SHALLOW WATER METHANE-DERIVED CARBONATES IN SILICICLASTIC SETTINGS: CRETACEOUS TEPEE BUTTES AND EOCENE STONE CITY BLUFF

A Dissertation

by

JENNIFER KATHLEEN HENDRICKS

Submitted to the Office of Graduate and Professional Studies of
Texas A&M University
in partial fulfillment of the requirements for the degree of

DOCTOR OF PHILOSOPHY

Chair of Committee,	Anne Raymond
Committee Members,	Michael C. Pope
	Ethan Grossman
	Thomas E. Yancey
	Michael Tice
	Dan Thornton
Head of Department,	Julie Newman

December 2019

Major Subject: Geology

ABSTRACT

Methane-derived carbonates occur in siliciclastic settings globally and precipitate from bicarbonate derived from methane oxidation. Methane-derived carbonates, which occur from the Archean to the present, take diverse forms, and have developed in a variety of depositional settings. This dissertation explores methane-derived carbonates from the Late Cretaceous Tepee Buttes (western US) and the Eocene Stone City Bluff (TX).

The Tepee Buttes are large carbonate mounds in the Pierre Shale. This study of 28 separate mounds from six different locations in southern Colorado identified six carbonate lithofacies comprised of the same common components in different proportions. Lithofacies have gradational boundaries and are randomly distributed on the mound surface, rather than concentrically zoned around a large, central vent. Horizontal beds visible on some mounds lie haphazardly on top of lower beds, which suggests formation as planar beds beneath the sediment-water interface, rather than as tall, elevated mounds with steeply dipping sides: the present-day configuration of the Tepee Buttes results from weathering and erosion. Mounds near Florence, CO, on the western side of the study area have a unique, lithofacies characterized by early diagenetic, iron-rich micrite.

Mound locations differed in degrees of matrix heterogeneity, but without a discernable pattern. Seep carbonate was formed from bacterial methane, likely sourced

from the underlying Pierre Shale; there is no evidence for a change in the source of methane through time. A forebulge acted as a trap to accumulate migrating methane.

The Stone City Bluff, TX, preserves barrel-shaped, vertically oriented septarian carbonate concretions associated with methane seeps. Barrel concretions preserve an internal micropipe, lined in pyrite, that preserves shell fragments and sedimentary features demonstrating fluid migration. The concretions have shrinkage cracks partly infilled with two generations of calcite. The $\delta^{13}C$ values of barrel carbonates are associated with the oxidation of bacterial methane generated in shallow shelf sediments during the Middle Eocene Climate Optimum that was expelled by sediment compaction.

The Tepee Buttes are the surface expression of a cold seep system; concretions from Stone City Bluffs preserve the subsurface plumbing. Together, these localities illustrate methane seeps from source, migration through the subsurface, to the surface expressions.

DEDICATION

I dedicate my PhD to my grandfather, W. J. Richmond, who attended A&M in the late 40s as a geology major; but was 6 hours short of earning his degree before his service in the Korean War. My grandmother, Brockie McCasland Richmond, was a kind, loving, and strong woman who taught me to prioritize learning. I dedicate this degree to my advisor, Anne Raymond, who guided, supported, uplifted, encouraged, championed, and even housed me through the highs and lows of grad school. I dedicate this work to the Thesis and Dissertation Goal Setting Group, its founder Dr Brian Williams, and my fellow grad students from different disciplines: without your help, encouragement, advice, insight, and accountability, I would have quit long ago. This dissertation would not have been feasible without my parents, Gary and Melissa Hendricks, who supported and cared for me always, sponsored me when I needed it, loved and advocated for me my entire life, and encouraged my pursuit of STEAM early in my life. I dedicate my dissertation to my sister, Renée Hendricks, a great friend and confidant throughout my life, and who I was able to commiserate with and turn to for emotional support, as she earned her master's degree in Anthropology. I thank Chris Nygren, my partner, who loved, encouraged, reassured, inspired, supported, comforted me, and cheered me on as I finished my dissertation. To Sandra Marek, who supported, reassured, sympathized, cheered me on, and listened to me through my graduate career. Finally, to Mrs. Tamara Lee, my high school anatomy teacher who advocated STEAM, and demonstrated to me what being truly passionate about your career is truly about.

ACKNOWLEDGEMENTS

I would like to thank my committee chair and advisor, Dr. Anne Raymond, for her guidance, support, encouragement, knowledge, writing assistance and understanding throughout my graduate school journey. I want to thank my committee members, Dr. Michael Pope, Dr. Ethan Grossman, Dr. Thomas Yancey, Dr. Michael Tice, and Dr. Daniel Thornton for their guidance, support, and revisions throughout my graduate career and this research. Thanks go to Dr. Cheryl Metz, for her immense knowledge about all things cold seeps, assistance in writing, and her aid.

I am grateful to my parents, Gary and Melissa Hendricks for their love and support, emotional and otherwise, throughout my entire graduate school experience, undergraduate career and my entire life. I am appreciative of Chris Nygren, my supportive significant other, for his love, and who boosted my mental health and encouraged me through the hardest part of my dissertation writing and my defense. I thank my sister Renée Hendricks, who I was always able to talk to about the struggles of graduate school and writing, and who understand what I was always going through.

I am appreciative of my fellow graduate students, especially my fellow paleo students, Michelle Chrpa and Samuel Neely for their friendship and encouragement and moral support. I am also grateful for the friendship and support of my other graduate student friends Angie Van Boening, Lauren Holder, Page (Jones) Alexander, Emily Schultz, Julian Correa, Robert Grajeda, III, John Hayes along with many other students in and out of the Geology Department.

I am extremely grateful to my friend, Sandra Marek for her friendship, emotional support, for her help with editing, and for always being available to talk. I want to thank my friend, Joseph Mery for his friendship, encouragement and assistance throughout grad school. I am incredibly grateful to the Thesis and Dissertation Goal setting group and its founder Dr Brian Williams, without their help I would not have finished grad school or writing my dissertation.

I am thankful for my close friends Maddie Pike and Thomas Petersen and for the many meals we shared and their friendship through my dissertation. Thanks go to my friends at the eATMe Hash House Harriers, the running group I am a part of. I am thankful to Suma Datta and Scott Dawson for teaching me to love dance and helping to introduce me to the world of West Coast Swing, and to the rest of the dancing community. I am grateful to my friend Laura Cottle for her continued friendship. I am thankful for the friendship of my friends Noura Randle and Matthew Etchells and their understanding of the trials of graduate school.

I am also thankful to Daniel Chaikin and Chris Piela who have helped mentor me in my career.

CONTRIBUTORS AND FUNDING SOURCES

Contributors

This work was supervised by a dissertation committee consisting of Professors Anne Raymond, advisor, Michael Pope, Ethan Grossman, Thomas Yancey, and Michael Tice of the Department of Geology and Geophysics, and Professor Daniel Thornton of the Department of Oceanography.

Jian Gong, Page Alexander, Kai Tao, and Shih-Yi Hsiung assisted in the field collecting samples, taking notes, and prepared initial lab samples data for Chapter 2 and Chapter 3. James Flis and Christopher Flis collected and prepared samples, and Dr Earl McBride of the University of Texas cut the barrel concretions for Chapter 4.

John Robbins, Brendan Roark, Chris Maupin and staff at the Texas A&M University Stable Isotope Geosciences Facility ran samples for Chapter 2, 3, and 4. Peter Larson and the staff at the Peter Hooper GeoAnalytical at Washington State University ran samples for Chapters 2 and 3.

Dr Anne Raymond assisted with writing, and along with Dr Michael Pope, and Dr Ethan Grossman assisted with editing prose for Chapters 2 and 3. Dr Thomas Yancey assisted with writing, editing and figure making for Chapter 4. Dr Anne Raymond assisted with editing Chapters 1 and 5.

All other work conducted for the dissertation was completed by the student independently.

Funding Sources

This graduate study was supported by two fellowships from the Berg-Hughes Center for Petroleum and Sedimentary Systems, the ConocoPhillips Fellowship and the Anadarko Fellowship, and a dissertation research grant from the Chevron Basin Modeling Center of Research Excellence.

This work was also made possible in part by the Geological Society of America (GSA) under Grant Number 9963-12, as well as the American Association of Petroleum Geoscientists (AAPG) Foundation under the James E. Hooks Memorial Grant. This dissertation's contents are solely the responsibility of the author and do not necessarily represent the official views of the GSA, the AAPG, the Berg-Hughes Center, ConocoPhillips, Anadarko or Chevron.

NOMENCLATURE

AOM	Anaerobic oxidation of methane
C	Carbon
CO	Colorado
Co.	County
DIC	Dissolved inorganic carbon
Fe	Iron
GoM	Gulf of Mexico
IRMS	Isotope ratio mass spectrometer
JVR	JV Ranch
m.y.	Million years
Ma	Million years ago
MECO	Middle Eocene Climate Optimum
NBS	National Bureau of Standards
O	Oxygen
SEHR	Southeast Hanna Ranch
TX	Texas
VPDB	Vienna PeeDee Belemnite
WIS	Western Interior Seaway

TABLE OF CONTENTS

Page

LIST OF FIGURES

Page

LIST OF TABLES

Page

CHAPTER I

METHANE DERIVED CARBONATES INTRODUCTION

Methane-derived carbonate concretions and beds occur in siliciclastic settings globally (Campbell, 2006; de Boever et al., 2006; Enos and Kyle, 2002; Gaillard et al., 1992; Kauffman et al., 1996; Nyman and Nelson, 2011; Shapiro, 2004; Sibuet and Olu, 1998). These carbonate concretions precipitated from bicarbonate derived from the oxidation of methane, and as such, retain a negative stable carbon isotopic signature (Konhauser, 2006; Whiticar, 1999). Methane-derived carbonate concretions and beds take diverse forms, have developed in a variety of depositional settings, and are present throughout geologic time (Campbell, 2006; Shapiro, 2004; Whiticar, 1999). Methane-derived carbonates and hydrothermal deposits occur from the Archean to the present and form on shallow shelves, in the deep ocean, in swamps, in eperic seaways, and even in lacustrine deposits (Campbell, 2006). Carbonate derived from methane is important geologically and commercially: it can help identify petroleum source rocks, enable scientists to reconstruct hydrocarbon movement in shelf systems, preserve unique fossil assemblages and original mineralogies, and records the progression of carbonate diagenesis in these features. Methane cold seeps are additionally important as they are thought to act as refugia during time of extinction, with numerous and diverse organisms colonizing and living at seeps (Campbell, 2006).

My dissertation considers methane-derived carbonates from two depositional settings: The Tepee Buttes, formed in a shallow eperic seaway, and The Stone City

Bluff, formed on a shallow shelf system. Methane-derived carbonate from both settings has a different morphology: the Tepee Buttes are large carbonate mounds (up to 10 m in height) preserving a diverse faunal community and are surface expressions of a vast methane cold seep system (Kauffman et al., 1996; Metz, 2010); the Stone City Bluff preserves the subsurface plumbing of a methane cold seep as barrel concretions, the largest of which is 70 cm in height and 20 cm in diameter and preserves evidence of methane-rich fluid migration in the form of micropipes. The Tepee Buttes have been studied for over a hundred years and have been widely reported upon in the literature (Gilbert and Gulliver, 1895; Bretsky, 1978; Howe, 1987; Beauchamp et al., 1989; Gaillard et al., 1992; Kauffman et al., 1996; Shapiro and Fricke, 2002; Birgel et al., 2006; Krause et al., 2009; Metz, 2010), whereas the barrel concretions at Stone City Bluff have not been described previously (Hendricks et al., 2012). The Tepee Buttes formed in the Late Cretaceous and the mounds examined in this study occur in southeastern Colorado; the Stone City Bluff barrel concretions occur in Upper Middle Eocene siliciclastic sediments in Burleson Co., TX.

My dissertation is broken into three parts. In the first, I will identify carbonate facies and their distribution on the Tepee Buttes mounds. Petrography and stable isotopic geochemistry allow me to determine a detailed paragenetic sequence and reveal a unique carbonate facies not yet reported in the Tepee Buttes seep system (Hendricks et al., in review). Combining these I propose a model of mound formation and diagenesis. In the second part, I examine temporal and spatial variations in the Tepee Buttes in southeastern Colorado. Most studies of the Tepee Buttes have focused on one or a few

mounds, despite evidence that mounds formed over 10 million years and range from southern Colorado to Montana (Kauffman et al., 1996; Metz, 2010). This study examines whether the model of mound formation, the paragenetic sequence, or the source of methane changed through time or varied geographically. In the third part, I examine unique, elongate, cylindrical concretions, called barrel concretions, recovered from Middle Eocene transgressive siliciclastic sediments at the Stone City Bluff, Burleson Co., TX. I record the morphology, petrography and stable isotopic geochemistry of these barrel concretions to determine a model of formation.

In the modern day, cold seep carbonates take diverse forms ranging from cm-scale carbonate crusts, to meter-scale chimneys, to brine pools and pockmarks, to large mounds rising tens meters above the seafloor to reef-like bioherms (Levin, 2005). Investigation of modern-day cold seeps is challenging due to the need for submersibles to study them at the depths where they usually form (Callender and Powell, 1999; Levin, 2005). Due to the challenge and high cost of exploring the sea floor, most cold seep carbonate studied today is the surface expression of methane seeps on the seafloor. By examining the Tepee Butte seep system through time and geographic space, and incorporating the Stone City Bluff barrel concretions, I can present a model of cold seep formation that extends to the subsurface.

CHAPTER II

ORIGINAL MORPHOLOGY OF THE TEPEE BUTTES MOUNDS: IMPLICATIONS FOR MOUND PALEOECOLOGY AND FORMATION

Introduction

The Tepee Buttes carbonate mounds (Fig. 1) of the Western Interior Seaway (WIS) are the most extensive fossil methane cold seep system known in both outcrop

Figure 1: Tepee Buttes, Southeast Hanna Ranch, Colorado; showing elevated mounds with resistant carbonate caps within the surrounding Pierre Shale A) Horizontal aspect showing profiles of the mounds B) Oblique view showing linear orientation some mound groups.

area and numerical abundance (Gilbert and Gulliver, 1895; Kauffman et al., 1996; Metz, 2010). In addition, this system was active over 10 million years from the mid-Campanian through the Maastrichtian, making it the longest-lived seep system yet

discovered (Scott and Cobban, 1975; Scott and Cobban, 1986; Kauffman et al., 1996; Shapiro and Fricke, 2002; Metz, 2010). These unique seeps provided centers of biologic diversity, productivity, and carbonate production in diverse marine settings. Because of this, ancient seeps offer a window into one of the most unique ancient marine habitats. On a larger scale, Metz (2010) hypothesized that the Tepee Buttes system was both long-lasting and geographically extensive because it was a sedimentary response to the reorganization of basin tectonics in the mid-Campanian, associated with the end of the Sevier orogeny and the beginning of the Laramide orogeny. For these reasons, the Tepee Buttes allow for an investigation of links between basin tectonics, sedimentology, paleoecology and seep development in a retro-forearc basin setting.

Both low original relief and elevated models were proposed for the Tepee Buttes mound formation (Fig. 2). These mounds were originally interpreted (Gilbert and Gulliver, 1895) forming as low-relief, stacked carbonate beds, similar to a stack of pancakes (Fig. 2A), with beds precipitating at calcareous springs and not forming high-relief features projecting above the surrounding siliciclastic seafloor (Gilbert and Gulliver, 1895; Arthur et al., 1982; Metz, 2010). The horizontal partings of the shale between carbonate beds indicate the carbonate was not built up faster than the surrounding Pierre Shale (Gilbert and Gulliver, 1895). According to the low original relief model of Gilbert and Gulliver (1895), the modern morphology of the Tepee Buttes results from differential weathering the carbonate beds and surrounding shale (Metz, 2010). Gaillard et al. (1992) described similar carbonate mound from the Jurassic of

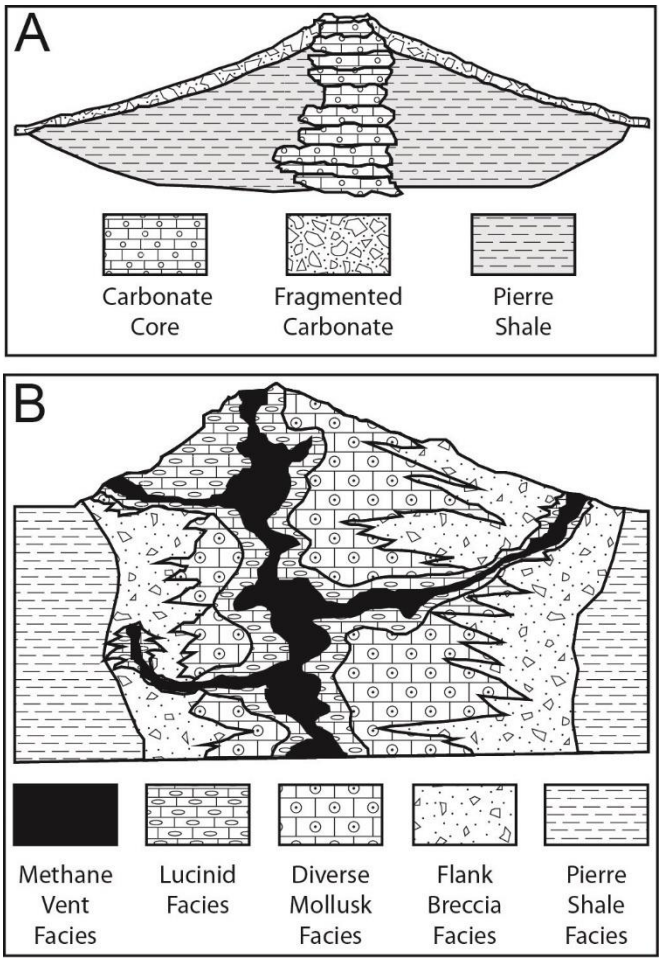

Figure 2: Historic models of Tepee Buttes morphology and zonation. A) A central limestone core surrounded by Pierre shale, with carbonate rubble on the slopes. Modified from Gilbert and Gulliver, 1895. B) Concentric zonation of facies around a central methane vent spring core facies. Modified from Kauffman et al., 1996.

France as "pseudobioherms" that are reconstructed as forming at the sediment-water interface. The elevated model became widely accepted after Kauffman et al. (1996) described the mounds as forming as elevated carbonate mounds, with dipping flanks and concentrically zoned facies around a central limestone core (Fig. 2B).

Most studies of the Tepee Buttes have focused on only a single mound or just a few mounds (e.g. Callendar, 1992; Kauffman et al., 1996; Shapiro and Fricke, 2002; Birgel et al., 2006; Krause et al., 2009), because of this, the method of mound formation is still not completely understood. Modern methane seep morphology is extremely diverse, with forms ranging from pockmarks (depressions in the seafloor) to flat lying carbonate crusts to tower-like carbonate build-ups to high relief carbonate mounds or mud volcanoes (Michaelis et al., 2002; Levin, 2005; Reitner et al., 2005; Campbell, 2006). This diversity of modern methane seep morphology makes it difficult to draw a comparison from the modern to the ancient. Since the Tepee Butte seep system formation occurred over a long period of time and the mounds cover an extensive geographic area (Metz, 2010), characterization of this system requires investigation of mounds throughout the interval of formation and across a broad geographic area. This contribution presents a detailed description of mound lithofacies and their distribution within individual mounds, as well as a comprehensive paragenetic sequence. These are used to evaluate current models of mound formation and trace their diagenetic history, and to also discuss a unique carbonate lithofacies not yet reported in the Tepee Buttes cold seep system. By studying this ferroan micrite lithofacies and its formation at the Tepee Buttes, a better understanding of other early diagenetic ferroan-rich carbonate can be reached.

Background

The Tepee Buttes are carbonate mounds located within the Pierre Shale from southern Colorado to South Dakota and Montana (Fig. 3). These mounds have been

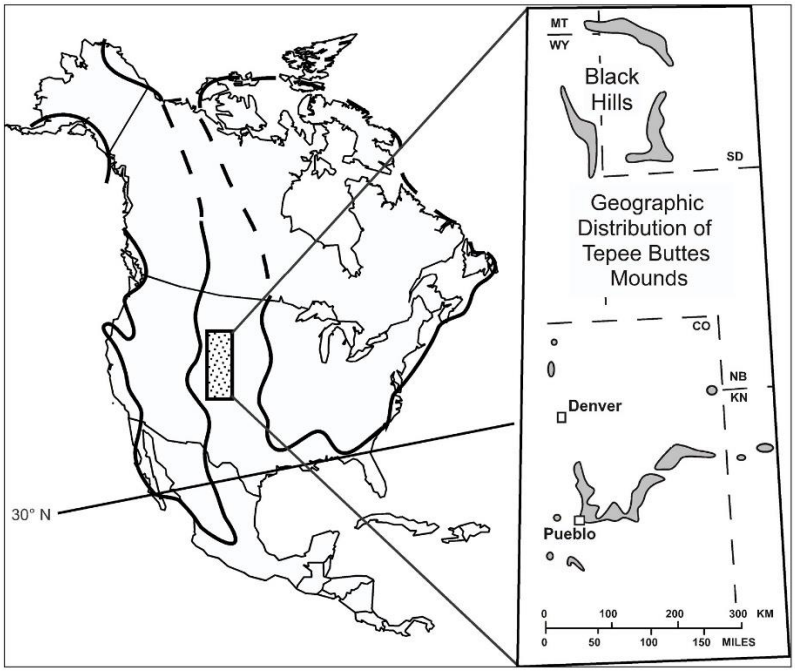

Figure 3: Location map of the extent of the Tepee Buttes. Black lines show the extent of the Western Interior Seaway and orientation of North America in the late Cretaceous when the Tepee Buttes were active. Reprinted from Metz, 2010.

studied for over 100 years and take their name from their resemblance to Native American tepees (Gilbert and Gulliver, 1895; Metz, 2010). The mounds are reconstructed as ancient methane seeps active during the Late Cretaceous, forming in a shallow epeiric seaway around methane-rich fluids seeping from the subsurface, when the WIS was at its maximum extent (Arthur et al., 1982; Howe, 1987; Kauffman et al., 1996; Birgel et al., 2006; Krause et al., 2009; Metz, 2010).

Seep activity occurs intermittently over 10 million years: from the Middle Campanian (78.7 Ma) to the Early Maastrichtian (69.1 Ma), occurring in four distinct stratigraphic intervals with the longest lasting less than three million years (Kauffman et

al., 1996; Metz, 2010). Formation of the Tepee Buttes occurred as tectonic depozones within the Western Interior Basin (a retro-foreland basin) shifted to the east, towards the craton (Metz, 2010). This shift was associated with a shallowing in the subduction angle of the Farallon Plate beneath North America to the west, most likely marking the onset of Laramide tectonics within the distribution area (Kauffman et al., 1996; Metz, 2010). The geographic extent (~212,000 sq. km) of the Tepee Buttes is attributed to the occurrence of a 'fixed' forebulge within the basin resulting from the tectonic reorganization associated with lithospheric loading and migration of the tectonic depozones (Metz, 2010). The longevity (> 10 m.y.) and recurrence of Tepee Butte seep activity over this 'fixed' forebulge can be tied to changes in shoreline positions, the region of maximum sediment loading, and sediment redistribution coincident with regressive-transgressive cycles within the basin (Metz, 2010). These changes affected lithospheric flexure of the forebulge region, opening and closing hydrocarbon conduits necessary for seep activity (Metz, 2010). Timing of shoreline migration compared to the timing of seep formation (seen in the stratigraphic distribution of the mounds) show that seep activity occurred between maximum transgressions and maximum regressions (Kauffman et al., 1996; Metz, 2010); this may account for the variation of mound formation in more localized geographic areas at the various intervals of Tepee Butte activity.

Based on planktic foraminiferal and macrofaunal analysis, the Tepee Buttes formed in shallow water, between 30 and 100 m depth (Howe, 1987). Lucinid bivalves (*Nymphalucina occidentalis*) dominate the mounds, while other organisms on and

around the mounds include inoceramid bivalves, ammonites, foraminifera (pelagic and benthic), gastropods, and echinoderms (including crinoids), while microbial mats also are present (Howe, 1987; Kauffman et al., 1996; Hunter et al., 2016). A tube-worm biofacies has been linked with the seep vent at the mound center (Arthur et al., 1982; Kauffman et al., 1996). Studies of the surrounding Pierre Shale suggest that the bottom waters of the WIS were dysoxic with slow circulation (Kauffman et al., 1996).

Methods

I visited and collected samples from over 28 different mounds and their satellite mounds in Colorado near Pueblo, Florence and Colorado Springs (Fig. 4). These

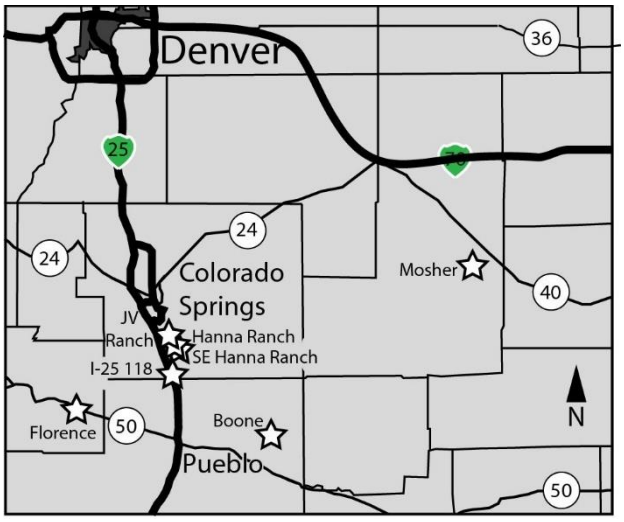

Figure 4: Map of area of southeastern Colorado surrounding Colorado Springs, showing the six locations (stars) of mounds visited in this study. Thick lines show major road, and thin lines show county lines.

mounds occurred in six locations: Boone, I-25, Hanna Ranch, JV Ranch, Mosher, and Florence. Due to its easy accessibility and with one mound bisected by a road cut, the

Boone location is the most commonly studied. Building on previous work (Gilbert and Gulliver, 1895; Arthur et al., 1982; Howe, 1987; Callendar, 1992; Kauffman et al., 1996; Shapiro and Fricke, 2002; Bash et al., 2005; Dahl et al., 2005; Anderson, 2006; Birgel et al., 2006; Lyons et al., 2007; Krause et al., 2009), six carbonate lithofacies were identified in the field based on fossil distributions, depositional and petrographic features, and weathering fabrics, then lithofacies distribution were mapped on three mounds. In addition, overall mound geometries were noted, carbonate bed morphology, bedding planes and the relationship of carbonate beds and shale partings. General orientation and relationships of mounds were noted in the field, as well as using Google Earth.

Sixty-four thin sections and 81 cellulose acetate peels were prepared of the six distinct lithofacies from all six mound locations. The relative iron and magnesium content of the samples was determined based on staining done with Alizarin red S and potassium ferrocyanide (Table 1; Dickson, 1965). A paragenetic sequence for the five

Carbonate types	**Formula**	**Combined Stain Color**
Calcite	$CaCO_3$	Pink to pale pink
Aragonite	$CaCO_3$	Pale pink
Ferroan Calcite	$(Ca,Fe)CO_3$	Mauve - purple - royal blue
Dolomite	$CaMg(CO_3)^2$	No color
Ferroan Dolomite	$Ca(Mg,Fe)(CO_3)^2$	Pale to deep turquoise

Table 1: Alizarin red S and potassium ferrocyanide staining used to identify mound carbonate (modified from Dickinson, 1965).

main lithofacies was determined using samples from the "classic" Boone location, and a modified paragenetic sequence for the Florence location, and verified the paragenetic sequence with thin sections of all lithofacies from all locations. All thin sections and slabs are stored in the Texas A&M Paleontology collections.

Stable isotopic analyses were conducted to characterize the carbon and oxygen isotopic signatures by collecting samples from each generation of carbonate fabric from the six different lithofacies with a dental drill. Table 2 lists the different carbonate fabrics, their general morphology, stain color, and carbon and oxygen stable isotope ranges. Samples from the dense lucinid lithofacies were analyzed for carbon and oxygen stable isotopes using a Kiel IV Carbonate Device attached to a Thermo ScientificMAT253 at the Stable Isotope Geosciences Facility at Texas A&M University. Characterization samples from other locations were sent to the Peter Hooper GeoAnalytical Laboratory at Washington State University for carbon and oxygen stable isotopic analysis on a Finnigan Delta S gas source isotope ratio mass spectrometer. Analytic results are reported versus Vienna Pee Dee Belemnite (VPDB) using the NBS-19 standard. Precision values for Texas A&M University were ± 0.06‰ and ± 0.04‰ for $\delta^{18}O$ and $\delta^{13}C$ respectively; whereas Washington State University precision values were ± 0.02‰ and ± 0.05‰ for $\delta^{18}O$ and $\delta^{13}C$ respectively. Stable isotopes are used to confirm the paragenetic sequence, and depositional and diagenetic conditions.

Fabric	Petrographic Character	Staining Color	Stable Isotopes (‰)
Peloids in micrite	Dark to medium brown circular to semi-circular peloids surrounded by fine-grained micrite	Pink	$\delta^{13}C$: -44.5 to -32.6 $\delta^{18}O$: -10.7 to -0.1
Peloids in calcite	Dark to medium brown circular to semi-circular peloids surrounded by calcite cement	Pink	$\delta^{13}C$: -47.4 to -34.8 $\delta^{18}O$: -9.3 to -0.2
Micrite	Fine-grained	Pink	$\delta^{13}C$: -44.9 to -34.5 $\delta^{18}O$: -11.2 to -0.3
Botryoidal cement	Radiating fibrous calcite, often in multiple generations	Pink to purple	$\delta^{13}C$: -46.5 to -25.1 $\delta^{18}O$: -8.4 to -1.5
Early sparry calcite	Sparry anhedral calcite infills vugs, lucinids and surrounds peloids. Has varying amounts of iron based on staining	Pink to purple to blue	$\delta^{13}C$: -24.5 to -7.1 $\delta^{18}O$: -12.7 to -7.1
Lucinid Shells	Replaced by iron-rich calcite spar	Blue	$\delta^{13}C$: -21.1 to -10.7 $\delta^{18}O$: -12.8 to -9.9
Inoceramid	Fragments of inoceramid shells, retains original shell mineralogy	Pink	$\delta^{13}C$: -6.6 to 2.4 $\delta^{18}O$: -6.4 to -2.1
Forams	Forams, many different species	Pink	N/A
Micritization	Iron rich micrite has neomorphosed sparry calcite on the interior of vugs or lucinid shells. Fine grained.	Purple	$\delta^{13}C$: -26.5 to -12.6 $\delta^{18}O$: -13.1 to -9.7
Silica replacement	Microcrystalline silica has replaced some lucinid shells	No stain (white)	N/A
Dolomite	Clear anhedral dolomite, found in the center of some vugs and replacing some lucinid shells	No stain (Clear)	$\delta^{13}C$: -19.2 to -15.7 $\delta^{18}O$: -12.8 to -10.2
Ferroan micrite	Iron-rich fine-grained micrite	Blue to turquoise	$\delta^{13}C$: -4.7 to 5.3 $\delta^{18}O$: -3.4 to -0.1
Fractures	Either open thin fractures or filled with botryoids or sparry calcite	Blue to unfilled	N/A

Table 2: Fabrics seen in the facies found at the Tepee Buttes describing the petrographic character, the staining color from Alizarin Red and Potassium Ferrocyanide, and the range of oxygen and carbon stable isotopic values.

Results

Field Observations

Today, the Tepee Buttes are steep-sided carbonate hills, rising to 10 m in height above the surrounding flat-lying Pierre shale, as typified by Kauffman et al.'s (1996) reconstruction (Fig. 1, Fig 3B). Mounds range in both height and width, from short (one to a few meters in height) and wide, to tall (up to 10 m) with relatively narrow bases (< 20 m). Mounds occur in groups of 10 to 100, arranged in linear arrays; lone mounds are rare (Scott and Cobban, 1975; Sharps, 1976; Scott and Cobban, 1986; Callendar, 1992). Satellite mounds associated with larger mounds generally have lower elevation and are connected by a saddle of shale and carbonate rubble.

Mounds show different degrees of weathering; some were completely covered in vegetation, soil and rubble, whereas others have resistant carbonate beds exposed on the sides and tops. These irregular beds range from 15 – 75 cm in thickness, and are most prominent at the tops of mounds, though they also occur exposed at the sides and bases of mounds. Mounds at Hanna Ranch, Southeast Hanna Ranch, and I-25 consist of unevenly stacked carbonate beds, interfingered with the surrounding Pierre Shale (Fig. 5) as similarly noted by Gilbert and Gulliver (1895). Carbonate lenses at the base and edges of the Boone mound also interfinger with the Pierre Shale, as noted by Kauffman et al. (1996; Fig. 6).

Petrographic Results

Based on field and petrographic observations, six different carbonate lithofacies were identified in the mounds: dense lucinid, vuggy, anastomosing ropey, brecciated,

Figure 5: Thin carbonate beds or lenses can be seen, with roughly parallel bedding. Beds were seen best when the angle of the sun was low. Arrows mark some of the bedding planes. Hammer (~30 cm long) for scale. Large photo taken at Southeast Hanna Ranch. Photo inset taken at I-25-118 mound, human for scale.

Figure 6: Shale interbeds on Boone mound, pointed out with arrows. Inset shows close up between shale and carbonate boundaries, with shale marked by arrows on Boone mound.

carbonate nodules, and ferroan micrite. The dense lucinid and vuggy lithofacies are the most common and abundant lithofacies, occurring on all the mounds. The anastomosing ropey and brecciated lithofacies are relatively abundant and occur on most mounds. The ferroan micrite lithofacies is a rare but distinct lithofacies defined by a unique ferroan-rich micrite fabric, encountered only on the westernmost mounds near Florence.

The four main lithofacies (dense lucinid, vuggy, brecciated, and anastomosing ropey) and the ferroan micrite lithofacies have the same major carbonate fabric constituents (Table 2): peloids, micrite, lucinid shells, vugs, and carbonate cements (sparry calcite, botryoids, microcrystalline); however, they have different amounts of these fabrics. Peloids (85 – 647.2 μm) are a mixture of both fecal and microbial pellets; smaller, more amorphous peloids are potentially due to the breakdown of a microbial mat, while the large peloids are likely fecal in nature from a variety of different organisms (Chafetz, 1986). Minor fabric constituents include secondary organisms, dolomite, quartz and carbonate sediment, pyrite and silica replacement. The organisms on mounds include: lucinid and inoceramid bivalves, ammonoids, benthic foraminifera, gastropods (minor), ostracods (minor), crinoids, and sponge spicules. There is no evidence of tube worms or stromatolites. A detailed description of the six lithofacies and their constituents appears in Table 3.

The dense lucinid lithofacies, characterized by a high density of lucinid shells and shell hash, as well as numerous vugs, is the most common lithofacies in the Tepee Buttes mounds (Fig. 7). In thin sections and peels, the matrix is composed of micrite and

	Lithofacies	Dense lucinid	Vuggy	Brecciated	Anastamosing ropey	Carbonate nodule	Ferroan micrite
Constituents							
Micrite		Common	Common	Frequent	Common	Abundant	Frequent
Peloids		Common	Common	Frequent	Frequent	Not Present	Observed
Botryoidal cement		Observed	Frequent	Frequent	Frequent	Rare	Observed
Vugs		Observed	Frequent	Frequent	Frequent	Rare	Observed
Sparry calcite cement		Observed	Frequent	Frequent	Frequent	Rare	Frequent
Dolomite		Rare	Rare	Rare	Observed	Rare	Rare
Ferroan Micrite		Not Present	Not Present	Not Present	Not Present	Not Present	Common
Silica		Rare	Rare	Rare	Rare	Rare	Rare
Pyrite		Observed	Observed	Rare	Observed	Rare	Rare
Fractures		Rare	Rare	Frequent	Rare	Rare	Frequent
Lucinid bivalves		Frequent	Frequent	Frequent	Observed	Rare	Observed
Inoceramid fragments or molds		Rare	Rare	Rare	Rare	Rare	Observed
Foraminifera		Rare	Observed	Rare	Observed	Rare	Observed

Table 3 : Facies chart describing the constituent makeup of the six different lithofacies and their approximate frequency. Rare: < 6%; Observed: 6 – 12%; Frequent: 12 – 25%; Common: 25 – 50%; Abundant: > 50%.

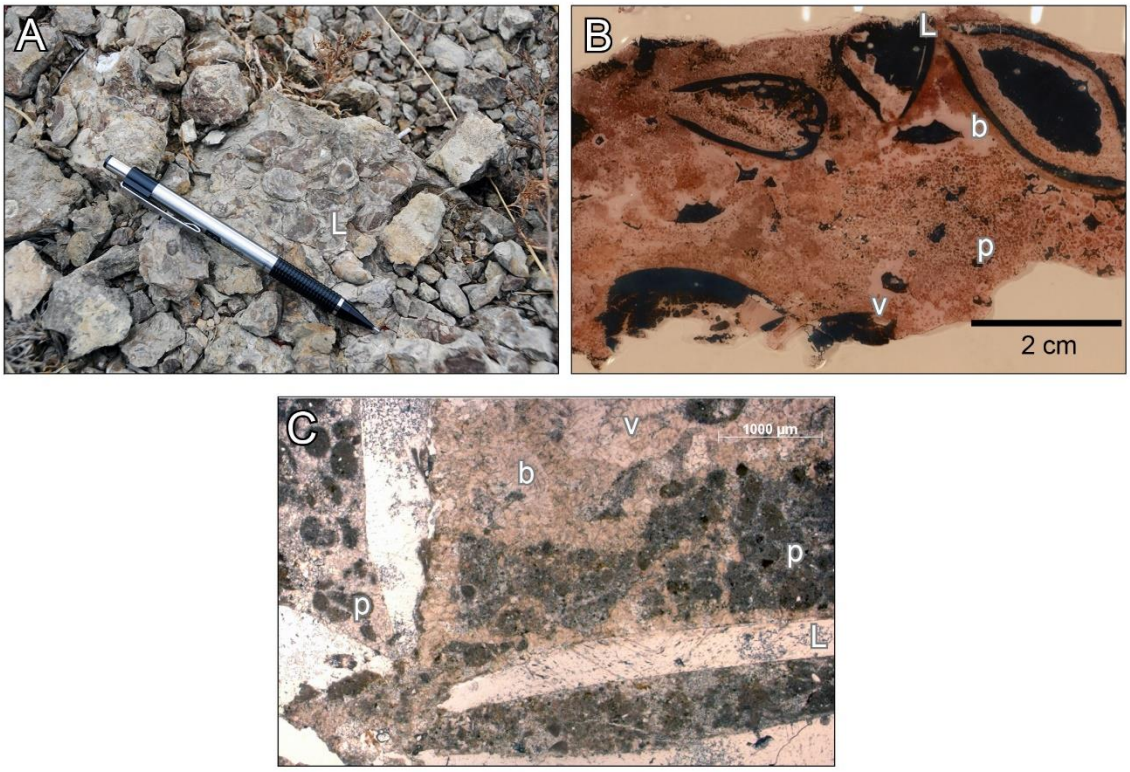

Figure 7: Dense lucinid lithofacies. A) Field photo showing large amount of lucinids and cement; B) Stained peel of slab Boone-DL; C) Thin section JVR2-01 photo showing lucinid shells, peloids and sparry calcite. L – Lucinid bivalves; p – peloids; v – vug; b – botryoids.

peloids (fecal pellets and microbial peloids), and frequently contains foraminifera (Fig. 7B,C). Articulated lucinids are filled with peloids, blocky spar, botryoids, or a combination of these; some shells have geopedal structures (Fig. 7C). Vugs, filled with one to many generations of botryoids and sparry calcite cement, range in size from 0.49 cm to greater than 5 cm. Sparry ferroan calcite has replaced all the lucinid shells and occurs in the interior of some vugs and fractures; some lucinid shells have areas of minor silica replacement (Fig. 7B).

The vuggy lithofacies, characterized by a high quantity of cement filled vugs, is the second most abundant lithofacies (Fig. 8). This lithofacies contains fewer whole lucinid shells and lucinid hash than the dense lucinid lithofacies (Fig. 8B). In thin section and peels, this lithofacies contains frequent vugs filled with sparry calcite cement and multi-generational botryoids (Fig. 8C).

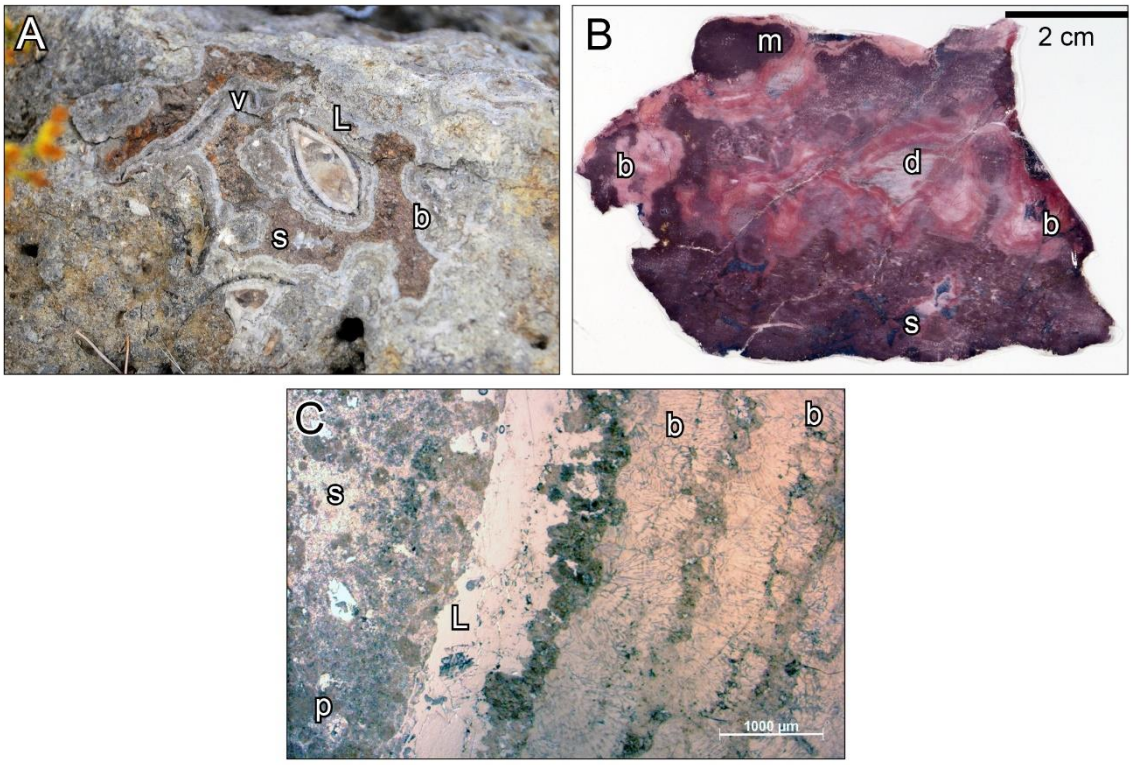

Figure 8: Vuggy lithofacies. A) Field photo showing large vugs surrounding a lucinid; B) Stained peel of slab B-11; C) Thin section photo of JVR1-07b showing lucinid shell with many generations of botryoids surrounding it. L – lucinid bivalve; v – vug; s – sparry calcites; b – botryoids; m – micrite; d – dolomite; p – peloids.

The anastomosing ropey lithofacies is characterized by anastomosing ridges (from 0.3 – 1.21 cm, averaging 0.76 cm in diameter) on weathered surfaces of the rock, micrite, minor lucinid shells and vugs (Fig. 9). Previous workers may have interpreted

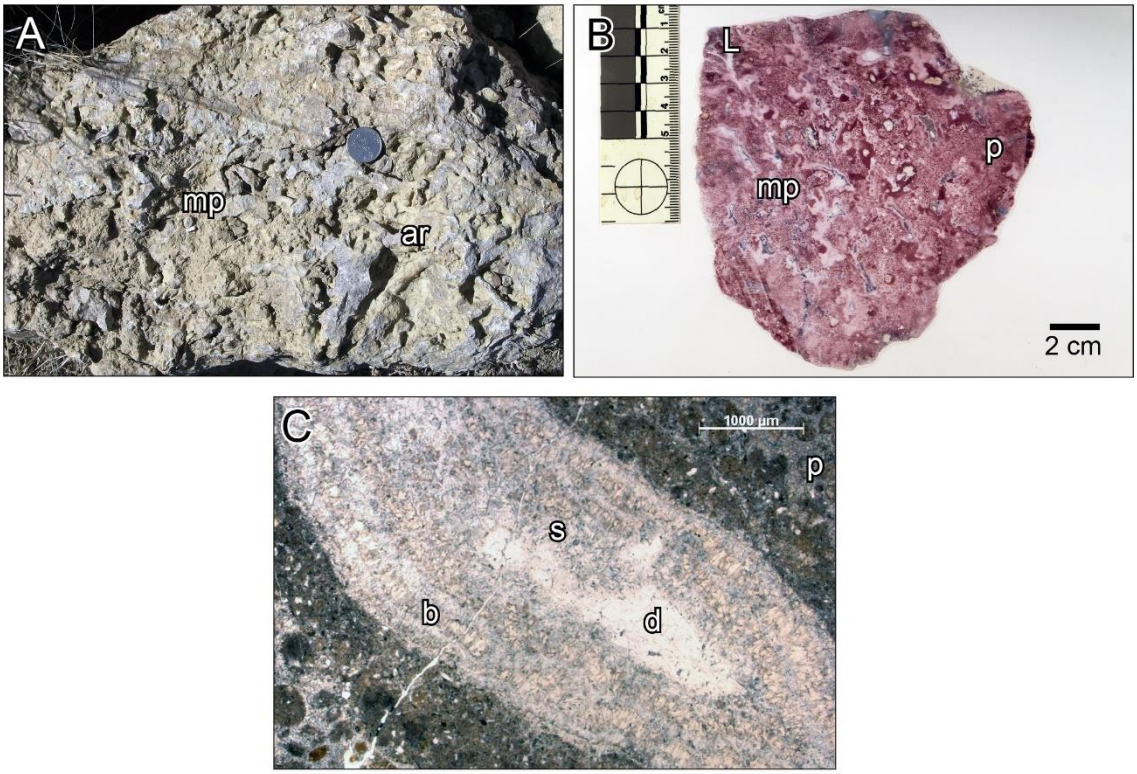

Figure 9: Anastomosing ropey lithofacies. A) Field photo showing the anastomosing ropey texture and micropipes; B) Stained peel of slab B-32; C) Thin section SEHR4-06B photo showing micropipe filled in with botryoidal calcite and sparry calcite. mp – micropipe; ar – anastomosing ropey texture; L – lucinid bivalve; p – peloids; b – botryoids; s – sparry calcite; d – dolomite.

these anastomosing ridges as tube worms (Howe, 1987; Kauffman et al., 1996; Shapiro and Fricke, 2002). In hand sample, the ridges when broken appear darker (gray brown) than the surrounding tan rock (Fig. 9A). 'Micropipes' occur in the interior of these larger

ridges (Fig. 9A,B); they are circular, averaging 0.25 cm (ranging to 0.5 cm) in diameter, rimmed in dark brown calcite, and filled with botryoids and sparry calcite.

In peel and thin section, pockets of orange shale occur throughout the rock (Fig. 9C; 10). Vugs are filled with large amounts of multi-generational botryoidal cement and

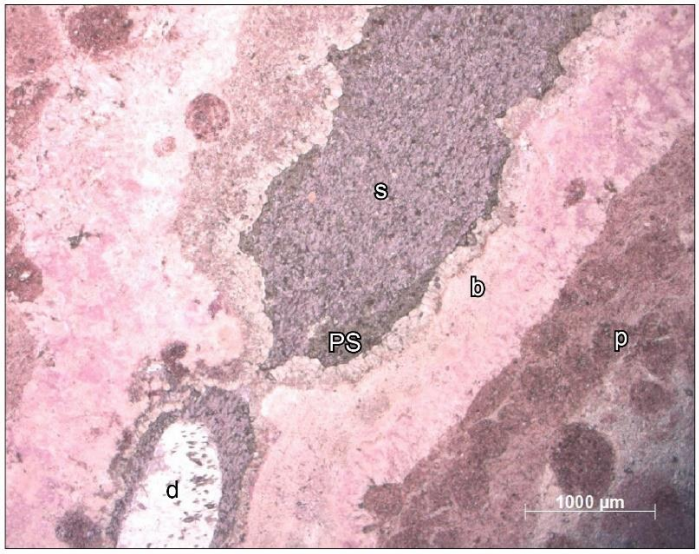

Figure 10: Anastamosing ropey lithofacies stained peel microscopic photo of B-32, showing the micropipe and the progression of the fill. p – peloids; b – botryoids; PS – Pierre Shale; s – sparry calcite; d – dolomite.

sparry calcite cement. Small tubes (micropipes), 1 - 7 mm in diameter and up to 40 mm long, distinguish this lithofacies and also were described by (Krause et al., 2009; Fig. 9B,C). Starting at the rim and working inward, micropipes are filled with micrite or botryoids, followed by ferroan sparry calcite, and in some, dolomite at the center (Fig 10). Towards the outer edges of the micropipes and within of botryoids, peloids are frequent, whereas foraminifera (or other small shells) are rare (Fig. 9C; 10). Micropipes

may be lined with orange to tan siliciclastic mud. These micropipes in the anastomosing ropey lithofacies were interpreted as methane gas pipes/conduits (Krause et al., 2009).

The brecciated lithofacies occurs on most mounds, and vug fill can exhibit small-scale brecciation and fractures (Fig. 11). This lithofacies has more micrite than other

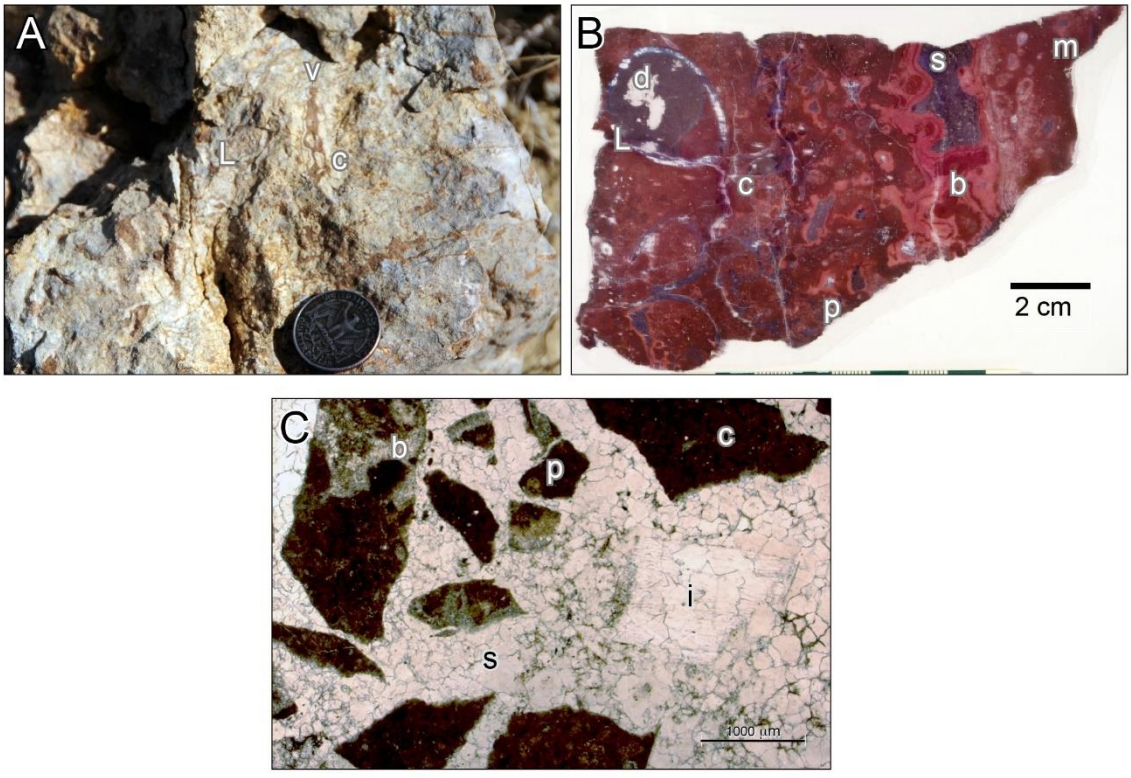

Figure 11: Brecciated lithofacies. A) Field photo showing brecciated clasts in a vertical vug; B) Stained peel of slab BS-3C-10; C) Thin section M1-01 photo showing clasts in a sparry calcite matrix. L – Lucinid bivalve; c – clasts; v – vug; d – dolomite; p – peloids; m – micrite; b – botryoids; s – sparry calcite; i – inoceramid shell fragment.

lithofacies and contains frequent vugs (1 cm to over 7 cm) filled with brecciated clasts surrounded by botryoids or sparry calcite cement, and occasional peloids (Fig. 11C). Clasts are angular, ranging in size from less than a millimeter to a few millimeters.

Frequent fractures (both large and small) filled with ferroan sparry calcite cement cross-cut foraminifera and other fabrics.

The carbonate nodule lithofacies consists of smooth, spherical to sub-spherical carbonate concretions (from 5 - 15 cm) that occur on the sides or tops of mounds and in the surrounding Pierre Shale (Fig. 12). In thin section or peels, concretions are

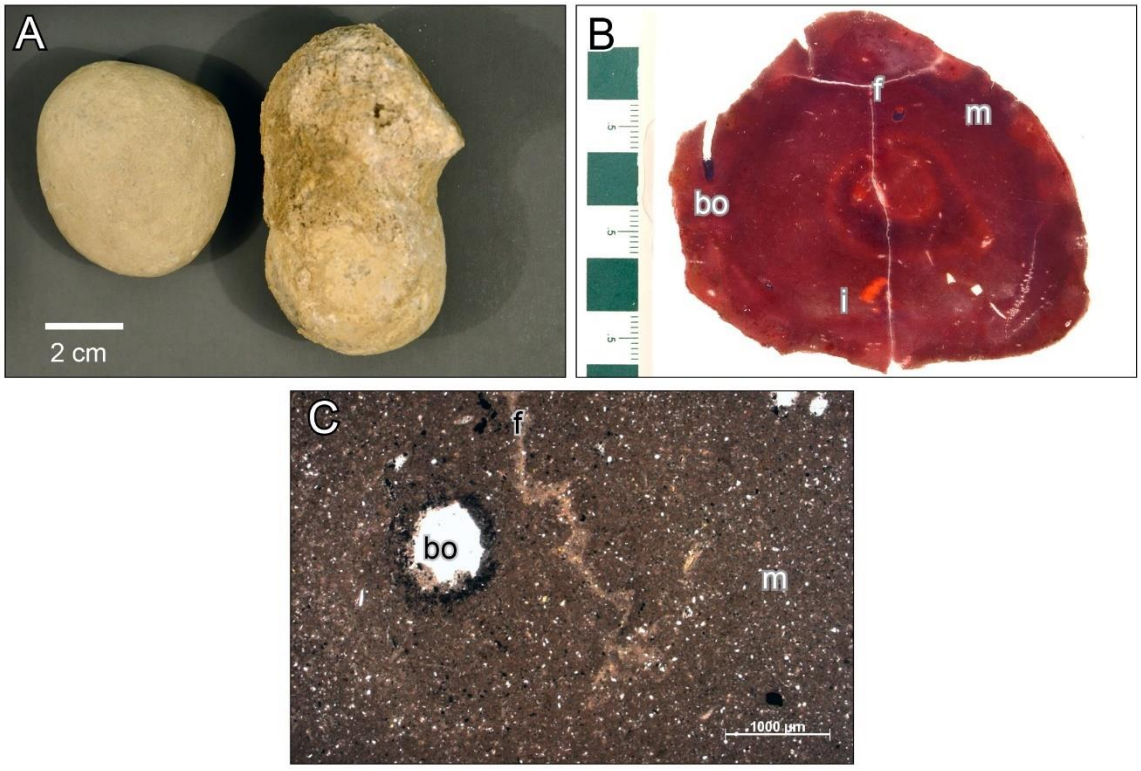

Figure 12: Carbonate nodules lithofacies. A) Uncut carbonate nodules; B) Stained peel of slab B-25; C) Thin section HR2B-06 showing boring and micrite matrix. m – micrite; f – fracture; i – inoceramid shell fragment; bo – boring.

characterized by a micrite matrix devoid of peloids and foraminifera (Fig 12B), with occasional small borings (1-3 mm diameter; Fig 12C). Some nodules contain small inoceramid or lucinid fragments.

The ferroan micrite lithofacies occurs only in mounds near Florence, CO, the western side of the study area. Hand samples contain a large amount of orange micrite, less lucinid shells, and less other constituents (peloids, vugs, etc.) than other lithofacies (Fig. 13). Iron staining is a significant characteristic in this location. In thin section and peel, much of the micrite stains completely blue, reflecting a high iron content unique to this lithofacies and location (Fig. 13B). Three phases of ferroan micrite can be distinguished petrographically, evident through: different stain colors (light blue, dark blue and grey-blue), cross cutting relations, and different levels of homogeneity (Fig. 13B,C). Peloids are less prevalent, appearing replaced or partially replaced by ferroan micrite. Fractures are frequent and are open or filled with ferroan sparry calcite cement. Lucinid shells are rare, replaced by ferroan calcite or partially by silica. Botryoids and vugs are less common than in other lithofacies, as much of the rock is composed of ferroan micrite. Foraminifera, inoceramid fragments, ostracods, and gastropods are rare; sponge spicules are rare but are not seen in other locations.

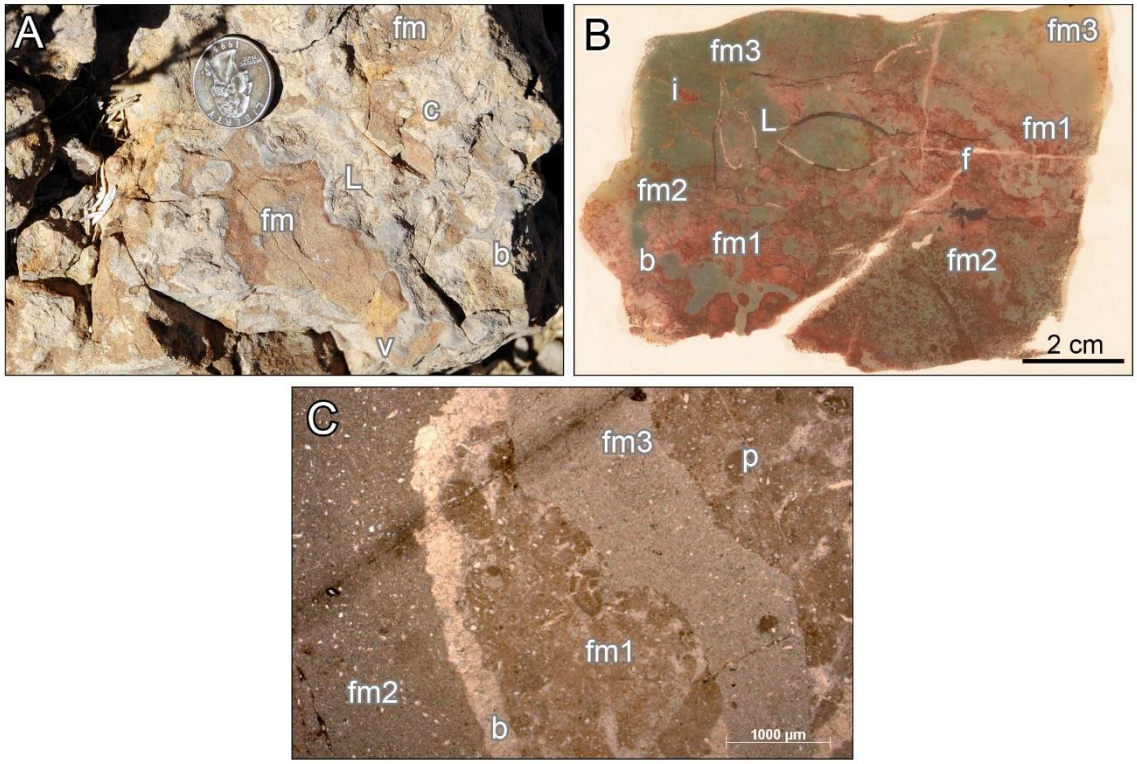

Figure 13: Ferroan micrite lithofacies. A) Field photo showing ferroan micrite and iron staining found only at the westernmost Florence mounds; B) Stained peel photo of slab F1-11 showing the different staining colors of the three generations of ferroan micrite; C) Thin section F1-11 showing differences in heterogeneity and cross cutting relations of the three generations of ferroan micrite. fm – ferroan micrite; L – lucinid bivalve; c – clasts; v – vug; b – botryoids; i – inoceramid shell fragment; f – fracture; fm1 – 1st generation (earliest) of ferroan micrite; fm2 – 2nd generation (middle) of ferroan micrite; fm3 – 3rd generation (latest) of ferroan micrite; p – peloids.

Lithofacies Distribution

Lithofacies are not arranged concentrically around the center of mounds, and instead appear patchily distributed within carbonate beds, with gradational boundaries between lithofacies (Fig. 14). The two most abundant lithofacies (dense lucinid and

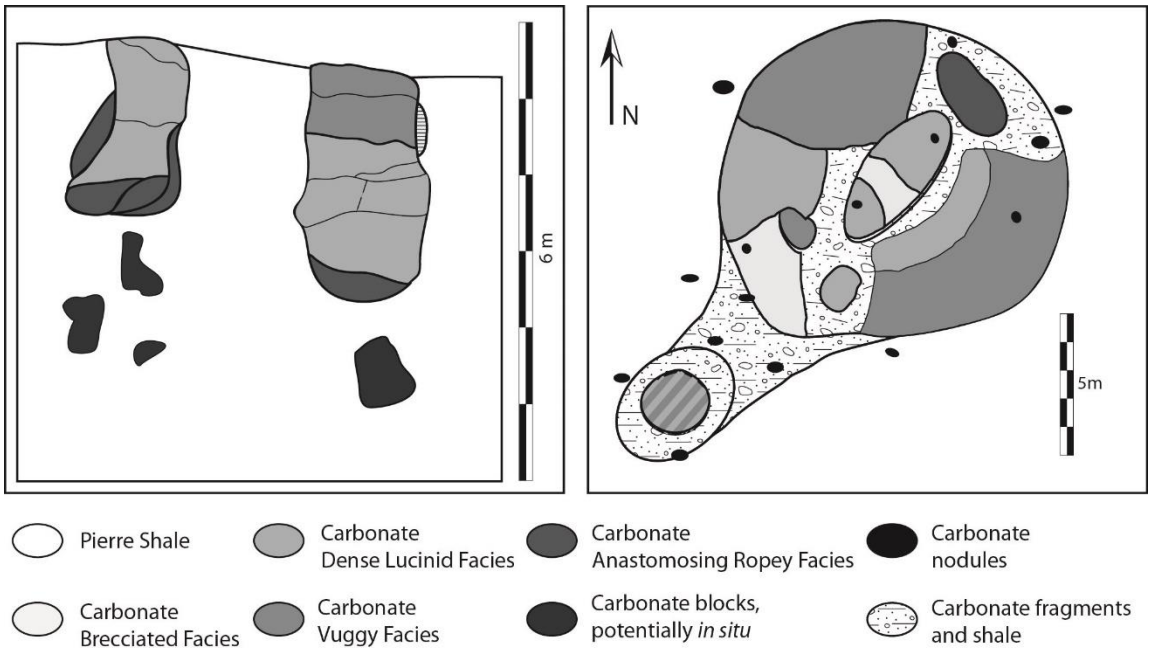

Figure 14: Lithofacies distribution on the I-25-118 (left) mound and generalization of the lithofacies documented Southeast Hanna Ranch (right). Lithofacies boundaries are gradational and not sharp delineation as depicted in the figure. Lithofacies were randomly oriented on the mound and were not concentrically zoned or found in the same location as has been historically suggested.

vuggy) comprise most of the mound surface, occurring near the apex and on the slopes. Field observations show no evidence of a large, central vent described by Kauffman et al. (1996) at the Boone mound, or any other location (Fig. 14). The ropey anastomosing lithofacies (Fig. 9) is the spring vent core limestone as described by Howe (1987) and (Kauffman et al., 1996), where it was placed in the center of the mounds through the entire length of the mound (Fig. 2A). The ropey anastomosing lithofacies occurs on the flanks of mounds (Fig. 14B), was never found directly in the center of a mound, and was patchily distributed, never crossing through multiple beds (Fig. 14A).

Stable Isotopic Results

Fabrics of the Tepee Butte mounds exhibit a wide range of oxygen and carbon stable isotope value: all show evidence of methane influence, except the ferroan micrite. However, there is a narrower range of oxygen and carbon stable isotope values within individual fabrics (Fig. 15). The carbon stable isotopic values of different Tepee Butte mound fabrics from the main lithofacies have a wide range, with $\delta^{13}C$ values as depleted as -47.4‰, ranging up to 2.4‰. The $\delta^{18}O$ values of fabrics varied as well, ranging from

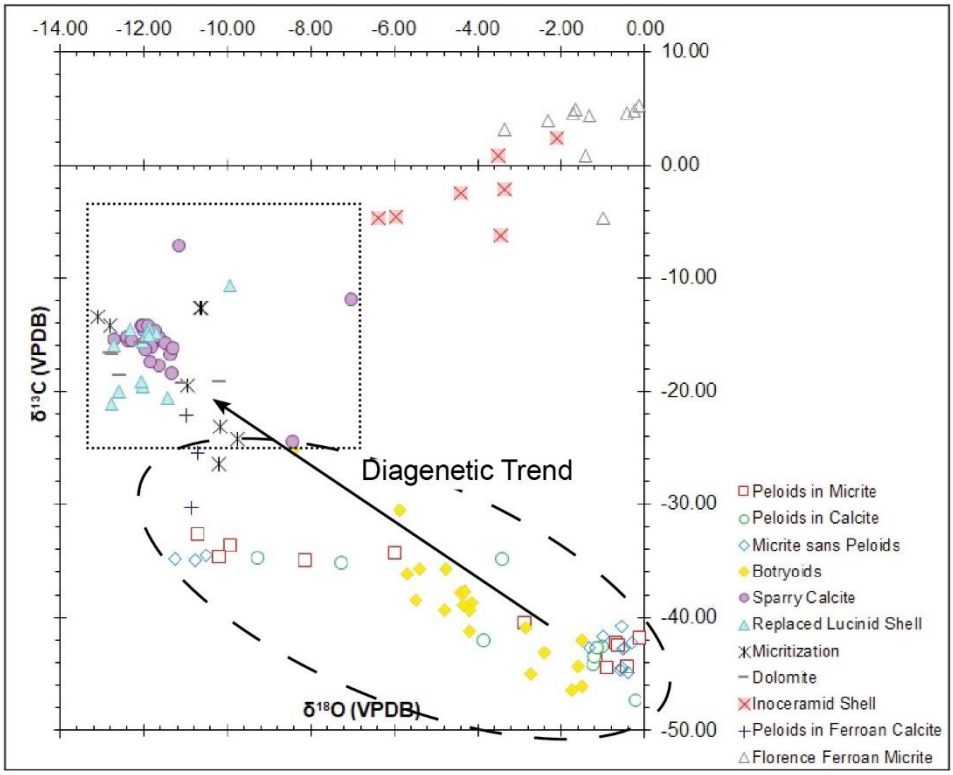

Figure 15: Stable isotopic characterization samples from the Boone location and Florence ferroan micrite. Dotted circle denotes the isotopic values of early fabrics, with the arrow marking the isotopic diagenetic trend towards the dotted square denoting of late diagenetic fabric values.

-0.1‰ to -12.8‰. The most depleted $\delta^{18}O$ values and the least depleted $\delta^{13}C$ values are associated with higher amounts of iron as seen by staining.

Non-ferroan carbonate fabrics (micrite, peloids in micrite and calcite, botryoids) have more depleted $\delta^{13}C$ values, ranging from -47.4‰ to -25.1‰, and have $\delta^{18}O$ values ranging from -0.2‰ to -11.2‰. Ferroan fabrics (ferroan sparry calcite, replaced lucinid shells) and dolomite have less depleted $\delta^{13}C$ values (-24.5‰ to -7.1‰), whereas the $\delta^{18}O$ values of these fabrics range from -7.1‰ to -12.9‰. Ferroan micrite from Florence had stable carbon isotope values that ranged from -4.7‰ to 5.3‰ and oxygen stable isotope values ranging from -3.4‰ to -0.1‰.

Discussion

Mound Formation

Stable carbon and oxygen isotopic values confirm that the Tepee Buttes are ancient methane seeps formed from microbial methane (Fig. 15; Kauffman et al., 1996; Birgel et al., 2006). Microbes produce methane in anoxic conditions when organic matter is combined with sulfate or other chemical substrates through a number of different pathways (Sibuet and Olu, 1998; Whiticar, 1999; Campbell, 2006). Early carbonate fabrics from the Tepee Buttes (micrite, peloids in micrite, peloids in calcite, and botryoids) have depleted $\delta^{13}C$ values (-47.4‰ to -25.1‰; Table 2; Fig. 15). Extremely depleted $\delta^{13}C$ values were measured in organic compounds from the Tepee Buttes (-118‰ to -102‰) and were interpreted as evidence for the presence of microbial methane at Tepee Buttes (Birgel et al., 2006).

Field observations support the original low-relief mound (Fig. 2A) models of Gilbert and Gulliver (1895) and Gaillard et al. (1992) with patchy lithofacies distributions (Fig. 14) similar to those seen in modern cold seeps (Levin, 2005), rather than the elevated mound model of Kauffman et al. (1996) with facies concentrically zoned around a large, central vent (Fig. 2B). Field observations show the dense lucinid and vuggy lithofacies dominate mounds with patchy distribution and gradational boundaries (Fig. 14; Anderson et al., 2005; Bash et al., 2005; Anderson, 2006; Lyons et al., 2007; Metz, 2010). This mirrors observations of modern methane seeps: in the Eel River Basin facies are randomly distributed around the cold seep, with multiple vents located on a mound (Levin, 2005), and in the Gulf of Mexico, Feng et al. (2008) saw no evidence of zonation within seep carbonate from Alaminos Canyon.

This work shows that Tepee Buttes seep carbonate formed as beds of microbial carbonate below the sediment water interface. Field observations of stacked horizontal carbonate beds (50 – 75 cm; Fig. 5; Fig. 16) on several mounds closely resemble the model of Gilbert and Gulliver (1895; Fig. 3B). Historical and modern photographs show stacked carbonate beds throughout the Tepee Buttes range (Gilbert and Gulliver, 1895; Darton, 1919; Close, 2006; Larson et al., 2013). The relatively horizontal orientation of the carbonate beds suggests that they formed parallel to the seafloor, not as dipping beds on the flank of a raised carbonate mound. Although some carbonate beds are not completely horizontal (Fig. 5), this most likely reflects alteration of original bedding morphology due to burial, compaction, and uplift in the area, related to burial and uplift in the Denver Basin (Higley and Cox, 2007). Modern lucinid accumulations in the Gulf

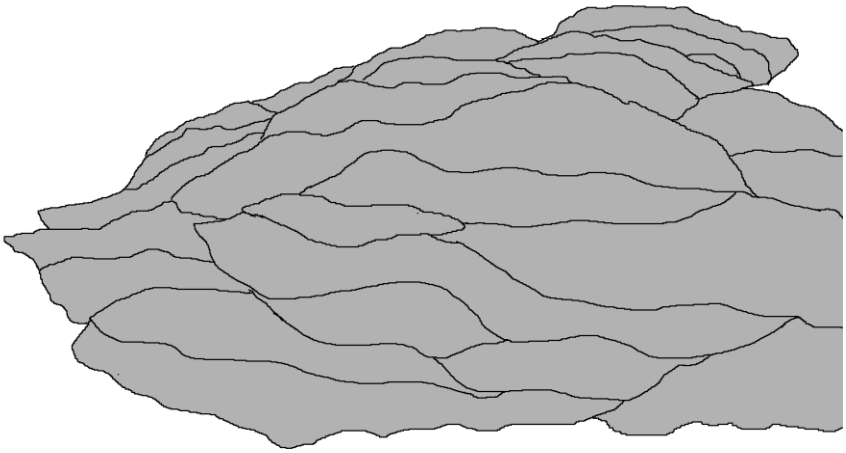

Figure 16: Stacked pancake model, modeled from mound at Southeast Hanna Ranch, pictured in Figure 5. Each carbonate bed rests haphazardly on underlying beds, with beds tapering on the sides.

of Mexico form thick (> 65 cm) lenticular or tabulate shell beds, with seep carbonate forming below the sediment water interface, and which outcrop when the surrounding sediment erodes (Callendar, 1992; Levin, 2005; Campbell, 2006). Similarly, pockmarks in the North Sea (believed to form due to expulsion of methane) reveal scattered lithified slabs and cemented layers below the surface of the seafloor (Hovland et al., 1987).

The formation of seep carbonate below the sediment water interface, coupled with the upward force of the methane and the addition of biomass and accumulation of shell material would have resulted in mounds that were at most a few meters in height. The modern high relief form of the Tepee Buttes results from the weathering and erosion of the surrounding Pierre Shale. In the relatively arid modern climate of eastern Colorado, the slowly weathering carbonate of the mound core remains emergent,

whereas carbonate beds at the edge have been reduced to rubble as the surrounding Pierre Shale erodes, resulting in ‘tepee-shaped’ mounds. Transport of weathered carbonate down the slopes of the mounds makes the mound base appear wider than the inner carbonate core.

The underlying carbonate beds may not form a precise vertical stack, as shown by Gilbert and Gulliver (1895; Fig. 2A). The methane vents of recent cold seeps in the Gulf of Mexico are short-lived, with old vents closing and new vents forming over ecological time scales (Hovland, 2002; Levin, 2005). However, because the delivery of methane in the Gulf of Mexico to the surface is controlled by faults, new vents and new beds of seep carbonate form near previous vents and carbonate beds (MacDonald et al., 1995; Sibuet and Olu, 1998; Levin, 2005; Kennicutt, 2017). Given this model of seep carbonate formation, beds of seep carbonate in the subsurface would form a ‘messy’ stack, in which succeeding carbonate beds overlapped, and did not form directly on top of one another (Fig. 16).

However, modern day cold seeps have a wide range of sizes and a wide variety of forms. In the modern Gulf of Mexico, mud mounds can be greater than 10 m in height and over 100 m wide, whereas other carbonate mounds are smaller, less than a few meters in height and 10 or so meters wide, and pockmarks may be small depressions or many meters deep and wide (MacDonald et al., 1995). Some Mediterranean mud volcanoes have decimeter scale carbonate crusts forming at the sediment water interface, which follow the contours of the mud volcano flanks and lack large organisms typical of modern cold seeps (Aloisi et al., 2002). In the Black Sea, methane seeps form globular

columns up to 4 m high and 1 m in diameter (Michaelis et al., 2002). These seep buildups, which resemble the chimneys at hydrothermal vents form from thick (10 cm) microbial mats that are internally supported by carbonate precipitates (Michaelis et al., 2002; Reitner et al., 2005). Modern seeps also tend to form at depths much greater than those generally associated with the Tepee Buttes or many other fossilized seeps (Callender and Powell, 1999; Kiel, 2010).

Carbonate Petrography and Stable Isotopes

The main carbonate constituents of the Tepee Buttes observed in this and previous studies are peloids, micrite, lucinid bivalve shells, vugs and carbonate cement (Howe, 1987; Kauffman et al., 1996; Bash et al., 2005; Anderson, 2006; Birgel et al., 2006; Krause et al., 2009). The paragenetic sequence paired with stable isotopic analysis shows two different phases of carbonate precipitation. Early carbonate formed below the sediment-water interface while the seep was active. Later diagenetic processes precipitated and altered seep carbonate within the subsurface after burial. Mounds across the study area show the same carbonate fabrics and similar organisms, suggesting formation under similar marine conditions (with the exception of the westernmost Florence mounds).

There is no evidence of vestimentiferan or serpulid tube worms at Tepee Buttes as reported by Kauffman et al. (1996), and the anastomosing ropey lithofacies is a weathering feature. These ridges do not appear to be tube worms, as they do not have critical morphological characteristics of worm tubes such as a preserved, mineralized wall structure or tube wall ornamentation, and they lack a uniformity in shape, size and

fill like that seen among the lucinids (Beauchamp and Savard, 1992; Hilário et al., 2011; Georgieva et al., 2019). Narrow tubule structures (2 – 10 mm) from the Tepee Buttes, originally interpreted as possible vestimentiferan worm tubes by Shapiro and Fricke (2002), were re-interpreted as 'tubes' preserving relict methane migration pathways (Krause et al., 2009). This study confirms these narrow tubes, rimmed in calcite and filled with calcite cement and fine-grained sediments, suggest the movement of fluids from lower in the subsurface. Similar interconnected methane pathways occur in the microbial mats in the modern Black Sea (Hovland, 2002; Levin, 2005; Konhauser, 2006). In the Gulf of Mexico, the permeability of the overlying sediment, faults or fractures influence the hydrocarbon flow pathways, while concretions, precipitates or biological organisms can block the flow of upwardly diffusing gas or liquid (Hovland, 2002; Levin, 2005). There is no evidence of stromatolites (i.e. layered carbonate produced in microbial mats) as described by Howe (1987) or Kauffman et al. (1996). Nonetheless, some small amorphous peloids (Fig. 7C; Fig. 8C) could be derived from the breakdown of microbial mats (rather than being fecal pellets), thus some of the carbonate could be considered microbialitic (Chafetz, 1986).

Ferroan Micrite Lithofacies

The ferroan micrite lithofacies presents a conundrum given its geochemistry and petrography. The oxygen stable isotopic values of ferroan micrite indicate formation near the surface in relatively cool water like other early carbonate fabrics, despite having more iron than later diagenetic, iron-rich fabrics. These later diagenetic fabrics have depleted $\delta^{18}O$ values (Fig. 15), whereas the $\delta^{18}O$ values of the ferroan micrite (average -

1.4‰) are only slightly enriched compared to the inoceramid values or non-ferroan peloidal carbonate, both of which are interpreted as early and are the closest values to marine DIC. Early diagenetic iron-rich calcite might suggest localized anoxia in sediments of the WIS; in oxygenated waters, the iron would quickly be oxidized and not preserved in the micrite.

Cross cutting relationships identify ferroan micrite as an intermediate lithofacies at the Florence mounds, cross cutting botryoids, peloids, and even other ferroan-rich micrite phases. In addition, it does not preserve the carbon isotopic signature of methane; instead, the $\delta^{13}C$ values are close to zero (average 3.2‰), which suggests precipitation from marine DIC. In contrast, the early carbonate from the Tepee Buttes have lower $\delta^{13}C$ values as a result from a mixing of carbon sources (marine DIC and AOM). The $\delta^{13}C$ values and high iron content of the ferroan micrite suggest the cessation of methane migration and pore-water anoxia during its precipitation.

I cautiously interpret the ferroan micrite as an early diagenetic event, happening in low temperatures relatively near the sediment-water interface (unlike the later diagenetic fabrics which have depleted $\delta^{18}O$ values, and may have formed deep in the subsurface). Preceding the formation of ferroan micrite, redox reactions occurring within the sediment resulted in a corrosive acidic zone at the base of the aerobic zone. This acidic zone produced patchy dissolution of "early" carbonate fabrics (i.e. peloids and botryoids). Iron freed in the iron reducing zone below provided the high iron content in the ferroan micrite, which filled the space created by this corrosion event. The positive (slightly enriched) $\delta^{13}C$ in an overall methanogenic system indicates carbonate formation

in the zone of methanogenesis, where the remaining pore fluid is enriched in ^{13}C due to the sequestration of light carbon in methane. This light carbon moved out of the system through methane venting. It should be noted that this entire process requires an oxic zone at the top of the sediment column, creating a calcium flux down into the sediment. As oxygen was progressively consumed in the sediment, the pH in the sediment would continue to decrease, until the sediment becomes acidic and prone to dissolution. The iron reducing zone would then supply the large amount of reduced iron (Fe^{2+}) in the ferroan micrite. This explanation requires a reduced or absent sulfate reduction zone within the vicinity of the ferroan micrite. In general, sulfate reduction coupled with reduced iron would result in pyrite formation, which is not seen at Florence. Pyrite formation would leave relatively small amounts of iron for the formation of ferroan micrite. The ferroan-rich micrite would be precipitated in or just above the methanogenesis zone, which again, would allow for the micrite to have a methanogenic, rather than a methanotrophic isotopic signature. The carbon came from a combination of: original bicarbonate dissolved in the acidic zone (that had a methane signature), marine DIC, and carbon that is enriched in ^{13}C due to the formation of methane.

The apparent lack of significant corrosional evidence at other Tepee Butte locations may indicate a reduced or absent oxic zone in the sediment, which would contribute to less corrosion and space for the precipitation of ferroan micrite. Additionally, other locations may have had a larger sulfate reducing zone in the sediment above the methanogenic zone, which could have consumed much of the free

iron. The presence of this lithofacies only in the Florence mounds suggests specific and unique environmental and geological conditions at these mounds.

Paragenetic Sequence for the Tepee Buttes in Southeastern Colorado

The paragenetic sequence is based on the dense lucinid lithofacies from the Boone mound; the other three main lithofacies (vuggy, brecciated, and anastomosing ropey) follow the same paragenetic sequence (Fig. 17). As the Pierre Shale was deposited, methane was expelled from the subsurface as the underlying sediment compacted (Whiticar, 1999; Hendricks et al., 2012). Early methane seepage would have facilitated large concentrations of chemosynthetic bacteria, i.e. methanotrophic, thioautotrophic and sulfate-reducing. These were free living, attached to the substrate in microbial mats, or symbionts within larger organisms like lucinids (Callendar, 1992; Sibuet and Olu, 1998; Levin, 2005). After the formation of a microbial mat, the area was colonized by larger organisms including lucinid bivalves, foraminifera, inoceramids, ammonites, gastropods, ostracods among others. Increased bicarbonate production in the subsurface through the anaerobic oxidation of methane (AOM) leads to the formation of seep carbonate.

Micrite (with and without peloids) appears to be the earliest carbonate fabric in the Tepee Buttes mounds. In all four common Tepee Butte lithofacies, peloids also occur surrounded by calcite. In this fabric, sparry calcite precipitates around peloids (or possibly replaces the micrite that originally surrounded the peloids). Micrite (with and without peloids) and peloids in calcite is the earliest fabrics based on the petrography and stable isotopes. However, these fabrics have a range of isotopic values along a

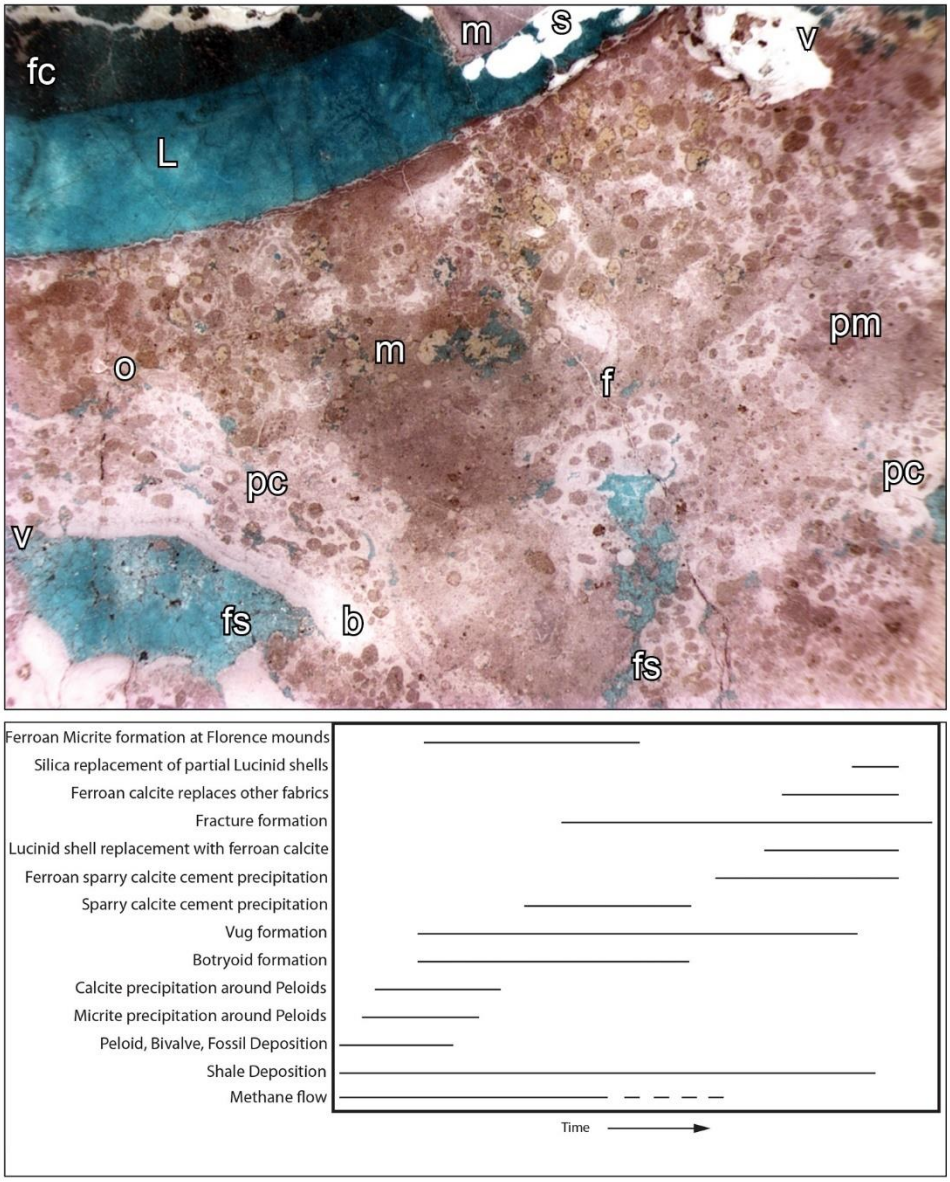

Figure 17: Paragenetic sequence for the Tepee Buttes mounds in Southeastern Colorado. Annotated paragenetic sequence on a stained peel of the dense lucinid lithofacies, with a relative time chart of the fabrics. m – micrite, o – organism (foraminifera), L – lucinid shell, pm – peloids in micrite, pc – peloids in calcite, b – botryoids, v – vug, fsc – ferroan sparry calcite, fc – ferroan calcite, f – fracture, s – silica.

diagenetic trend from extremely depleted $\delta^{13}C$ values coupled with marine $\delta^{18}O$ values, to less depleted $\delta^{13}C$ values coupled with $\delta^{18}O$ values indicative of early diagenesis (Fig. 15). This range in stable isotopic values suggests that micrite and both peloidal fabrics formed over a similar, extended period of time, and stable isotopes cannot distinguish which was the earliest carbonate fabric. Carbonate formation and increased organismal density also occur in modern seeps in the Gulf of Mexico (Levin, 2005). In these modern seeps, methane does not travel up one central vent; instead it takes multiple pathways, which move and shift through time (Hovland, 2002). These changing methane pathways may account for the stacked carbonate beds comprising the Tepee Buttes. The Tepee Butte seep carbonate formed below the sediment water interface and had low topographic relief during deposition.

Vug formation began within peloidal fabrics and lucinid body cavities relatively early in paragenesis while methane venting was still active and continued well past the cessation of methane seepage. Following vug formation, calcitic botryoids precipitated inside of vugs, around peloids, and inside articulated lucinid shells. Botryoids show a similar range of stable isotopic ratios as peloids in both micrite and calcite, suggesting formation over a similar, extended period. Deposition of the Pierre Shale continued throughout this interval, ultimately covering the mounds. During mound deposition as seep carbonate formed and experienced early diagenesis, the base of the mound would have undergone diagenetic processes associated with later parts of the paragenetic sequence. Eventually, methane seepage slowed or ceased, stopping mound growth.

After burial, subsequent generations of carbonate at the Tepee Butte mounds are ferroan (staining purple to blue), indicating diagenetic alteration of seep carbonate in anoxic or formational water. The earliest ferroan carbonate is ferroan sparry calcite that replaces lucinid shells and fills vugs and other voids. The stable isotopic values indicate formation from burial fluids (Fig. 15). Dolomite intermittently formed in the very interior of vugs but only occurs rarely. Fractures formed during burial and filled with various forms of calcite. Finally, silica replaced small patches of some lucinid shells.

Paragenetic sequence for ferroan micrite lithofacies from Florence, CO

In addition to the lithofacies at the Boone mound, the Florence mounds have a unique ferroan micrite (Fig. 13) that cuts across the early, methane-influenced fabrics (i.e. micrite, peloids in micrite, peloids in calcite and botryoids). Stable isotopic analyses reveal $\delta^{18}O$ values from -3.4‰ to -0.1‰ and $\delta^{13}C$ values from -4.7‰ to 5.3‰. These $\delta^{18}O$ values are indicative of carbonate formed from marine water (Fig. 15). However, the carbon values of this ferroan micrite indicate that methane was not a major contributor to its formation (ferroan micrite stable isotopic averages are $\delta^{18}O$ -1.4‰ and $\delta^{13}C$ 3.2‰). Based on petrographic characteristics, there are three different phases of ferroan micrite that cut across one another: dark blue micrite, light blue micrite, and gray-blue micrite. However, their isotopic values are indistinguishable. Ferroan micrite itself is cross-cut by the later fabrics, such as fractures filled with ferroan-rich sparry calcite.

This unique ferroan micrite suggests that the westernmost mounds at Florence, CO experienced different depositional or diagenetic conditions than other Tepee Buttes

mounds examined in this study. The ferroan micrite lithofacies follows the Boone paragenetic sequence for the early carbonate fabrics. However, the Florence mounds apparently experienced a large corrosion event that dissolved much of the original carbonate material deposited earlier in the paragenetic sequence (peloids in micrite, peloids in calcite and micrite), resulting in more dissolution than the Boone mounds. This event created a large amount of space for the precipitation of ferroan micrite. The iron in the ferroan micrite may have come from the overlying ferric reducing zone. The carbon in ferroan micrite predominately derives from marine DIC, since this is not a closed system, or a combination of methanogenic and methanotrophic carbon. The different ferroan micrite units apparently precipitated in close succession, with the different staining colors reflecting slightly different amounts of iron in the pore water. After the precipitation of the ferroan micrite, this lithofacies follows the Boone paragenetic sequence for later diagenetic fabrics.

Conclusions

The Tepee Buttes are one of the most extensive, long lived, and well-studied cold seep systems in the world. The stable isotopes of early carbonate confirm that these were formed through the anaerobic oxidation of methane. Mound lithofacies are not concentrically zoned around a central methane vent; instead, they are randomly distributed on the mound with gradational boundaries, similar to modern seeps in the Gulf of Mexico and off the coast of California. Different lithofacies correspond to the amount of methane that part of the mound was receiving. The five different lithofacies observed on the main Boone mound share the same paragenetic sequence. Seep

carbonate formed below the sediment-water interface, resulting in mounds that were low relief features, elevated less than a few meters above the seafloor. The mounds formed as stacking carbonate beds (< 75 cm) that interfinger with the surrounding Pierre Shale. Previous studies identified a tubeworm facies, equivalent to the anastomosing ropey lithofacies that preserves relict methane pathways rather than worm tubes. The ferroan micrite lithofacies, observed only on the westernmost mounds in Florence, is unique due to iron-rich micrite with original marine isotopic signatures. This lithofacies formed during early diagenesis due to a large corrosion event in the ferric sediment zone under unique environmental conditions that are absent at other locations.

CHAPTER III

TEMPORAL AND SPATIAL ISOTOPIC AND PETROGRAPHIC VARIATIONS IN SOUTHEASTERN COLORADO TEPEE BUTTES

Introduction

The Tepee Buttes are one of the longest lived and most extensive cold seep systems and were studied long before methane seeps were discovered (Fig. 18; Gilbert and Gulliver, 1895; Kauffman et al., 1996; Metz, 2010). They formed in the Late Cretaceous in the Western Interior Seaway (WIS) while the Sevier Orogeny was active to the west (Fig. 18D). The mounds stretch from the Black Hills region in South Dakota and Montana south into Colorado and New Mexico; and span four distinct episodes of formation (Metz, 2010) from the Middle Campanian (78.7 Ma) to the Early Maastrichtian (69.1 Ma).

Tepee mound formation has been discussed in depth, by Gilbert and Gulliver (1895) who suggested that the mounds formed as colonies of lucinid bivalves, while proposing the possibility that they formed as calcareous springs. In the 1980's, the Tepee Buttes became accepted as forming from submarine springs during the oxidation of methane (Arthur et al., 1982; Howe, 1987). Kauffman et al. (1996) proposed that the mounds originally formed high relief features, up to 5 m above the seafloor, as they ar seen today. This high relief model of mound formation was the generally accepted method of formation for many years. More recently, a number of workers have proposed

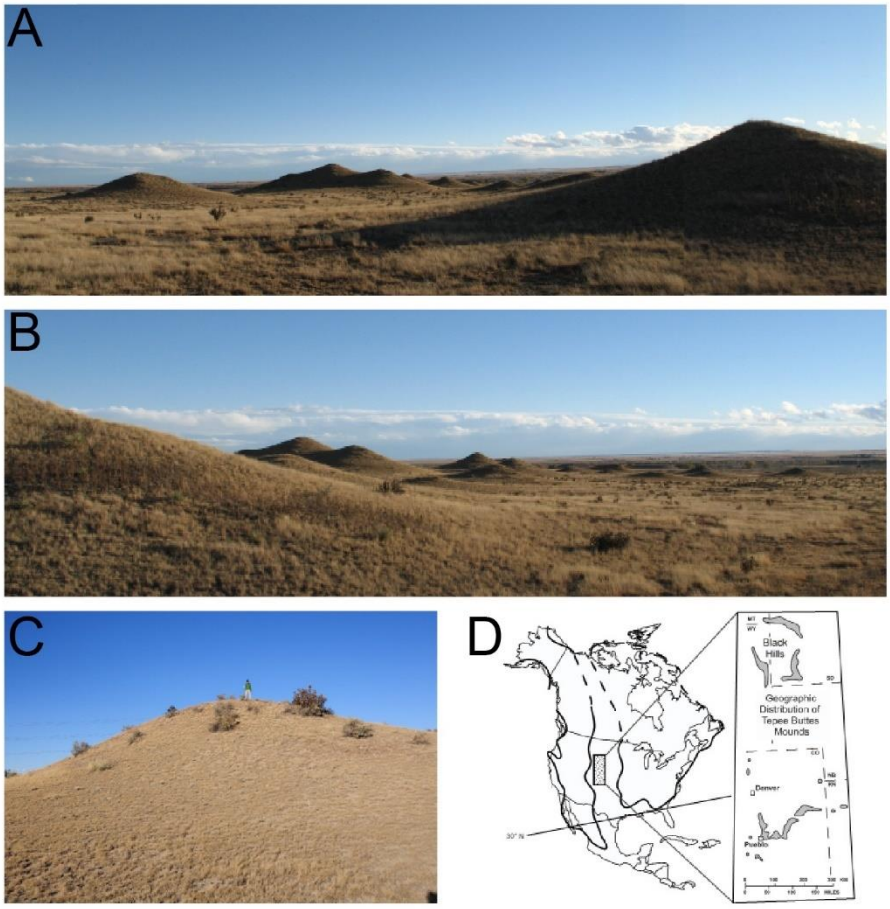

Figure 18: A&B) Photograph of the Tepee Buttes showing classic conical shape, Southeast Hanna Ranch; C) 1.5 m human for scale, JV Ranch; D) Reconstruction of Tepee Buttes in the Western Interior Seaway during the Late Cretaceous; reprinted from Metz (2010).

a low original relief model in which mound carbonate formed at or near the sediment water interface with little relief (Gaillard et al., 1992; Dahl et al., 2005; Anderson, 2006; Close, 2006; Metz, 2010; Hendricks et al., in review). In this scenario, differential weathering of the surrounding Pierre Shale relative to the resistant mound carbonate formed the high-relief structures recognized today as the Tepee Buttes.

Problem

Despite this longevity and geographic range of the Tepee Buttes, the seep system is generally discussed in broad terms without considering spatial and temporal trends in mound carbonate texture, lithofacies, and chemistry. This study seeks to investigate geographic and temporal variations in the Tepee Buttes mounds from southeastern CO by examining petrographic and geochemical differences in a wide range of mounds and locations.

The source of methane to the mounds was assumed to be constant through time (Birgel et al., 2006); however, this hypothesis was not tested by systematic investigation of the stable carbon isotopic variation of mound carbonate through time and space. In this study, stable isotopic geochemistry of early carbonate fabrics from the dense lucinid lithofacies is used (*Nymphalucina* coquina of Kauffman et al. (1996)) to examine whether the source of methane was constant through time, and whether it varied spatially or across the zone of mound formation. The dense lucinid lithofacies was chosen due to its abundance on the mounds studied and the abundance of early carbonate fabrics it preserves, which can preserve more of the original methane isotopic signature. Changes in the stable isotopic ratios of mound carbonate through time and space will help to identify the source of methane, whether there was a change in methane pathways through time, and if mounds experienced differences in post depositional diagenesis. This study will also determine the most likely source of the methane, and if there was a change in migration pathways through time. The westernmost mound in the study area, near Florence, CO, occurs adjacent to an oil field sourcing the Pierre Shale.

Documenting possible changes in the hydrocarbon source of the Tepee Buttes mounds over their 10 m.y. formation interval will contribute to the understanding of petroleum systems and hydrocarbon migration in ancient epeiric seas and at continental margins.

Methods

Twenty-eight mounds were sampled from six separate locations in southeastern CO near Colorado Springs, Pueblo and Florence in the Fall of 2010. The six locations are: Boone, I-25, Hanna Ranch (which includes southeast Hanna Ranch [SEHR]), JV Ranch, Florence, and Mosher (Fig. 4). GPS locations were used to establish accurate mound locations for use in Google Maps™ and to plot the location of the study mounds on the relevant maps showing ammonite biozones (Scott and Cobban, 1975, 1986; Sharps, 1976). These biozones are well established and allow for determination of the relative age of each of the 28 mounds. Mound locations spanned six ammonite biozones and approximately 3.5 million years (Fig. 19). These biozones were used to determine the oldest and youngest mound locations to compare temporal variations; they were also used to determine the locations farthest north, east, south, and west within the *Didymoceras nebrascense* biozone. The carbonate fabrics, lithofacies distributions in the mounds, and overall mound characteristics in the field are discussed in detail in Hendricks et al. (in review).

Cellulose acetate peels and thin sections were made from the dense lucinid lithofacies from all mound locations to examine petrographic differences between locations, focusing on comparing the oldest and youngest mounds, and the most

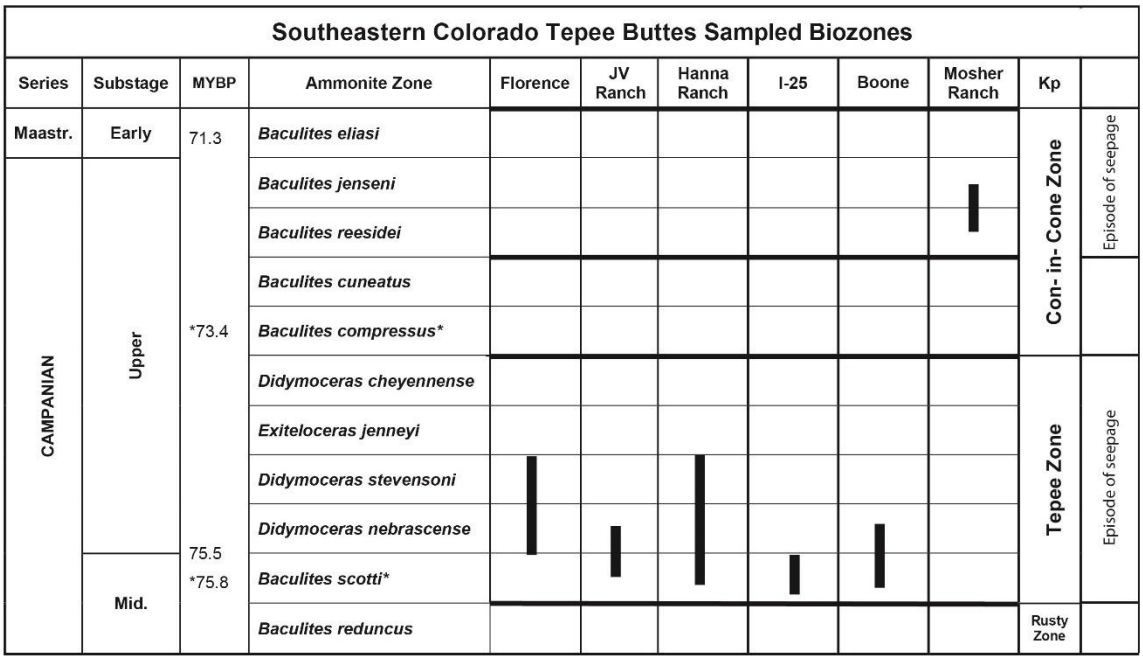

Figure 19: Age of the six locations based on well-established ammonite biozones (Scott and Cobban, 1975, 1986; Sharps, 1976), with the episodes of active seepage and mound formation.

northern, eastern, southern and western mounds in one biozone. Finally, at SEHR, the dense lucinid lithofacies was sampled along a closely spaced linear array of buttes. Samples were stained with alizarin red and potassium ferrocyanide to indicate the relative iron and magnesium contents of the carbonate fabrics (Table 1; Dickinson, 1965). A detailed petrographic description of the dense lucinid lithofacies at each mound location was recorded and used to assess differences in mound carbonate due to stratigraphic age and spatial distribution.

In order to compare the carbon and oxygen isotopic composition of mounds across a geographic and temporal gradient, samples of peloidal or micritic fabric, and botryoidal cements from the dense lucinid lithofacies of mounds from each location

were collected using a dental drill to ensure that each sample included only one carbonate fabric. Initial characterization carbon and oxygen stable isotopic analyses were determined at Texas A&M University's Stable Isotope Geoscience Facility using a Kiel IV Carbonate Device attached to a Thermo Scientific MAT253 isotope ratio mass spectrometer (IRMS). Additional samples were analyzed at the Peter Hooper GeoAnalytical Laboratory at Washington State University, using a Finnigan Delta S IRMS. Analytic results are reported versus VPDB using the NBS-19 standard. Precision values for Texas A&M University were ± 0.06‰ and ± 0.04‰ for $\delta^{18}O$ and $\delta^{13}C$ respectively; while Washington State University precision values were ± 0.02‰ and ± 0.05‰ for $\delta^{18}O$ and $\delta^{13}C$ respectively.

The Mann-Whitney U test was used to determine if there were significant differences among the carbon and oxygen isotopic ratios of mound carbonate based on age, the spatial distribution of mounds within a biozone, or along a line of mounds in one location. This is a non-parametric test for detecting differences in central tendency between two samples with small population sizes, in which variables are not normally distributed. P values of less than 0.05 were considered statistically significant.

Results

Stratigraphic and Spatial Distribution of Mound Locations

The oldest location sampled in this study is the I-25 mounds, located off the side of interstate I-25 southbound between mile markers 117 and 118, in the beginning of the *Baculites scotti* biozone (Fig. 20). The Boone mounds, Hanna Ranch mounds, and JV Ranch mounds also extend into this biozone, but not as far (Fig. 20). The youngest

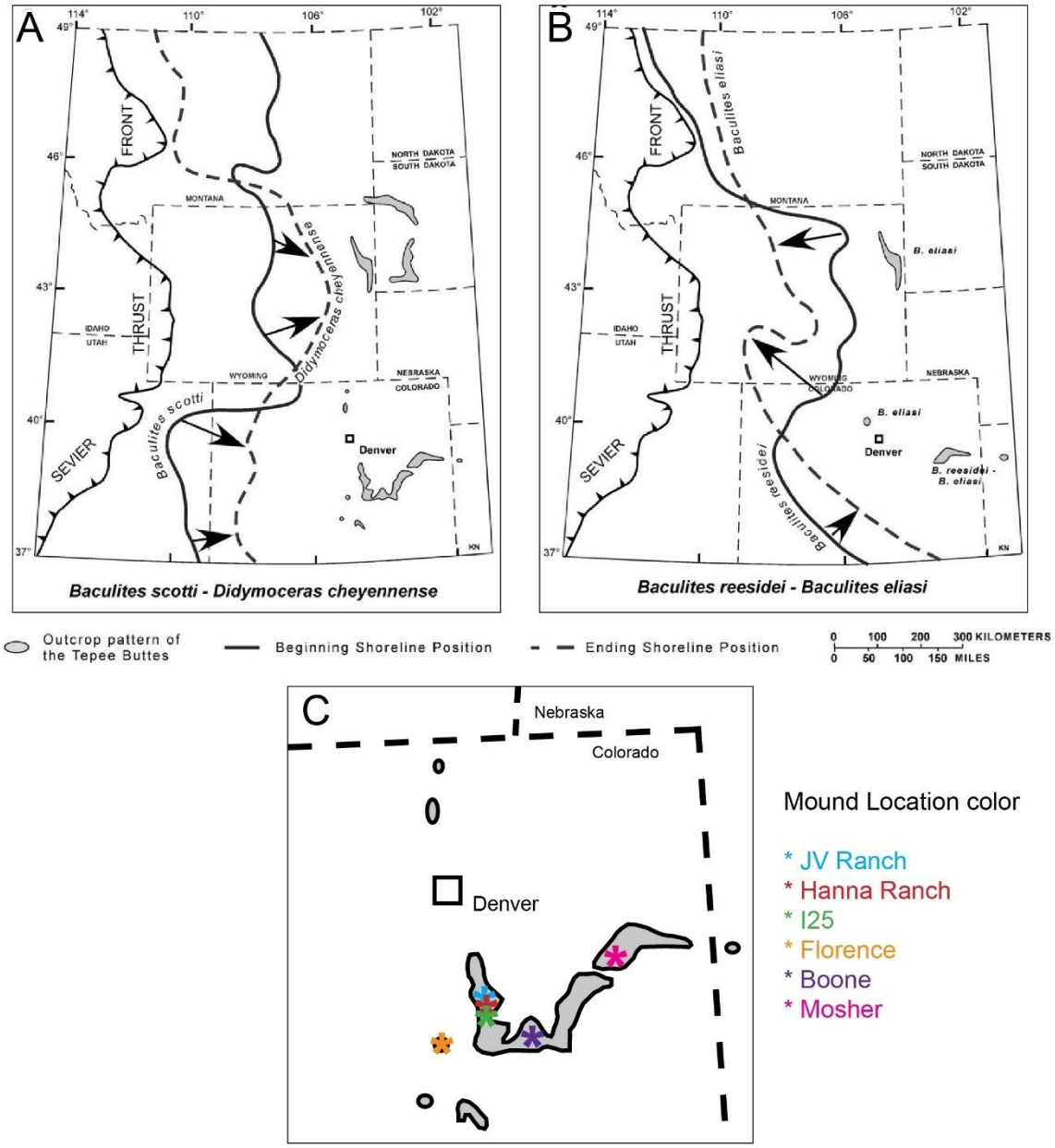

Figure 20: A&B) General paleoshoreline compilations for the two episodes of mound formation in this study; with permission from Metz (2010); C) Approximate mound locations are plotted in different colors (represented in the key) in a blown-up area of eastern Colorado; A) I-25, Boone, Hanna Ranch, JV Ranch, and Florence mound locations formed spanning biozones *Baculites scotti* through *Didymoceras cheyennense*; B) episode of mound formation spanning biozones *B. reesidei* through *B. eliasi*; Mosher formed from *B. reesidei* though *B. jenseni*.

mound location is the Mosher mounds, in the *B. reesidei* biozone. The Mosher mounds are also the farthest north and east of the mound locations studied (Fig. 20); however, they are not included in the study of geographic variation, because none of the other locations extend into this biozone (Fig. 20).

Within the *D. nebrascense* biozone, the JV Ranch mounds are the northernmost mounds, whereas Florence are the westernmost mounds, and Boone mounds are the southern and easternmost mounds studied. A linear array of closely spaced buttes at SEHR (also spanning the *D. nebrascense* biozone) was also studied to evaluate small scale temporal or spatial variations. This array had seven individual mounds and was around 800 m long and includes mounds from three biozones, beginning at the end of the *B. scotti* biozone through the beginning of *D. stevensoni* biozone. Hanna Ranch was 3.5 km south of the JV Ranch location. Linear arrays of mounds are thought to form along Cretaceous faults (Callendar, 1992; Kauffman et al., 1996; Metz, 2010). Despite their geographic and stratigraphic proximity, the buttes at JV Ranch and Hanna Ranch do not share a common lineation, suggesting that the mounds at these locations formed along different faults.

Locations varied in the abundance, size and clustering of mounds and also in the proportion of carbonate lithofacies present, and their general characteristics are summarized in Table 4. The I-25 location consists of two small carbonate build-ups, exposed in a road cut. These small mounds are not prominent features on the landscape, yet their presence suggests that there are many more mounds still buried within the Pierre Shale. Mounds at Boone and Hanna Ranch occur in multiple linear arrays,

Mound Location	Relative Age	Biozones	Geographic location	Rough # of mounds	Mound orientations	Mound preservation	Notable Lithofacies
I-25	Oldest	Baculites scotti		2	N/A	Well	Anastamosing ropey
Mosher	Youngest	Baculites reesidei		3	clustered	Poor	Brecciated; Anastamosing ropey
Boone		Baculites scotti - Didymoceras nebrascense	Eastern/ Southern	~100	linear arrays	Adequate	Dense Lucinid
Florence		Didymoceras nebrascense - Didymoceras stevenoni	Western	6	clustered	Adequate	Ferroan micrite
JV Ranch		Didymoceras nebrascense - Didymoceras stevenoni	Northern	8	linear arrays	Poor	Brecciated
Hanna Ranch		Baculites scotti - Didymoceras stevensoni	Line of buttes	100+	linear arrays	Well to Poor	Dense Lucinid

Table 4: Facies chart of the six different locations in this study, describing their relative age, biozones spanned, relative geographic location, approximate number of individual mounds and mound orientation, general mound preservation, notable prominent lithofacies, general petrographic characteristics, common mound organisms, other noteworthy features, and overall matrix texture.

Mound Location	Thin section characteristics	Common organisms	Other noteworthy features	Matrix
I-25	Heterogeneous matrix - abundant siliciclastic grains, pyrite is common	Lucinid bivalves; Radiolarians; Plant fragments - plants cells and wood fragments; Echinoid spines	Vertical cross section Bedding visible	Heterogeneous
Mosher	Fine-grained, homogeneous micrite in matrix	Lucinid bivalves; Plant spores or pollen; Sponge or Algal rods; Radiolarions; Foraminifera	Possible microbial striations	Homogeneous
Boone	Abundance of micrite, peloids	Lucinid bivalves; forams	Vertical cross section	Heterogeneous
Florence	Large quantities of iron; Fine grained matrix; abundant fractures	Lucinid bivalves; Sponge spicules	Ferroan micrite facies	Homogeneous
JV Ranch	Abundant amounts of cement (botryoidal cement and sparry calcite); fractures and microfaults	Lucinid bivalves; Pyrite replaced plant cells, forams, inoceramid fragments	Large amounts of cement, both botryoidal and sparry calcite cement	Heterogeneous
Hanna Ranch	Abundant carbonate nodules and cement, with minor amounts of microfaults	Lucinid bivalves; Ostracods and echinoid spines	Bedding visible; Compressed or elongated fossils Includes Southeast Hanna Ranch	Heterogeneous

Table 4 Continued.

whereas the JV Ranch mounds occur in a single linear array, consistent with mounds forming along fault lines. Mounds at the Mosher and Florence locations occurred in small clusters rather than linear features. Mound locations also differed in the degree of weathering, shale coverage and vegetation coverage. The clustered mounds of Florence and Mosher, along with the mounds at JV Ranch, tended to be vegetated and covered with shale and carbonate rubble (Fig. 21). The mounds at Hanna Ranch, Boone and I-25 had at least a few mounds with well exposed *in situ* carbonate beds. Differences in the distribution of mound lithofacies among the locations are discussed below.

Petrographic Results

Petrographically, mounds have many more similarities than differences. The mounds all had the same carbonate fabrics, generally the same organisms, and lithofacies; with the one exception of Florence, which is the only location with the ferroan micrite lithofacies. Nearly all thin sections of mound carbonate contain micrite, peloids, sparry calcite, and organisms to some degree.

Mounds at different locations had differing amounts of (1) clastics or sand-sized grains (both carbonate and siliciclastic); (2) pyrite, which affected the heterogeneity of the matrix and fabrics; (3) volumes of cement (both botryoidal and sparry cement); and (4) abundances and preservation of organisms, especially smaller microorganisms like forams, radiolarians, and plant matter. Mound locations also differed in the abundance of fractures or stylolites.

I-25 Mounds. As discussed above, the I-25 mounds, the oldest location studied, consist of two vertical carbonate buildups, around 5 m in height, with large amounts of

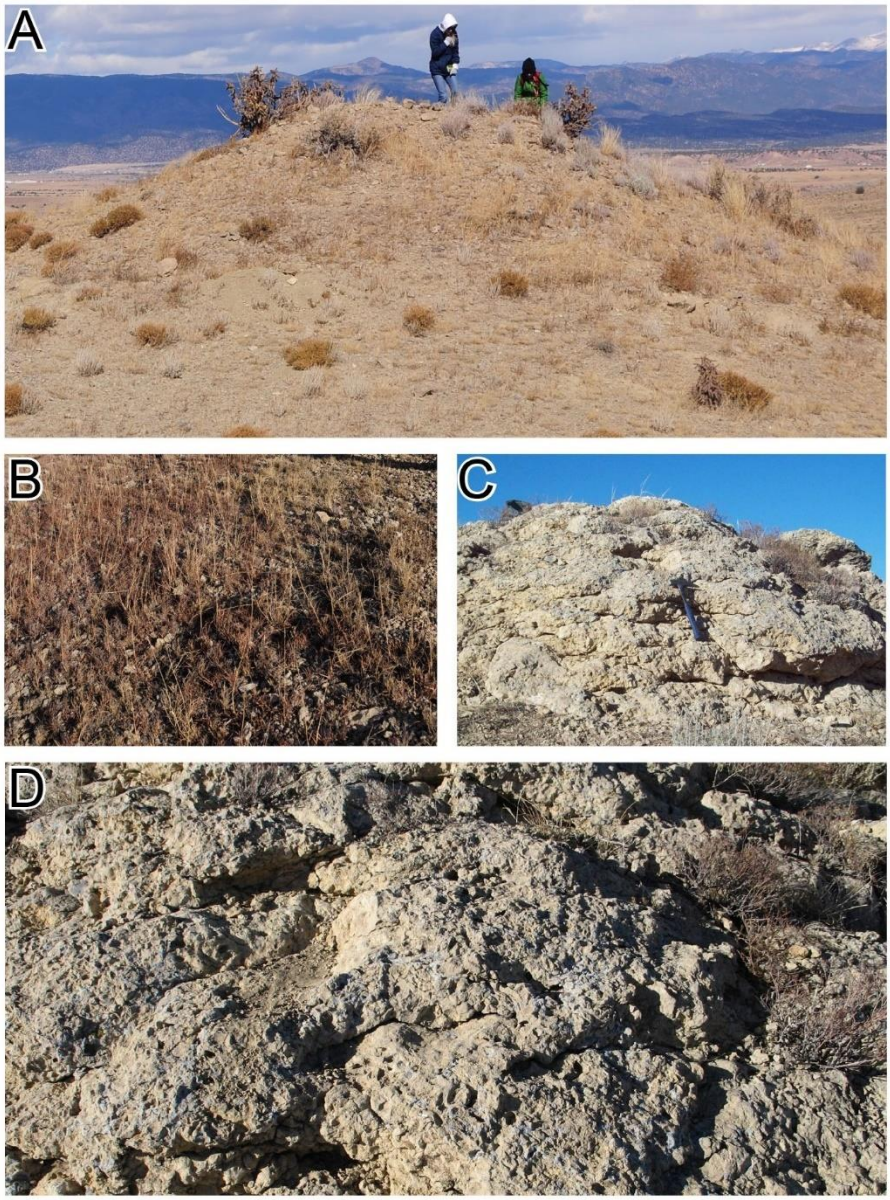

Figure 21: A) Typical outcrops of Tepee Butte mounds, with shale, carbonate rubble, and vegetation covering the sides, Florence; B) The top of one of the Mosher mounds, no *in situ* carbonate exposed; C) Stacked carbonate beds at SEHR3, the tapered lens shape of bed can be seen, hammer for scale; D) Stacked and tilted carbonate beds from Hanna Ranch, note the irregularity of the beds and their formation as stacked carbonate lenses.

carbonate rubble at the base and sides. The smallest mound location studied, the I-25 mounds occur on the side of interstate I-25 in a roadcut, which reveals a vertical section of the mounds rather than the typical conical tepee form which inspired the name the Tepee Buttes (Gilbert and Gulliver, 1895). No other mounds occur close to I-25. One of the carbonate buildups has carbonate beds up to 50 cm thick (Hendricks et al., in review). This mound location had an abundance of the anastomosing ropey lithofacies, which is not as common on other mounds. However, since I-25 is in a road cut, carbonate lithofacies that occur in the interior of mounds may be more exposed.

Thin section of mound carbonate from this location show a very heterogeneous matrix, which differentiates it from other locations (Fig. 22A,B). There are abundant quartz and carbonate sand grains in the matrix, as well as within peloids (Fig. 22A). Peloids are less numerous but still present, and often have less well-defined borders than seen in other mounds. Pyrite grains are common in the matrix, concentrated along fractures, and within vugs (Fig. 22B). Organisms include forams (large and small), lucinid shells and inoceramid shell fragments, small spines (potentially sponge or echinoid), and plant organics including wood fragments and algal or plant cells (Fig. 22A). Some of these organics, as well as poorly preserved radiolarians, were replaced by pyrite, giving them a dark brown color.

Mosher mounds. The Mosher mounds are over three million years younger than the I-25 mounds and contain the youngest buttes in this study. This location has three isolated mounds approximately 250 m apart, with no other buttes visible in the area. This mound location also has a greater amount of the brecciated lithofacies as compared to

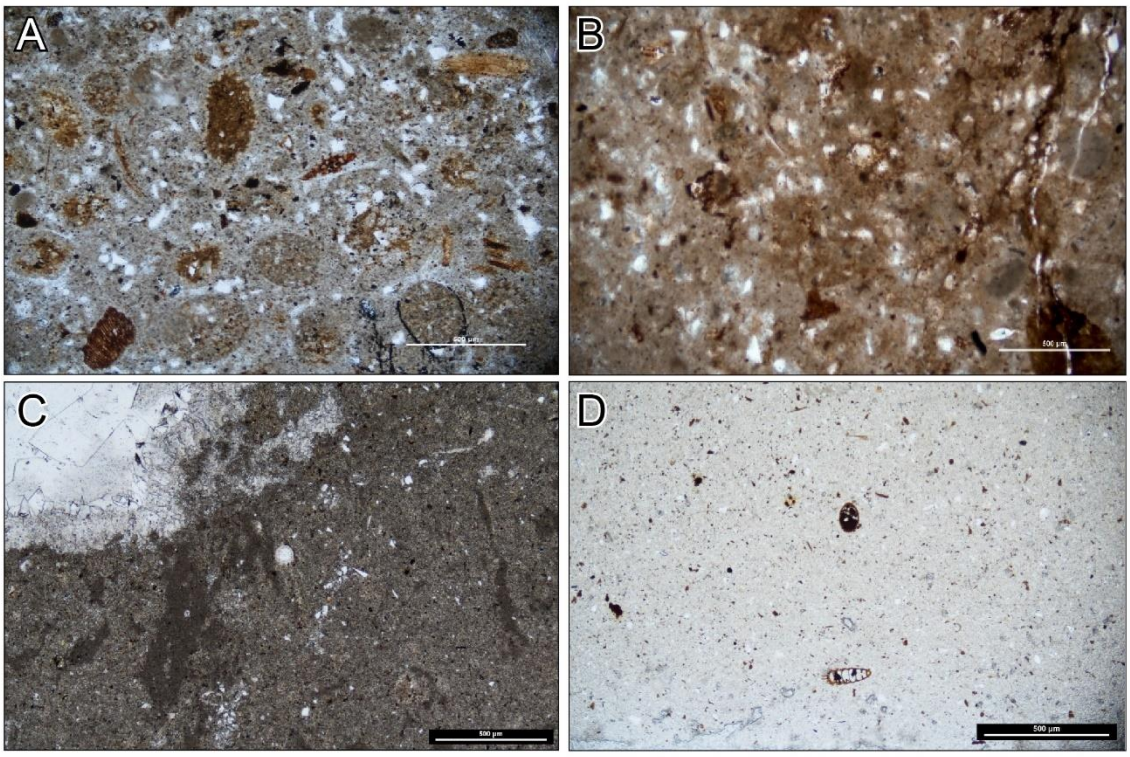

Figure 22: A) I-25: peloidal and micritic fabric with sand sized siliciclastic grains, pyrite, plant and wood fragments showing the heterogeneous nature of this location; B) I-25: micritic and peloidal fabrics displaying heterogeneous nature of this location, with abundant sand sized siliciclastic grains, mottled texture and a stylolite on the right side. C) Mosher: homogenous micrite matrix with striped microbial texture, a sparry calcite filled vug in the upper right and echinoid fossil in the center. D) Mosher: very homogeneous micrite, with two well preserved radiolarians, and various pyritized microfossil fragments. Scale bar is 500 μm.

the other locations, while the ropey anastomosing lithofacies is common. In the field, either sponge or algal rods were visible, while lucinids were less abundant and less densely packed than other locations.

Overall, the carbonate at Mosher is finer grained than at other mound locations (Fig. 22C). The matrix was predominately micrite, yet still had abundant peloids. This results in a more homogeneous texture despite the presence of siliciclastic grains and

fossils in the matrix. One of the samples exhibits a texture that looks similar to microbial laminations (Fig. 22C). Pyrite occurs throughout the matrix, concentrated along fractures, and within vugs, including void spaces of fossils (e.g. radiolarians; Fig. 22D).

Thin sections of Mosher carbonate display a large number of microfossils: forams, ostracod shells, inoceramid shell fragments, plant fossils, and radiolarians (Fig. 22C,D). Some fossils from Mosher are incredibly well-preserved, like radiolarians, a lucinid shell that retains its original shell microstructure (not seen in any other locations), and possible land-plant spores and pollen. Some of the microfossils, especially radiolarians were replaced with pyrite. Yet there is also an interesting dichotomy because in addition to the very well-preserved organisms, a large number of heavily recrystallized forams and shells also occur at Mosher.

Florence mounds. The Florence location is the westernmost in both the study area, and in the *D. nebrascense* biozone. These mounds are located next to the longest continually producing oil field in the United States (Florence Oil Field), which has been operating since 1862 (Higley et al., 1995; Higley and Cox, 2007). This location has six mounds along the road, clustered into two groupings with three mounds each; only the southern grouping was studied. In the field, iron staining was abundant on some of the carbonate and interbedded shale, which was rare at other locations.

Florence is the only studied location that had the ferroan micrite lithofacies, an iron-rich micrite that contained little else (Fig. 23). The paragenetic sequence of the ferroan micrite lithofacies indicates three separate generations of ferroan micrite distinguished by increasing amounts of heterogeneity, different stain colors of blue

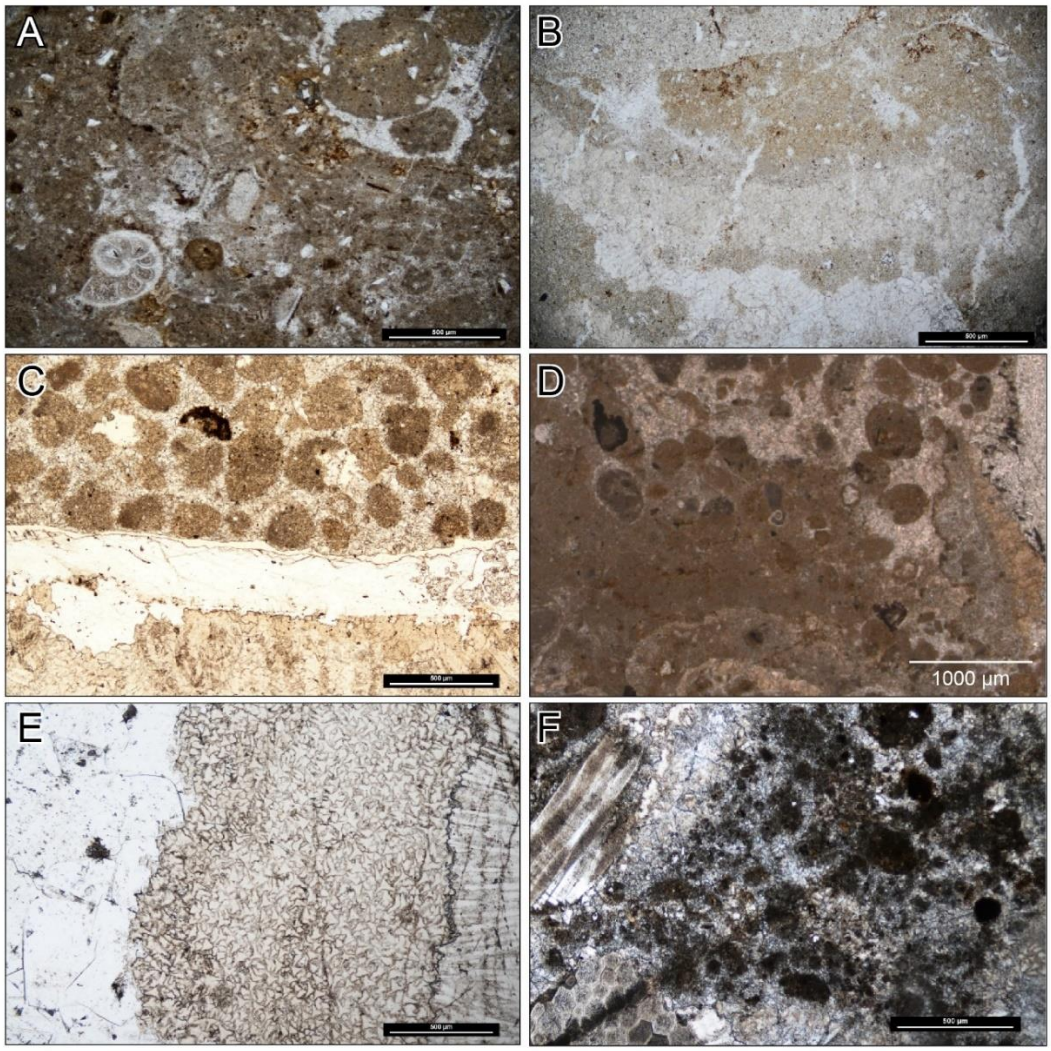

Figure 23: A) Florence: dense lucinid lithofacies showing peloids, dispersed siliciclastic grains, minor sponge spicules, an exceptionally well preserved foram and minor pyrite (possible siderite). B) Florence: ferroan micrite lithofacies; showing the three generations of ferroan rich micrite. Sparry calcite cement filling voids and minor pyrite also present. Significantly less siliciclastic sand sized grains present. C) Boone: dense lucinid lithofacies; peloids in calcite filling the interior of the replaced lucinid shell. Botryoidal cements have formed along the outside of the shell. D) Boone: peloids in micrite and peloids in calcite; stylolite on the right side along the recrystallized lucinid shell. Pyrite is concentrated along both the left and ride sides along the edges of voids E) JV Ranch: large amounts of cement typical of this location, with large sparry calcite crystals on the left, triangular botryoid terminations in the center, and fan like botryoidal crystals on the right. F) JV Ranch: Inoceramid fragments on the left with peloids in calcite. Pyrite within the peloids. Dark diagonal line across the thin section is a flaw of the manufacturing process. Scale bar A,B,C,E,F is 500 µm; scale bar D is 1000 µm.

(from grey-blue, to bright blue, to light-blue) indicating increasing amounts of iron, as well as cross-cutting relations (Fig. 23B). Hendricks et al. (in review) detailed the ferroan micrite lithofacies, identifying it as an early diagenetic lithofacies.

The Florence mounds preserve a large range of organisms: lucinids, forams (Fig. 23A), echinoid spines, sponge spicules, inoceramid shell fragments, and minor numbers of ostracods and microfossils (e.g. radiolarians). These organisms occur in the Florence mounds, but in fewer numbers than at other mounds. As at the Mosher location, fossils in the Florence location exhibit a range of preservation states, from well preserved to diagenetically altered. Both Mosher and Florence have a finer grained matrix than other mounds locations. At Florence, fossil preservation seems to be tied to the ferroan micrite lithofacies. The formation of ferroan micrite destroyed original fabrics and fossils through dissolution and reprecipitation, whereas other portions of Florence mounds have incredibly well-preserved carbonate. Peloids are less common in the ferroan micrite lithofacies but are present in the other lithofacies on Florence. There is less botryoidal cement in these mounds, and most of the cement was sparry calcite. There are abundant fractures at this location, both large and small, cemented and open (Fig. 23B).

Boone Mounds. Mounds at the Boone location are very abundant and occur in linear arrays that began forming in the *B. scotti* biozone and continued into the *D. nebrascense* biozone (Fig. 19). This location is the farthest east and south in the *D. nebrascense* biozone and includes the most widely studied Tepee Butte mound most likely due to its accessibility and its location on a county road (Fig 20; Howe, 1987; Callendar, 1992; Kauffman et al., 1996; Anderson, 2006; Close, 2006; Krause et al.,

2009; Metz, 2010; Hendricks et al., in review). One of the mounds was cut by the road, exposing the center and flanks. However, the Boone mound was heavily geo-eroded (i.e., sampled by geologists and fossil hunters; Fig. 24), slowly destroying and potentially masking the true nature of the mound. A number of contributions discussed the petrography of the mounds (Howe, 1987; Callendar, 1992; Kauffman et al., 1996; Anderson, 2006; Close, 2006; Krause et al., 2009; Hendricks et al., in review).

The Boone mounds have a large amount of micrite, as well as peloids surrounded by both micrite and calcite (Fig. 23C,D). Botryoidal cement and sparry calcite cement occur commonly, infilling vugs and organisms. Pyrite occurs commonly at the Boone mounds, mostly concentrated along fractures, voids (including interiors of organisms) and as stylolites (Fig. 23C). Organisms include lucinids, ostracods, echinoid spines, forams, and a small number of radiolarians. Dolomite occurs sporadically, in the interior of vugs, formed after the ferroan sparry calcite.

JV Ranch Mounds. The JV Ranch location is the farthest north in the *D. nebrascense* biozone (Fig. 19), and mounds occur in a singular linear array of seven mounds, two of which have smaller satellite mounds. JV Ranch mounds are fairly tall, between 4 – 6 m in height, and they contain abundant cement. The dense lucinid and vuggy lithofacies dominate these mounds; however, the brecciated lithofacies was more common at these mounds than other locations. Mounds here often are heavily weathered with a large amount of shale and carbonate scree on the sides and even tops and covered in vegetation.

Figure 24: Photographs of "geo-erosion" of the Boone mound from 1961, 2001 and 2005. Since this mound has been so extensively published about and is so easily accessible, as well as it is a road cut mound resulting in more mound carbonate on display, geologists assisted in the erosion of this mound, significantly faster than natural erosional processes. Slight carbonate bedding planes can be seen in both the 2001 and 2005 photos. Photos courtesy of Cheryl Metz.

Botryoidal cement (commonly formed through multiple generations) is much more abundant than at other mound locations (Fig. 23E). Sparry calcite is similarly abundant, and the crystals can be very large (Fig. 23E). Many of the peloids are surrounded by botryoids or sparry calcite. Peloids in micrite are still common in this location, but often do not have well defined edges as seen at Boone. Brecciation can be seen within the sparry calcite cement, and even peloids can be observed with small fractures through them. Pyrite occurs frequently scattered throughout the matrix but also can occur concentrated along corrosion lines. Organisms include: lucinid shells, inoceramid shell fragments, forams, and plant fragments with cells replaced by pyrite.

Hanna Ranch Mounds. The Hanna Ranch location is approximately three and a half km southeast of the JV Ranch mounds and seven km north of the I-25 mounds. Mounds at this location, which include SEHR, span the entire *D. nebrascense* biozone and almost two additional biozones (Fig. 19). Mounds at this location are incredibly numerous, numbering over 100 mounds along relatively linear rows, though there are some mounds in clusters. Some Hanna Ranch mounds are relatively weathered with vegetation growing over much of the mound, whereas others expose *in situ* stacked carbonate beds visible on the sides and tops of mounds.

The proportion of carbonate fabrics and lithofacies varied greatly between the mounds at this location (Fig. 25). Hanna Ranch mounds have abundant carbonate nodules. Mounds at both SEHR and Hanna Ranch had abundant sparry calcite and

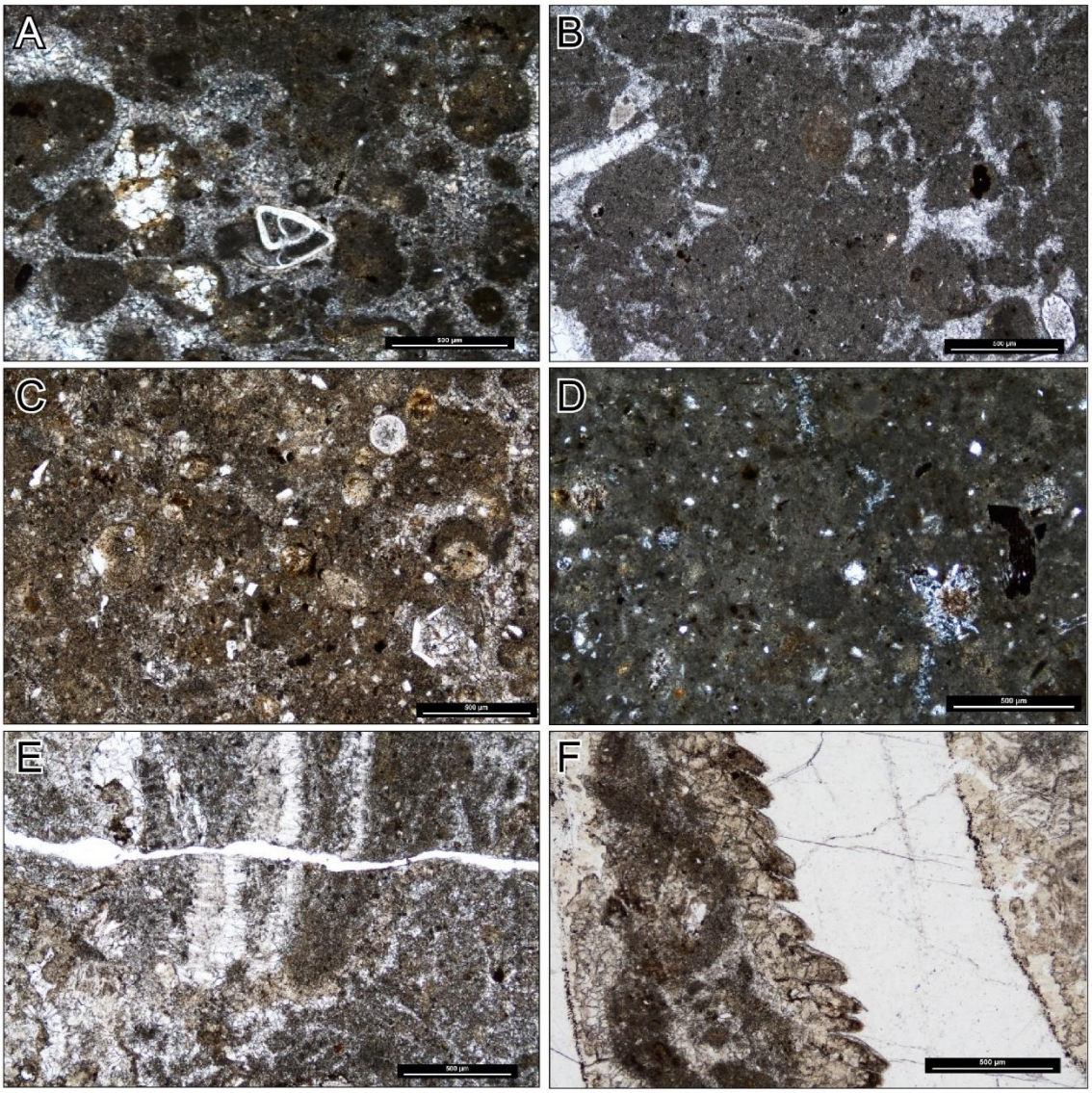

Figure 25: A) Hanna Ranch: Peloids in calcite and micrite with a well preserved foram; B) SEHR2: Homogeneous micrite, peloids, and sparry calcite cement; Compressed echinoid and other organism visible; C) SEHR4: Heterogeneous matrix with abundant siliciclastic grains, pyrite, and organisms (plant and foram fossils); D) SEHR5: Heterogeneous micrite with pyritized wood cells and poorly preserved organisms; E) SEHR7: Micro-fault of botryoidal cements and sparry calcite; F) SEHR6: Lucinid shell overgrowth, with micrite, botryoidal and calcite cement. Scale bar is 500 μm.

botryoidal cement, and both contain a large number of ostracods and echinoid fossils, which differentiates them from other mound locations (Fig 25B,C). Some mounds at Hanna Ranch and SEHR2 contain compressed or elongated microfossils, such as forams or echinoid spines, not seen at any other mound location (Fig. 25).

Seven mounds were examined from a linear array (around 800 m long) in a small geographic area at SEHR (Fig. 25). This array began forming at the end of the *B. scotti* biozone, through *D. nebrascense*, to the early *D. stevensoni* biozone, with SEHR2 forming first, and SEHR6 forming last based on their location in respect to ammonite biozone boundaries (Scott and Cobban, 1986). These mounds did not display a linear trend or pattern petrographically. SEHR2 had a homogeneous matrix with few clastics or sand sized grains in the matrix, and pyrite occurs concentrated along vugs and in voids. SEHR2 contained compressed fossils, in addition to well preserved fossils (Fig 25B). SEHR4 had a heterogeneous matrix, with a larger amount of siliciclastic sediment, large numbers of fractures and diverse and abundant fossil fauna (Fig. 25C). SEHR5 had similar fabrics to SEHR4. SEHR6 had more clastic sediment and more heterogeneity than SEHR2 but was more homogeneous than SEHR4. Both SEHR6 and SEHR7 had more fractures than previous mounds, and microfaults exhibit minor amounts of displacement (Fig. 25E).

Stable Isotopic Results

The locations examined have a range of stable isotopic values (Table 5), with $\delta^{13}C$ ranging from -45.1‰ to -26.7‰ with an average of -38.3‰, while the $\delta^{18}O$ ranged from -8.2‰ to -0.9‰ with an average of -2.8‰. Mosher had the lowest average $\delta^{13}C$ of

Location	Avg $\delta^{13}C$ ‰	Min $\delta^{13}C$ ‰	Max $\delta^{13}C$ ‰	Avg $\delta^{18}O$ ‰	Min $\delta^{18}O$ ‰	Max $\delta^{18}O$ ‰
I-25	-43.0	-48.0	-34.5	-1.2	-2.2	0.0
Mosher	-38.3	-49.5	-20.8	-6.4	-10.1	-3.4
Boone	-42.2	-46.5	-34.8	-1.8	-4.4	-0.1
Florence	-38.3	-45.1	-26.7	-2.8	-8.2	-0.9
JV Ranch	-37.7	-46.9	-19.4	-6.2	-9.9	-3.7
SEHR2	-34.1	-41.9	-25.4	-8.7	-10.6	-6.3
SEHR4	-32.7	-41.4	-28.9	-7.7	-10.7	-3.5
SEHR6	-40.7	-48.3	-37.4	-7.7	-10.2	-3.4

Table 5: Average carbon and oxygen stable isotopes for each location, with minimum and maximum values from all locations, reported VPDB.

-43.0‰, whereas SEHR4 had the highest average $\delta^{13}C$ of -32.7‰, though still a very low value (Fig. 26; Table 5). Mosher also had the highest average $\delta^{18}O$ of -1.2‰, whereas SEHR2 had the lowest average $\delta^{18}O$ of -8.7‰. Mosher, Boone, and Florence had the least negative $\delta^{18}O$ values. SEHR2 and SEHR6 have statistically different $\delta^{13}C$

Locations	$\delta^{13}C$ P1	Significant	$\delta^{18}O$ P1	Significant
Mosher vs I-25	0.2578	N	<0.0001	Y
Boone vs Florence	0.1867	N	0.0838	N
Boone vs JV Ranch	0.0643	N	0.0002	Y
Florence vs JV Ranch	0.5	N	0.0033	Y
SEHR2 vs SEHR4	0.3859	N	0.1922	N
SEHR2 vs SEHR6	0.0367	Y	0.1251	N
SEHR4 vs SEHR6	0.0047	Y	0.4761	N
Boone vs I-25	0.166	N	0.2946	N
I-25 vs Florence	0.0749	N	0.0179	Y

Table 6: Isotope Statistics using a Mann-Whitney U test to compare mound locations, with the outlier at JV Ranch removed.

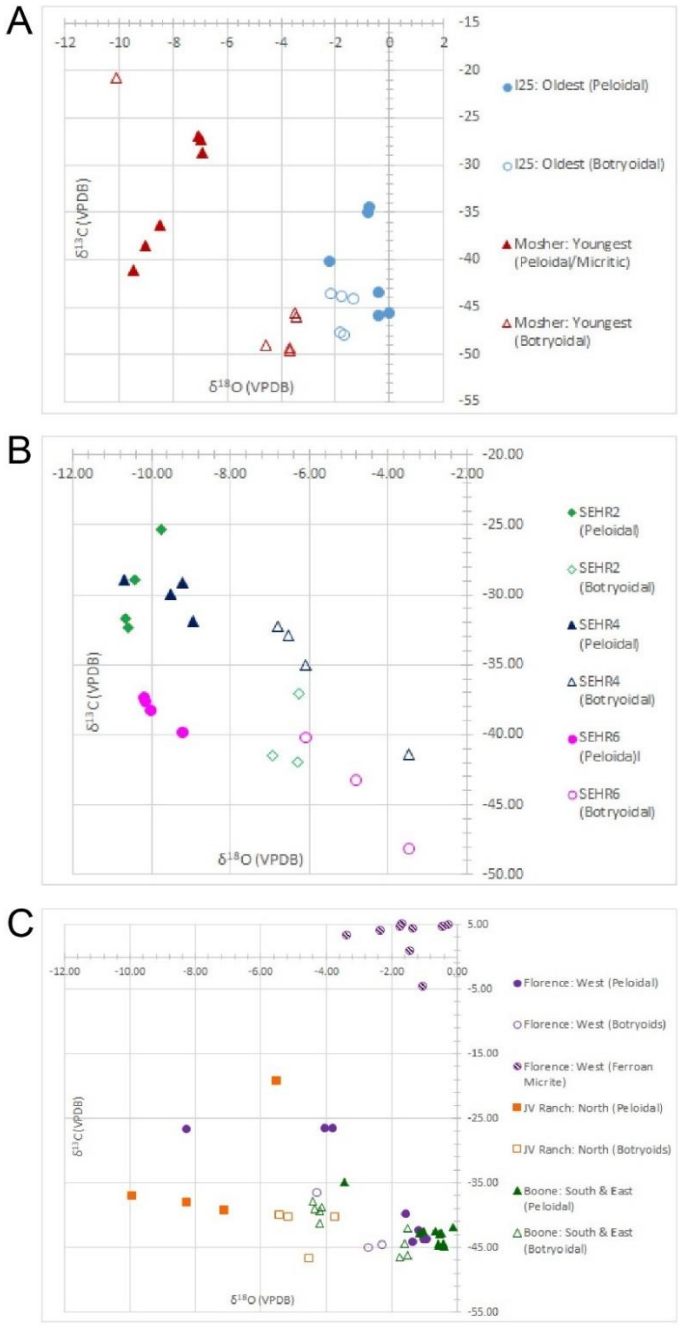

Figure 26: Carbon and oxygen stable isotopic values of mound carbonates from different locations in this study, A) Temporal variations: Oldest mound location I-25 compared to the youngest mound location Mosher; B) Southeast Hanna Ranch isotopes, SEHR2 is the oldest and westernmost mound, and SEHR6 is the youngest and easternmost mound; C) Spatial variations of the *Didymoceras nebrascense* biozone: Boone is the most southern and eastern mound location, JV Ranch is the northernmost mound location, and Florence is the westernmost mound location.

values, with a P value of 0.04 (Table 6). SEHR4 and SEHR6 have statistically different $\delta^{13}C$ values, with a P value of 0.005. There is no discernable pattern to the linear array of mounds tested at SEHR, however SEHR6, the oldest mound at this location, has lower $\delta^{13}C$ values than both SEHR2 and SEHR4 (Fig. 26B).

Florence and JV Ranch have statistically different $\delta^{18}O$ values, with a P value of 0.002, with Florence having much less negative $\delta^{18}O$ values than JV Ranch (Table 6). Boone and JV Ranch both have statistically different $\delta^{13}C$ values and $\delta^{18}O$ values, with P values of 0.03 and 0.0001, respectively. There is not much overlap between Boone and JV Ranch $\delta^{18}O$ values, whereas Boone has lower $\delta^{13}C$ values (Fig. 26C). However, there is one data point at JV Ranch that has much less ^{13}C-depleted carbon, which may contribute to the $\delta^{13}C$ value being statistically different (Table 6).

Discussion

Temporal and Spatial Variation in Petrography

The Tepee Buttes investigated in this study span two different episodes of mound formation, from the *B. scotti* biozone to the *B. jenseni* biozone and cover an area of approximately 6,500 km^2 (Fig. 4, 19; Metz, 2010). Compiled paleoshoreline data show that mounds formed at different distances from the shoreline, and likely at different depths (Fig. 19; Howe, 1987; Kauffman et al., 1996; Metz, 2010; van Cappelle et al., 2018). The mounds share more similarities than differences. All of the mounds investigated share the same carbonate fabrics and lithofacies (with the exception of Florence which had the ferroan micrite lithofacies, and the ferroan micrite fabric).

Mounds differ in the proportion of each lithofacies, and the percentage of larger grains and siliciclastic sediment, resulting in more heterogeneous or homogeneous fabrics (Figs. 22, 24, 25). The abundance of large grains and clastic sediments may reflect proximity to the paleoshoreline, shoreline migration and paleocurrents. Paleoshorelines for the four intervals of mound formation were compiled, and this study includes mounds from two of these intervals (Fig. 19, 20; Metz, 2010).

The mounds formed on the forebulge of the Sevier orogeny, regardless of which interval or biozone they formed in (Metz, 2010). Episodes of butte formation correspond to times of maximum transgression, and end at times of regression (Kauffman et al., 1996; Metz, 2010). Sediment loading in the foredeep proximal to the thrust belt, which increased flexure on the forebulge, appears to drive mound formation (Metz, 2010). Increased flexure generated pathways of methane migration, often allowing pre-existing faults to open. Mounds often form in linear arrays, parallel or adjacent to Laramide faults; however, not all locations have linear arrays, and some mounds arrays formed perpendicular to Laramide faults (Gilbert and Gulliver, 1895; Callendar, 1992; Kauffman et al., 1996; Birgel et al., 2006; Metz, 2010). The locations with the largest number of buttes, Boone and Hanna Ranch, do have linear arrays of mounds (Table 4).

A peninsula northwest of this study's sites at the beginning of the *B. scotti* biozone is suggested by paleoshoreline reconstructions (Fig. 20; Metz, 2010; van Cappelle et al., 2018). The oldest mound location in this study, I-25 began forming at the beginning of this biozone, whereas Boone, Hanna Ranch and JV Ranch all began to form during the middle of this biozone; Florence began formation at the end of the *B.*

scotti biozone (Fig. 19). This peninsula, which was approximately 300 km northwest of this study area, could be the source of the majority of the siliciclastic grains and wood fragments at I-25. Paleocurrents moving southward and westward would have brought siliciclastic grains to the forming mounds, despite the shoreline positioned approximately 400 km or more directly west (Parrish et al., 1984; Wright, 1987; Metz, 2010; van Cappelle et al., 2018). Though the Boone mounds were only 50 km away from I-25, they contain less siliciclastic sediment. Small-scale changes in topography, currents, and sediment influx among other factors, could have resulted in the different carbonate fabrics. Mounds that had more elevation would have disrupted small scale currents to accumulate larger size particles like microfossils and siliciclastic sand grains. Progradation of the shoreline into the basin during the Late Campanian, and a south-southeast longshore drift would have brought larger grains and wood to the Buttes (van Cappelle et al., 2018).

Throughout the episodes of mound formation, the shoreline to the west was predominately prograding into the basin (Fig. 20). The prograding shoreline could have brought more siliciclastic grains further into the basin, and thus produce more heterogeneous fabrics in later mounds (e.g. Florence and Hanna Ranch). This was not the case in the linear array of mounds examined at SEHR. Mounds at this location spanned the longest amount of time, almost three entire biozones from *B. scotti* to the end of *D. jenneyi* (Fig. 19). These mounds had a wide range of morphologies and fabrics, and different proportions of lithofacies. A trend of petrographic and isotopic changes along the line of buttes was expected; however, no definitive patterns in

petrographical differences or petrographic gradients in this linear array were observed. The abundance of siliciclastic grains and matrix heterogeneity increased from SEHR2 through SEHR4 and SEHR5, and then decreased slightly through SEHR6 and SEHR7 (Fig. 25). Changes in the delivery of siliciclastic grains to these mounds could result from changes in paleocurrents, shoreline migration and clastic delivery (Parrish et al., 1984). Based on the shoreline reconstruction, during the *B. scotti* through *D. cheyennense* time interval, the shoreline generally prograded, while the northwestern peninsula previously discussed regressed, suggesting a reorganization of siliciclastic delivery pathways (Fig. 20A; Metz, 2010; van Cappelle et al., 2018).

Although, lithofacies percentages differed between mounds with the exception of Florence and its ferroan micrite lithofacies, all locations had the same lithofacies. The dense lucinid and vuggy lithofacies dominated all of the mounds. However, mound preservation likely played a part in the lithofacies distribution. Lithofacies were more difficult to map at locations like Mosher and JV Ranch, where mounds were extensively covered in vegetation, shale and carbonate rubble (Fig. 21); though, all locations had some covered intervals. The mounds with the most *in* situ seep carbonate exposed occurred at road cuts (I-25 and Boone). Mounds at Hanna Ranch (and SEHR) also had significant amounts of *in situ* carbonate exposed. At all three locations, mounds exhbited sets of stacked carbonate beds, usually less than 50 cm thick, relatively horizontal, and often tapered at the edges to form carbonate lenses. However, most Tepee Buttes mounds are surrounded by so much shale and rubble, and have been buried and exposed, that well-defined carbonate beds may not be visible.

The Tepee Buttes have a unique diagenetic system due to extensive cementation at shallow depths. One Mosher mound has very fine-grained potential microbialitic striations, indicative of the bacterial mat that formed around the seep (Fig. 22C). Rapid cementation allows for extremely well-preserved organisms; in contrast, at some mounds other fossils were buried before cementation. At SEHR2 and certain Hanna Ranch mounds, occasional fossils (like echinoid fragments and forams) were compressed, indicating burial before cementation (Fig. 25B). Not all the fossils at these mounds were compressed, which suggests patchy early cementation.

All locations had well preserved microfossils, most commonly forams. Well preserved radiolarians, and plant and wood fragments, replaced with pyrite were evident at Mosher and I-25 (Fig. 22). The large amount of iron in the seeps system results in pyrite, siderite and at Florence, the ferroan micrite lithofacies.

Temporal and Spatial Variations in Carbon and Oxygen Stable Isotopes

The $\delta^{13}C$ averages of seep carbonate from six mound locations range from -43.0‰ to -32.7‰, with the lowest value at Mosher of -49.5‰ (Fig. 26, Table 5). The $\delta^{18}O$ averages of the six locations range from -8.7‰ to -1.2‰. Mounds that had higher average $\delta^{13}C$ values (I-25, JV Ranch, and SEHR2&4) also had lower average $\delta^{18}O$ values, ranging from -6.2‰ to -8.7‰. These values are well within the spread of published isotopic values, and support a microbial source of methane (Arthur et al., 1982; Birgel et al., 2006; Krause et al., 2009). The only values that do not fit within the published isotopic values are the ferroan micrite of the Florence mounds (Fig. 26C); high $\delta^{13}C$ and $\delta^{18}O$ values have not been reported in any Tepee Butte fabrics other than

those seen in inoceramids or ammonites (Krause et al., 2009). The ferroan micrite values are similar to inoceramid values (Hendricks et al., in review), but have higher $\delta^{18}O$ values, more like that expected for original marine dissolved inorganic carbon (DIC).

The paragenetic sequence at the Boone suggests that peloidal fabrics (peloids in micrite and calcite) formed before botryoidal cements (Fig. 26C; Hendricks et al., in review). At the Boone mounds, peloidal fabrics were less altered than botryoidal cements (Fig. 26C), yet at the Florence and I-25 mounds, the isotopic values of peloidal and botryoidal fabrics overlapped significantly (Fig. 26A,C). At half of the mound locations, botryoidal cements were less diagenetically altered and had more negative $\delta^{13}C$ values and less negative $\delta^{18}O$ values than peloidal fabric, suggesting less diagenetic alteration of botryoidal cements, which is was also reflected in the stain color, as botryoidal cements were usually pink indicating low iron content (Fig. 26). The peloidal fabric was often more purple, indicating more iron content, which is incorporated into the fabric during middle to late diagenesis. This was not expected since botryoidal cements come later in the paragenetic sequence than peloidal fabrics (Hendricks et al., in review). The reason botryoidal cements retain more of their original geochemistry could be due to their large crystal size which limits exposure to pore fluids, along with the fact that fine-grained peloidal cements are more likely to undergo recrystallization.

Mosher and Boone mounds had the most negative $\delta^{13}C$ values of -43.0‰ and -42.2‰ respectively, and also had the highest average $\delta^{18}O$ values of -1.2‰ and -1.8‰ respectively (Fig. 26, Table 5). This suggests that the peloidal carbonate at these locations have undergone the least post-depositional diagenetic alteration, and likely

reflect more of the original isotopic signature when the mounds were formed. Clumped isotopes of molluscs from the *B. compressus* biozone yielded a calculated $\delta^{18}O$ value of -1.2 ± 0.2‰ (Dennis et al., 2013). Boone, Florence and I-25 all have early carbonate $\delta^{18}O$ values that fall within a slightly larger range (-2 - 0‰) with the expanded range due to these locations being slightly older than the clumped isotope values measured (Fig. 26). SEHR, Mosher and JV Ranch have early carbonate $\delta^{18}O$ values that are lower, from -8.7 – -6.2‰, indicating carbonate was not formed in original marine conditions, and formed deeper in the subsurface.

Even with the potential diagenetic alteration of the other mound locations, there is no evidence of a drastically ranging methane source during carbonate seep formation. The $\delta^{13}C$ values of all the mound locations studied reflect precipitation from a mixture of marine DIC and bicarbonate derived from the oxidation of microbial methane. The $\delta^{13}C$ values do not change across locations to suggest any addition of bicarbonate from oxidation of thermal methane. This is confirmed when comparing I-25 and Mosher, the oldest and youngest mound locations: they do not have statistically different $\delta^{13}C$ values (Table 6), which shows that the original source of bicarbonate for the carbonate was not statistically different. This is also indicative of an unchanging source of methane since Mosher formed in a different episode of seep activity from the other mounds (Metz, 2010).

The ferroan micrite lithofacies is an early diagenetic lithofacies only occurring at the Florence mounds. The $\delta^{13}C$ signature of the carbonate suggests precipitation early in the sediment redox zone, despite the high iron content (Fig. 26C; Hendricks et al., in

review). The WIS during the time of Tepee Buttes formation had dysoxic, slowly circulating bottom waters (Parrish et al., 1984; Kauffman et al., 1996). The ferroan micrite at the Florence mounds may have resulted from decomposition of organic matter in an aerobic sediment zone, resulting in carbonate dissolution due to an acidic environment, which created space where the ferroan micrite precipitated (Hendricks et al., in review). Iron in the ferroan micrite may have been supplied from the overlying ferric reduction zone, and the lack of evidence for methane oxidation in the $\delta^{13}C$ signal suggest precipitation from marine DIC and in the methanogenesis zone (which would have the ^{12}C preferentially removed during methane formation). The difference in the environment at Florence is highlighted in comparison to JV Ranch, which also had a large amount of corrosion and void space but resulted in large sparry calcite crystals and multi-generational botryoidal cement (Fig. 24). Comparing JV Ranch to Florence, the difference in the early diagenetic environment is shown by the difference in the fill seen in the large void spaces; at Florence, ferroan micrite fabrics, and at JV Ranch large sparry calcite crystals and extensive botryoids. The ferroan micrite $\delta^{18}O$ values closely reflect an original marine $\delta^{18}O$ signature of -2 – 0‰, similar to $\delta^{18}O$ values calculated from clumped isotope measurements (Dennis et al., 2013). Temperatures from clumped isotope values were calculated to be 24.2 ± 0.4 °C, and calculated temperatures from the ferroan micrite $\delta^{18}O$ values are 22.0 ± 4.5 °C (Hays and Grossman, 1991).

Some mounds did have statistically different $\delta^{13}C$ values, but they do not indicate a change to thermogenic methane (Table 5, 6). Spatially, Boone and JV Ranch had statistically different mound $\delta^{13}C$, with a P1 of 0.028. However, removing one ^{13}C-

enriched point (peloids in calcite) from JV Ranch data, the $\delta^{13}C$ of Boone and JV Ranch are not statistically different (P1 = 0.064; Table 6). JV Ranch only had eight isotopic samples, so this small sample size could account for the difference in carbon isotopes. Spatially, none of the other mound locations (neither Boone and Florence, nor JV Ranch and Florence) had statistically different $\delta^{13}C$ values. JV Ranch did have statistically different $\delta^{18}O$ values from both Boone and Florence, with respective P1 values of 0.0001 (or 0.0002 with the outlier removed) and 0.0022. This shows that JV Ranch carbonate went through more diagenetic alteration than those from the other two locations formed within the same biozone. Even for the mounds closest to the south, SEHR, JV Ranch had statistically different $\delta^{18}O$ values (P1 = 0.032). This is reflected in the large amounts of cement seen at JV Ranch, which shows there was large amounts of dissolution and reprecipitation during burial through the large void space available to precipitate large sparry calcite crystals and multiple generations of botryoidal cement (Fig. 24E).

Looking at a smaller spatial scale, the line of buttes examined at SEHR had interesting isotopic values (Table 5, 6). There was not a linear pattern, instead SEHR6 had statistically different $\delta^{13}C$ values from both SEHR4 (P1 = 0.0367) and SEHR2 (P1 = 0.0047). Seep carbonate that formed so close to one another are expected to have formed from statistically similar methane (Sibuet and Olu, 1998), and while the $\delta^{13}C$ did not change along a linear line of buttes at SEHR through the biozones, the $\delta^{18}O$ values do not reflect original marine precipitation and may be reset through diagenesis. SEHR2 (youngest) had an average $\delta^{13}C$ of -34.1‰, SEHR4 had average $\delta^{13}C$ values of -32.7‰, and SEHR6 (oldest) had the most negative $\delta^{13}C$ of -40.7‰. Though the methane was

changing through time, it was microbial methane throughout the *B. scotti* through *D. stevensoni* biozones, and it was not changing in a linear direction. This also shows that there is more variability within a mound location than there is between them. The line of buttes tested at SEHR did not show statistically different $\delta^{18}O$ values, which is as expected since mounds from the same small geographical location are not expected to experience drastically different diagenetic histories.

$\delta^{13}C$ values of locations that reflect bottom water $\delta^{18}O$ (I-25, Boone and Florence) were not statistically different. This confirms that the source of methane for the Tepee Buttes in southeastern Colorado was constant through time. Minor changes in the $\delta^{13}C$ values could be from changes in methane pathways as a result of sediment loading and flexure of the forebulge. Changes in flexure would result in methane migration from different locations, and or changes in the flow. No oil inclusions in any of the Tepee Buttes samples show the source of methane was not thermogenic. Thermogenic methane migrating from deep would most likely carry oil with it to the surface, and some of it would get trapped in the seep carbonate. Any oil inclusions in the Tepee Buttes can be attributed to a later diagenetic event, and oil migrating long after the seeps were active and buried.

Methane Source

Based on oxygen and carbon stable isotope geochemistry, the methane source for all Tepee Buttes mounds examined in southeastern Colorado was microbial. The $\delta^{13}C$ values range from -32.7‰ to -43.0‰ (Table 5; Fig. 26), which all fall within the expected range of carbonate fabrics formed from microbial methane mixed with marine

DIC (Peckmann and Thiel, 2004). The small range in $\delta^{13}C$ values of original early carbonate supports the contention that the methane source was relatively constant through time. The minor variations seen in the $\delta^{13}C$ values could be related to changes in the makeup of the original organic matter, or amount of initial degradation the original organic matter experienced before burial.

The Pierre Shale has sandstone members (Richards, Terry, Hygiene) that conventionally produce hydrocarbons north of the study area in the Denver Basin (Higley et al., 1995; Higley and Cox, 2007). The source of these hydrocarbons was traced to the surrounding Pierre Shale, or the underlying shales of the Niobrara, the Graneros and the Mowry (Higley et al., 1995). The Pierre Shale is an unconventional source of hydrocarbons, due to its low permeability, and produces from very near the Florence collection site; the Florence oil field is the oldest continually working oil field in the United States, producing since 1862 (Higley et al., 1995; Higley and Cox, 2007). Early carbonate cements from mounds near the Florence oil field have carbon isotopic signatures consistent with microbial methane, despite its proximity to the oil field.

Further suggesting an original microbial methane source, the reconstructed burial history of nearby fields suggests hydrocarbon production began after the Campanian, when the earliest Tepee Buttes began to form (Higley and Cox, 2007). For example, in the Wattenberg field to the north of the study area, the Pierre Shale and underlying Niobrara Formation entered the dry gas window in the Oligocene (Higley and Cox, 2007). In the Denver Basin, the underlying Lyons Sandstone (Permian) began hydrocarbon generation at the very end of the Late Cretaceous, but migration is not

thought to have occurred until the Eocene (Higley and Cox, 2007). Likewise, the Lower Cretaceous D and Muddy J sandstones, also in the Denver Basin, began oil generation in the Late Cretaceous; however, thermal gas generation did not occur until the end of the Eocene (Higley and Cox, 2007). However, the burial history of the Pierre Shale and Niobrara Formation in the vicinity of the Florence oil fields, and the Tepee Buttes, remains undefined and undetermined.

Biomarkers in carbonate fabrics of the Tepee Buttes suggests that the methane was most likely shallow microbial methane sourced in the underlying sediments (Birgel et al., 2006). Biomarkers from both methanotrophic archaea and sulfate-reducing bacteria occur in Tepee Butte carbonate, suggesting an anaerobic oxidation of methane as the key source of DIC (Birgel et al., 2006). Some biomarkers for methanotrophic bacteria suggests aerobic methane oxidation occurred at the seeps (Birgel et al., 2006).

The occurrence of microbial methane in the Tepee Buttes suggests that the source of methane formed shallow in the subsurface. A shallow source of methane suggests very high and constant levels of productivity in the WIS to allow for such an extensive, long-lived seep system. This is supported by the very high organic carbon content (2-11%) of certain parts of the Pierre Shale, particularly the Sharon Springs in the study area, which would allow for a copious amount of original bacterial methane production (Timm and Sonnenberg, 2017). A shallow source of methane also supports the forebulge hypothesis of methane migration along pre-existing fractures beginning at times of maximum transgressions (Metz, 2010). The timing of maximum sea level might also change the oxygen levels of the bottom water and sediment allowing for more

organic carbon to be buried and thus converted into methane. This coupled with changing stress levels of the sediment due to increased flexure could account for the timing of active seepage. A forebulge would also act as a trap to accumulate methane that migrated along sediment layers, and account for the long-lived seep system.

Conclusions

Mound locations were more similar to one another than they were different. All mounds probably formed as low relief features with stacked carbonate beds. These beds can be seen at locations where large amounts of carbonate is exposed; they are difficult to see in mounds covered by shale, carbonate rubble or vegetation. The main petrographic difference between mounds was the amounts of larger sand sized siliciclastic grains, plant, and wood fragments in the early carbonate fabrics. Mounds at I-25 and some mounds at SEHR had heterogeneous carbonate. Despite reconstructions suggesting these mounds formed between 300 – 500 km from the paleoshoreline, terrestrial material was still able to reach them. Mounds at JV Ranch and Florence, formed at similar times and similar distances from the paleoshore, but had more homogeneous early carbonate fabrics. This difference in siliciclastic and terrestrial input to locations that are forming at similar times and geographically close to one another shows how difficult it is to recreate paleo currents, as well as predicting paleoshorelines.

The $\delta^{13}C$ values of early carbonate fabrics from the Tepee Buttes locations in this study coupled with previous biomarker studies indicates the source of methane was microbial methane. This is consistent with models of oil formation in surrounding petroleum basins. The rarity of oil inclusion in the seep carbonate also suggests that

thermogenic methane did not contribute to the formation of the Tepee Buttes. Differences in stable carbon isotope values between locations, some of which are statistically significant, may be due to diagenetic alteration, slight changes in the organic source, and changes in the methane pathways and flexure of the lithosphere. The methane source was most likely the coeval Pierre Shale. The dysoxic nature of the WIS would allow for large amounts of organic matter to be buried, permitting microbial methane to form, while leaving a large amount of unoxidized organic matter that was buried which formed the oil and thermogenic gas being produced today.

The Tepee Buttes preserve a unique diagenetic system where large amounts of pyrite form early in diagenesis which allows for pyrite to replace and preserve microorganisms like radiolarians, wood or plant spores. Also unique is the diagenetic difference between locations; JV Ranch and Florence both experienced significant dissolution, but only Florence developed the ferroan micrite lithofacies, whereas JV Ranch precipitated large sparry calcite crystals and botryoidal cements. The ferroan micrite shows that periods of oxic sediments occurred, at least at the Florence location.

In order to fully understand the Tepee Buttes seep system, work must be extended outside of just southeastern Colorado, to include the mounds in the Black Hills region, as well as the first and fourth episodes of mound formation. Petrographic and stable isotopic comparisons, especially clumped isotopes, on a large scale will allow for a better understanding of cold seep formation, paleoenvironmental differences in the Western Interior Seaway, and how subsurface methane can move through a system.

CHAPTER IV

FORMATION OF BARREL CONCRETIONS AROUND METHANE SEEPAGE PATHWAYS IN UPPER MIDDLE EOCENE SHELF SEDIMENTS, STONE CITY BLUFF, TEXAS*

Introduction

As carbonate concretions are common in siliciclastic sediments where carbonate shell or grains (especially aragonitic components) dissolve in pore fluids or calcium ions are available from the diagenetic alteration of sediment. Where saturation occurs, concretions form and continue to grow as pore fluids migrate through the sediment and bring additional ions to the surface of the concretion. In siliciclastic sediments of the Gulf Coastal Plain in Texas, carbonate is quickly mobilized in sediment because of the high content of land plant debris that generates organic acids during decomposition. These organic acids have removed most carbonate from sandstones and sandy sediments, adding the dissolved ions to the migrating pore fluids. The movement of these fluids to the margins of sand bodies, where chemical conditions change, frequently leads to the precipitation of carbonates that can produce prominent stratigraphic markers like the Seguin Formation at the base of the Wilcox Group. Where there are interbeds containing an abundance of shell material, the primary carbonate shell and bioclasts are buffered from dissolution and carbonate can persist and be retained in the sediment.

These conditions occur in the fine-grained marine sediment layers within the Claiborne Group. Units like the Stone City Member contain common round and elongate concretions, including the appropriately named Cannonball concretion bed at Stone City Bluff on the Brazos River (Fig. 27). The section is located on the banks of the Brazos

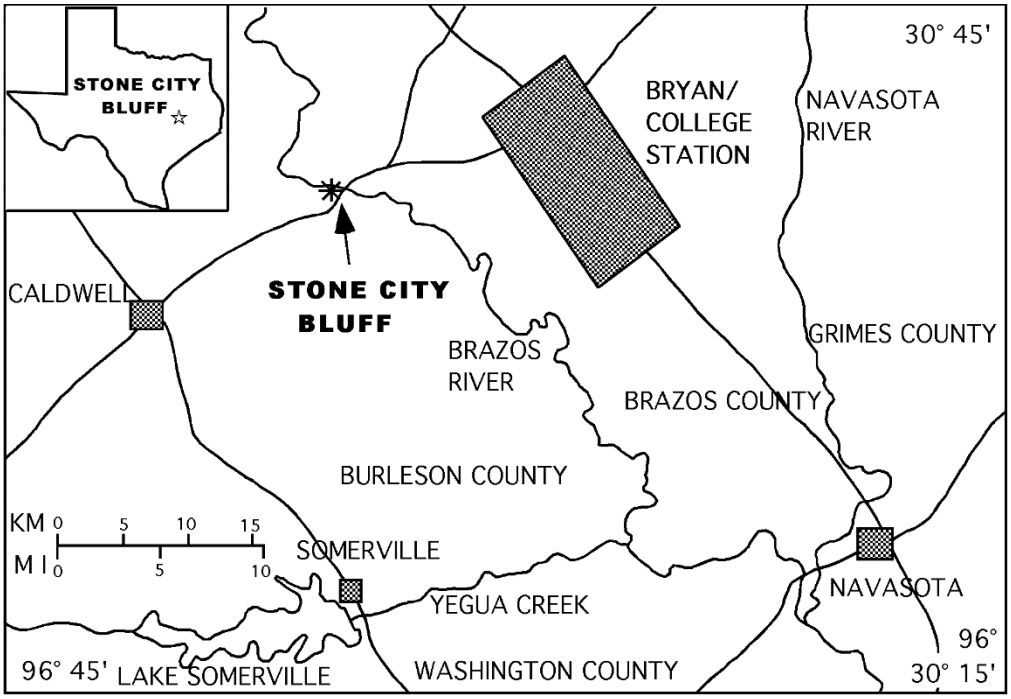

Figure 27: Location map showing the site of the Stone City Bluff, in Burleson County, Texas, marked by a star. Dark boxes denoted nearby towns.

River west of Bryan, Texas, on the Burleson County side of the river. The outcrop is known as the Whiskey Bridge site and is a well-known fossil locality.

This report documents the occurrence of an unusual type of calcite concretion present at Stone City Bluff, consisting of calcite concretions with an elongate shape, resembling barrels, which occur with the elongate axis extending vertically through

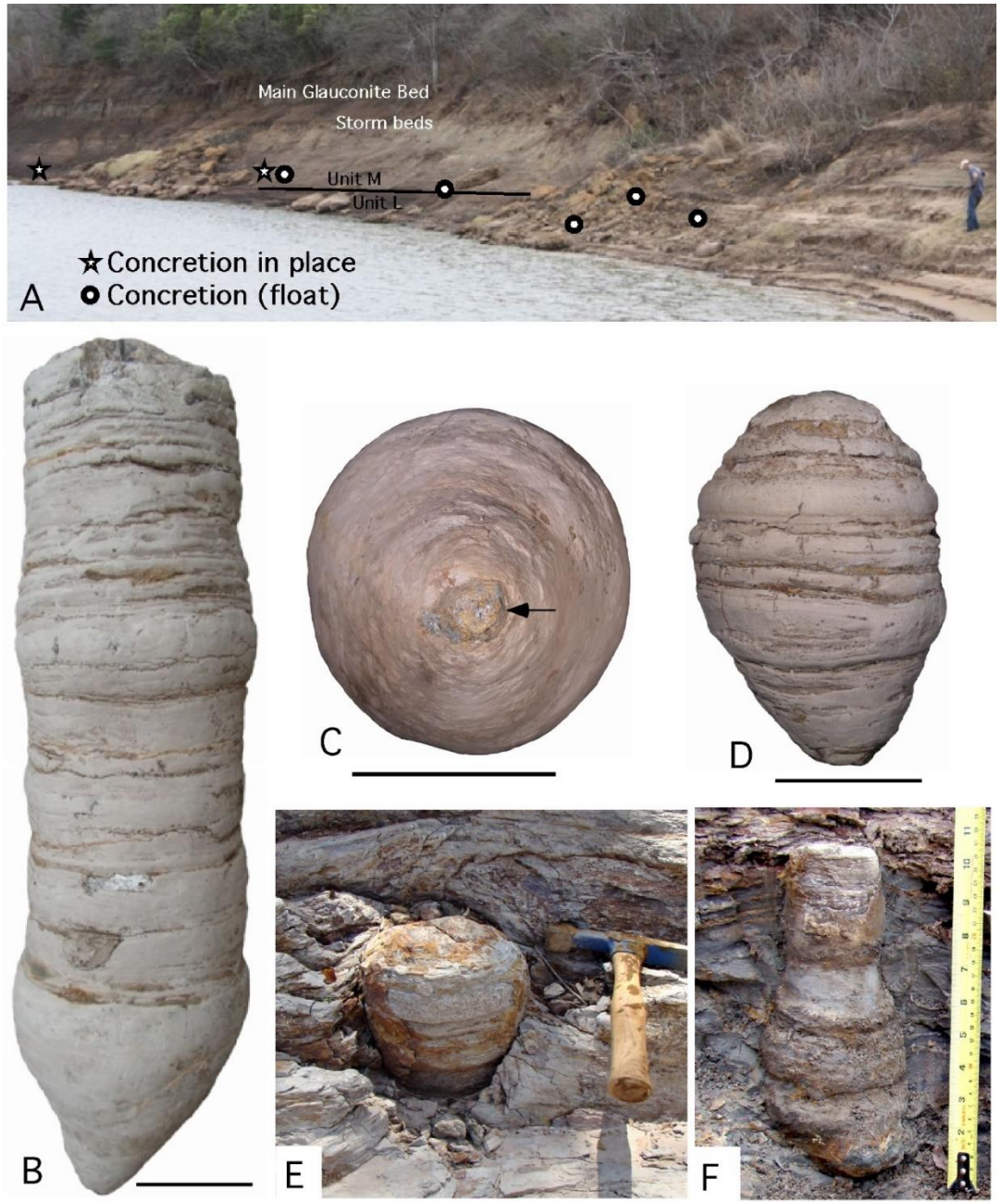

Figure 28: A) Location of barrel concretion site, Stone City Bluff on the Brazos River, upriver from bridge. Position of in-situ and float concretions shown and important beds in the section labeled. B) Largest barrel concretion, with incomplete top, showing variations in diameter related to changes in sediment grain size. C) Pyrite-lined micropipe (arrowed) at base of largest concretion. D) Short, large diameter concretion with tapered top and bottom. E) V-shaped barrel concretion in situ. F) Small, irregular shaped barrel concretion with incomplete top and curved base. Scale bar is 4 in (10 cm) long.

layers of sediment. These concretions are distinct from the more common subspherical concretions that occur in the Cannonball concretion bed near the base of the section and the Main Glauconite Bed higher in the section. Those rounded concretions occur laterally within beds of the same sediment type. The barrel concretions of this report extend vertically through alternating layers of mud-rich siltstone and fine sandstone (Fig. 28), pinching and swelling in diameter in response to the changing mean grain size of the sediment. Sediment layers surrounding the concretions drape over the tops and against the sides and the interiors of concretions shows similar arching of sediment layers (Fig. 29D), showing that barrel concretions formed while sediments were still compacting.

The growth of these concretions is related to the presence of small pyrite-lined pipes that extend the length of the concretion in its center. The concretions formed in response to the vertical migration of fluids following a well-defined pathway through the layers of sediment. This mode of formation is similar to the formation of large pipe concretions that occur in some parts of the world (De Boever et al., 2009; Nyman et al., 2010). Pipe concretions have been associated with the vertical migration of methane through sediments and the pipe-bearing barrel concretions at Stone City Bluff contain an isotopic signature that indicates a similar origin.

Geologic Setting

The Stone City Bluff section contains strata of an upper Middle Eocene transgressive systems tract (Yancey, 1995) deposited during flooding after deposition of the Sparta Formation (Stenzel, 1936; Stenzel et al., 1957). Stenzel (1936) interpreted this set of

deposits as the record of shoaling that terminated in subaerial erosion, but the depositional trend in the section is to deeper water (Yancey and Davidoff, 1991, their p. 79–80; Yancey, 1995; Fear et al., 2010) and the coarse-grained Moseley bed horizon considered to be an unconformity by Stenzel (1936) marks the surface of a submarine hardground (Thornton and Stanton, 1994) produced by sediment starvation in an offshore marine environment. The lower parts of the section are dominated by combined tidal and storm-controlled processes and the upper parts of the section contain coarser sandy layers that record storm deposition set in a background of mud deposition. These deposits are part of the regional record of a global highstand (Waterman et al., 2011) that corresponds with the late Middle Eocene Climate Optimum (MECO) of the lower Bartonian stage.

The barrel concretions occur in the lower part of the exposed section at Stone City Bluff, near the boundary between units L and M of Stenzel et al. (1957), a contact between a sandier, more porous lower layer and a finer grained upper layer (Fig. 28A). The barrel concretions are located 8 ft (2.5 m) above the better-known Cannonball concretion horizon. They were collected at the upriver end of the bluff outcrops during 2010 and 2011, but a barrel concretion from the same locality was collected by C. A. Thornton in 1993. The distinctive nature of the barrel concretions was not recognized until multiple specimens were found at the site. Three of these concretions were found in place in situ, permitting documentation of their orientation and character of the surrounding sediments that drapes over tops of the concretions. The other concretions were collected after erosion from the deposit and collected at the base of the cliff face.

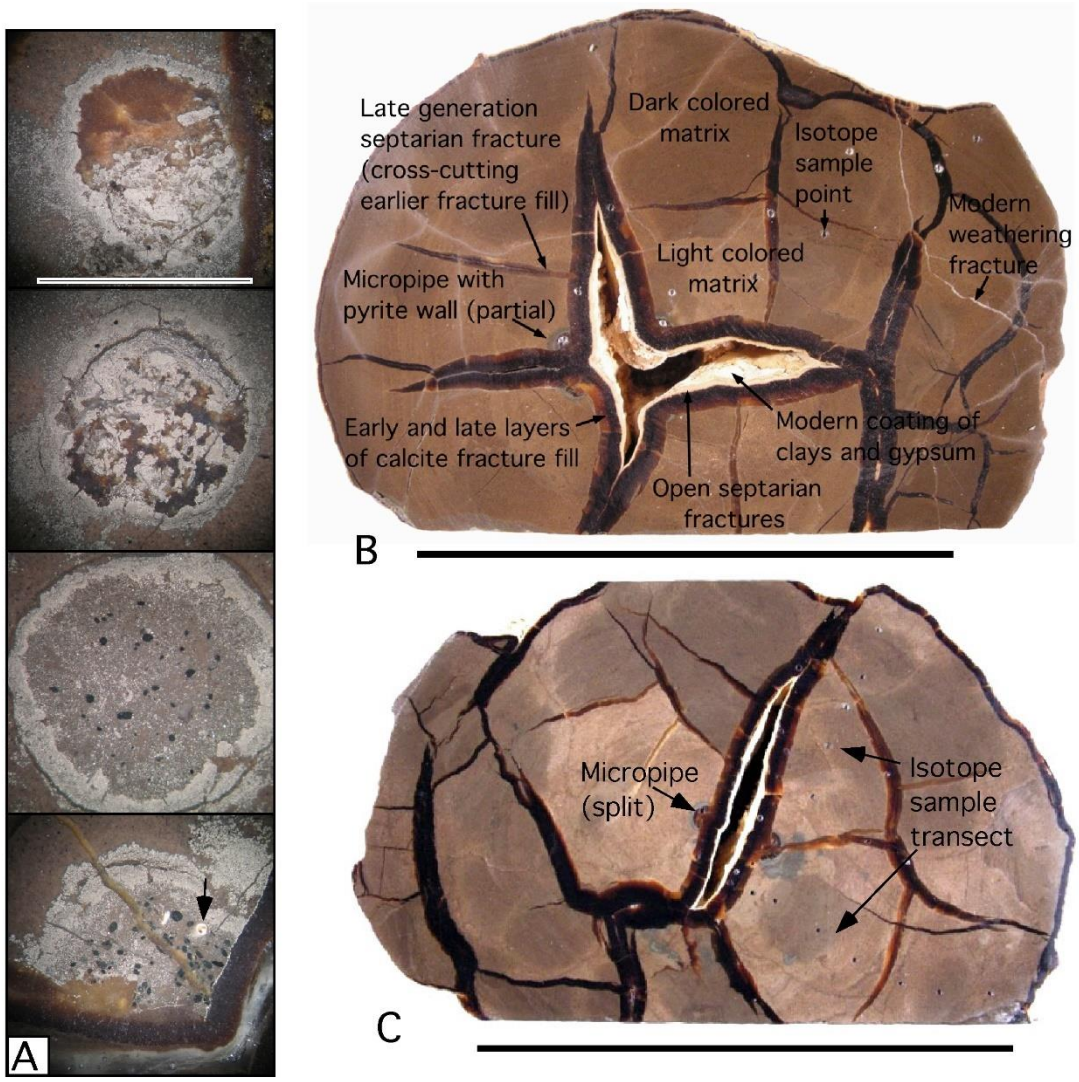

Figure 29: A) Serial section of a micropipe in concretion shown in Figure 1F, showing change from sediment fill at base to calcite and pyrite cement fill at the top; the arrow in lowest photo points to a gastropod shell bioclast in the sediment; dark grains in fill are glauconite and fecal peloids. B) Horizontal cut section of barrel concretion with features labeled. C) Horizontal cut section of same barrel concretion at lower level; isotope sample transects shown. D) Vertical slice of same barrel concretion showing doming of sediments associated with sediment compaction during growth of concretion, E) Surface of septarian fracture extending across barrel diameter, with dark layers of encrusting calcite; extent of open horizontal and vertical septarian fractures reveals the weak condition of barrel concretions and typical broken condition.

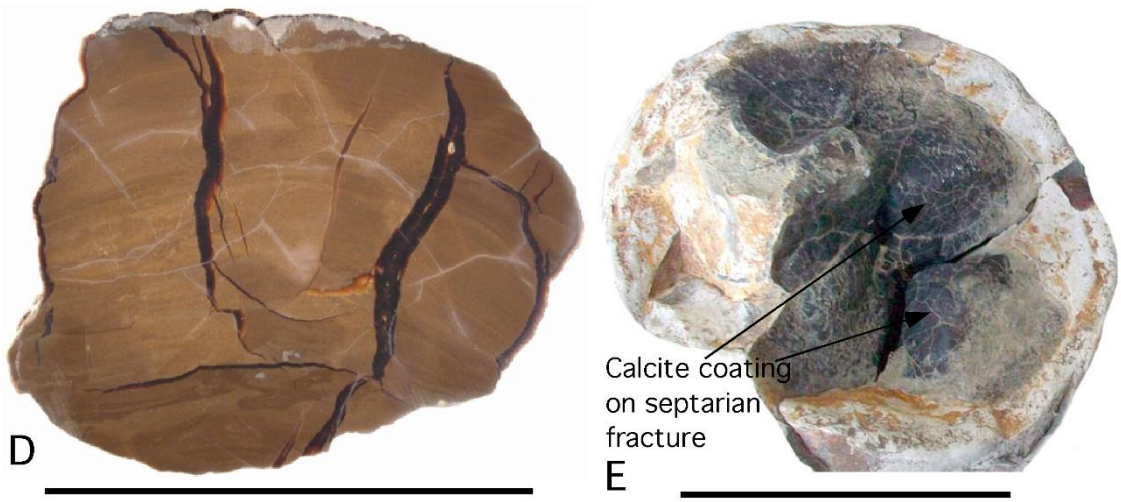

Figure 29 Continued.

All concretions have similar internal features, indicating a common origin, although they range in barrel diameter and length.

Methods

Initial characterization of the barrel concretions was done by cutting serial sections to reveal features of the interior. Upon determining that there was a possibility of methane-related diagenesis, sample powders were collected with a dental drill of the carbonate matrix, micropipe fill, partly open septarian fracture fill and healed fracture fill. These samples were analyzed for carbon and oxygen stable isotopes on a Kiel IV Carbonate Device attached to a Thermo Scientific MAT253 at the Stable Isotope Geosciences Facility at Texas A&M University. Data were calibrated to the VPDB standard using NBS–19. Precision was 0.03‰ and 0.07‰ for $\delta^{13}C$ and $\delta^{18}O$ respectively. A T-test of unequal variances was run on the appropriate diagenetic phases to determine whether they were significantly different, using a p value of < 0.05.

Description of Concretions

The barrel concretions are elongate and cylindrically shaped, ranging in size to 2 ft (0.7 m) in length and 8 in (0.2 m) in diameter (Fig. 28). Smaller concretions collected are short and squat, but this is the result of recovering only segments of the concretion, which tend to break into sections due to the presence of unfilled septarian fractures that segment the concretions. These concretions differ from pipe concretions reported by Nyman et al. (2010) and De Boever et al. (2009) in the absence of a large diameter open central cavity in the concretion and by the presence of septarian fractures. Barrel concretions have micropipes in the center that are filled with cement. They also differ from pipe concretions in the size, with the largest barrel concretion being less than 3 ft (1 m) long, while those in Bulgaria are over 30 ft (10 m) in length (De Boever et al., 2009). The bases of some of the barrel concretions taper, causing the ends to be cone shaped.

The concretions are composed of calcite-cemented sandy mudstone (~35 weight % sediment), with minor amounts (< 5%) of pyrite. Coarse sediment grains are imbedded in the calcite cement edge, producing a rough surface that reveals sedimentary structures (lamination, cross bedding, wavy bedding, and burrows) of the sediment layers. The carbonate matrix has two shades of gray color in irregular patches that are partly controlled by fractures in the concretion, giving the interior of the concretion a mottled look. A light gray color occurs along the outer margin of the concretion and along the sides of open fractures, whereas areas distant from the fractures have a dark gray color.

Concretions contain many large septarian fractures of both radial and concentric orientation, developed in two generations of fracturing (Fig. 29B). Early-formed septarian fractures are larger and dominantly radial in orientation but later-formed fractures tend to be irregular and smaller in size. They are lined with accretionary layers of dark calcite crystals, but the larger fractures are not completely filled. This is atypical for septarian concretions. Fractures in the concretion center have unfilled gaps as much as 0.4 in (1 cm) wide bounded by layers of dark calcite 0.3 in (4 – 5 mm) thick. Surfaces of the calcite layers facing the open spaces are lined with surficial coatings of microgranular white clay-rich material and small, clear, euhedral gypsum and calcite crystals. Septarian fractures commonly contain two layers of calcite cement, shown by small differences in color. Early formed calcite fracture fill layers are lighter orange-brown and clearer whereas later-formed layers are darker brown, presumably due to impurities in the calcite crystals.

Concretions contain pyrite-lined micropipes located in their centers that are approximately 0.4 in (1 cm) in diameter. Micropipes are filled with calcite and in some cases contain cemented sediment fill. The sediment fill in one concretion contains shell fragments, showing that sediments were carried into the micropipe before cementation was complete. Micropipe wall composition is pyrite and the pyrite extends into parts of the fill and the surrounding matrix in some areas. Serial sections of concretions reveal that the micropipe is generally centrally located but may occur off center, especially towards the ends of the concretion. In larger concretions with centrally located micropipes, the micropipes are usually broken apart into sections by later-formed radial

septarian fractures (Fig. 29C). In these concretions the micropipe is obscured and needs to be reconstructed by restoring the concretion to its pre-split condition.

Stable Isotope Geochemistry

Stable oxygen and carbon isotopic analyses of the concretions yield very low $\delta^{13}C$ values, from -28.9‰ to -34.6‰ (Fig. 30). The samples form a tight cluster of very low $\delta^{13}C$ values with $\delta^{18}O$ values close to 0‰. The lowest $\delta^{13}C$ values are from septarian carbonate fill, both late and early, averaging -33.6‰, with $\delta^{18}O$ values averaging -1.0‰. The micropipe fill also yields low $\delta^{13}C$ values, averaging -32.3‰, with $\delta^{18}O$ values

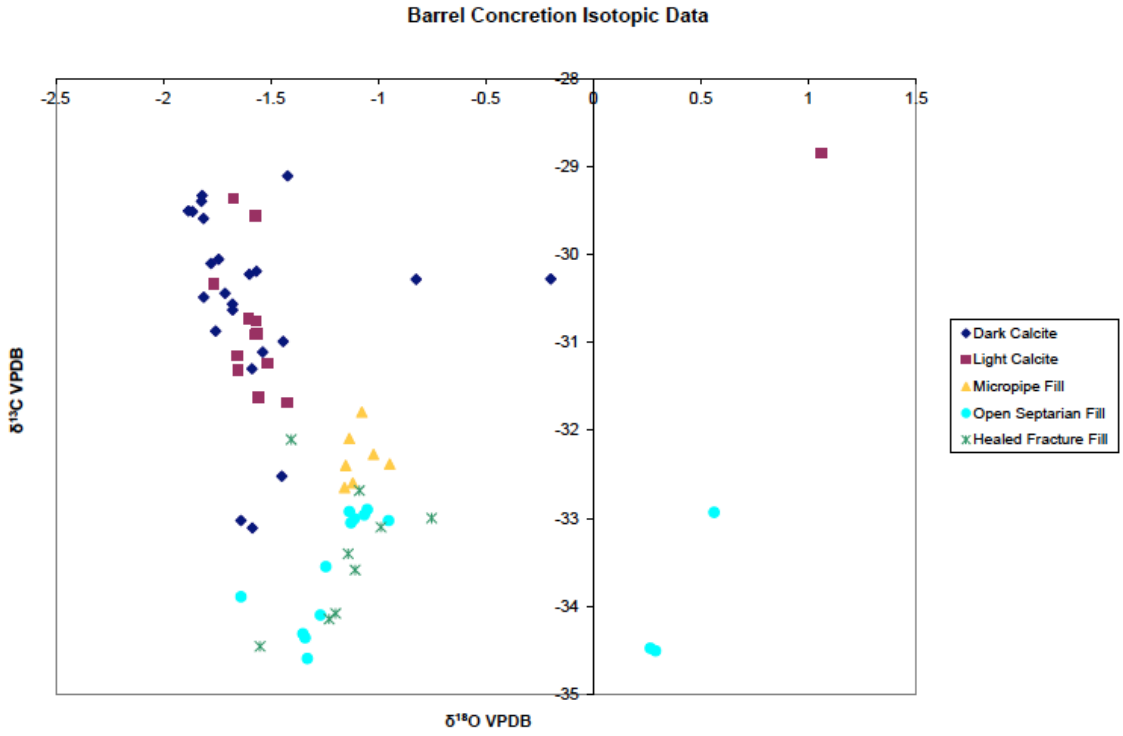

Figure 30: Plot of stable isotope values for matrix, micropipe and open septarian fracture and healed fracture fill in barrel concretions.

averaging -1.1‰. The matrix has the heaviest (highest) $\delta^{13}C$ values, averaging -30.6‰ for both the light and dark matrix, with $\delta^{18}O$ values averaging -1.6‰ for dark matrix carbonate and -1.3‰ for light matrix carbonate. A T-test of unequal variance run on the light and dark matrix carbonate yielded no statistical difference between the $\delta^{13}C$ values ($p = 0.39$). Sampling transects along four different paths from the center of the concretion outward through the matrix showed no discernible isotopic trend.

Paragenesis of Concretion Formation

Micropipes were the first component of the concretions to form, maintaining a pathway for methane and fluid migration. Pyrite precipitated to form the micropipe walls and calcite precipitation occurred around the pipe. Extension of pyrite into the surrounding calcite matrix in some areas indicates that pyrite and calcite precipitation occurred simultaneously as the concretion grew, with calcite being the dominant precipitate. The end of fluid migration is marked by the pipe filling with calcite and pyrite cements, preceded in some concretions by partial infilling with sediment carried by fluids. Following this, desiccation of the matrix produced large septarian fractures that radiate from the center of the concretion, resulting in splitting of the micropipe into segments. Two episodes of calcite precipitation occurred coating the sides of septarian fractures, but not filling the larger cavities. A later generation of smaller septarian fractures appeared and became filled with calcite, perhaps overlapping in time with the later episode of calcite fill in the first set of septarian fractures. Small amounts of pyrite occur scattered throughout the concretion matrix. Because small pyrite concretions are common in the surrounding sediments, it cannot be determined if the pyrite concretions

were incorporated by later-forming calcite cement or if they concurrent with concretion formation. The last set of fracturing (tight cracks) and coating of open septarian cavities by clays and euhedral gypsum and calcite crystals occurred during present day exposure of the concretions at the outcrop.

Discussion

Morphology and stable isotopic values show that these barrel concretions were formed as a result of methane expulsion in a shallow shelf system. Sediment and shell fill in the micropipes suggest that these tubes were not only used for gas expulsion, but for aqueous fluid expulsion as well. Compaction of thick piles of sediment could cause both gas and fluid expulsion. Evidence of compaction is seen in the vertical slices of the barrels, showing doming of the sediments related to compaction. The presence of the barrel concretions just above an interface between a more porous, sandier lower layer and a finer upper layer suggests a method of formation. Methane was able to more freely move through the sandier lower layer, but was unable to easily move up through the overlying finer grained layer on top of it. Methane preferentially moved upward through small micropipes, and the large concentration of methane resulted in the precipitation of calcite and pyrite in sediments surrounding the small pipe passageways. The different colors in the matrix may be due to recent alterations. The matrix has the least depleted $\delta^{13}C$ values, with both values close to -30.5‰, but there is no statistical difference between the light and dark matrix carbonate.

The low $\delta^{13}C$ values of the barrel concretions contrast sharply with the $\delta^{13}C$ of four serially-sampled gastropod shells from the Stone City section (0–2‰; T. Kobashi

and E. Grossman, unpublished data). On the other hand, the $\delta^{18}O$ values of the barrel concretions and matrix, averaging -1.6‰ to -1.0‰, are similar to those of the gastropod shells (mean = -1.6‰) after correcting for aragonite-calcite differences in fractionation (+0.6‰; Grossman and Ku, 1986). This shows that the barrel concretions formed in local marine waters at normal bottom temperatures, and provides evidence that the stable isotope values have not been reset through diagenesis by either interaction with meteoric water or burial.

The $\delta^{13}C$ values are very low suggesting that the carbon used to form the carbonate was derived, in part, from methane. The source of the bicarbonate was most likely microbial anaerobic oxidation of methane (Enos and Kyle, 2002). The less negative $\delta^{13}C$ values (-28‰ to -31‰) of early-formed matrix (Fig. 30), along with the pyrite occurrence, indicate formation during sulfate reduction in the presence of carbon derived from oxidized methane and marine dissolved inorganic carbon (DIC). None of the carbonate samples have $\delta^{13}C$ values low enough to suggest a pure methane source for the bicarbonate, and thus suggest that the carbon source was mixed. The pyrite in the walls of the micropipes and throughout the rest of the concretions also supports this conclusion of precipitation in the sulfate reduction zone of the sediment. The lower values (-32‰ to -35‰) of late generation septarian and micropipe fill (Fig. 30) suggest methane oxidation in sediments with less dilution by marine DIC, and thus less mixing with bottom waters.

Methane-derived carbonate concretions have been found in siliciclastic settings throughout the world and are often associated with methane cold seeps (Gaillard et al.,

1992; Kauffman et al., 1996; Enos and Kyle, 2002; De Boever et al., 2009; Nyman et al., 2010). Methane cold seeps are found throughout geologic time and have many different forms. Some cold seeps are large fossil-rich carbonate mounds or column shaped (Gaillard et al., 1992; Kaufmann et al., 1996). Modern cold seeps also have a range of shapes, from chimney-shaped carbonate columns to spheres to grape-shaped agglomerations. Other seeps have surface expression as microbial mats actively precipitating carbonate (Aloisi et al., 2002; Michaelis et al., 2002; Reitner at al., 2005).

Most research on methane cold seeps has focused on the surface morphology of the carbonates. However, carbonate pipes with hollow interiors have been found (de Boever et al., 2009; Nyman et al., 2010) and are thought to preserve the subsurface conduits that bring methane to the surface. Based on the isotopic and morphological data, these barrel concretions can also be considered as part of the subsurface plumbing of a cold seep acting as conduits for methane gas and fluids to move upwards through the sediment.

Conclusions

Barrel concretions discovered in the Stone City Bluff, Burleson County, Texas, are carbonate pipes that acted as conduits for methane and fluid migration. These barrels preserve the subsurface plumbing of a cold seep located on the shelf of the Gulf of Mexico. The concretions formed during pyrite formation, and in the presence of carbon derived from both oxidized methane and marine dissolved organic carbon. This discovery shows that methane was generated in shallow shelf sediments.

CHAPTER V

CONCLUSIONS

Cold seeps are complex systems governed by many different factor, because of this methane-derived carbonate can take many forms and occurs in many different depositional settings. The Tepee Buttes are the most extensive fossil cold seeps, and formed over 10 million years in the late Cretaceous Western Interior Seaway from southern Colorado to the Black Hills of South Dakota and Montana. Field observations, facies mapping and petrographic analysis of 28 mounds in the vicinity of Pueblo, CO, suggest that mounds originated as low-lying stacked carbonate beds that were not elevated significantly above the seafloor. The modern high-relief, conical shape is a result of weathering. Seep carbonate formed from a mixture of marine Dissolved Inorganic Carbonate and oxidation of bacterial methane, sourced from the underlying Pierre Shale. The methane source was constant through time, and no thermogenic methane contributed to the formation of mounds. Mound facies are a mixture of the same carbonate fabrics in varying proportions: micrite, peloids, carbonate cement, and organisms. Carbonate facies are not zoned concentrically around a large, central methane vent. Methane moved through small tubules, less than 10 mm in diameter, preserved in the anastomosing ropey facies. These tubules preserve dolomite, cement, and siliciclastic sediment, which is evidence of moving fluids and gases.

In order to evaluate changes in methane source to the Tepee Buttes mounds, my collaborators and I investigated the petrography, paragenetic sequence and stable

isotopic composition of mounds from six locations in southeastern and south-central Colorado, which formed over ~3 m.y. and which cover a geographic area of approximately 6,500 km^2. The Tepee Buttes mounds in southeastern Colorado show minor difference between study locations, mainly related to the heterogeneity of the micrite and early carbonate fabrics as a result of increased amounts of siliciclastic and sand sized grains. I did not find a geographic pattern to the increased grain size at most mound locations based on distance to the paleoshore. Changes in topography, currents, or sediment delivery could account for the heterogeneity in sediment supply. There was a difference in the heterogeneity of the Mosher mounds, which formed during a different episode of mound formation, had fine grained sediments, and preserved a microbial texture. Paleoshoreline reconstructions during the interval of formation of the Mosher mounds, place the shoreline further away, which may account for less delivery of clastics and the presence of smaller grains. I found no evidence for a change in the source of methane through time. Comparisons of stable isotope ratios of mound carbonate at the six locations yielded few significant differences, and when significant, the variation was minor. Seep carbonate was not formed from thermogenic methane, which is consistent with the timing of hydrocarbon formation in surrounding petroleum basins, like the Denver Basin to the north. Bacterial methane likely came from the underlying Pierre Shale.

Mounds sources by bacterial methane are usually ephemeral due to the patchy nature of organic matter distribution, and because methane rarely forms large reservoirs, making long lived seep systems fueled by bacterial methane rare. Despite this, mound

locations in the Tepee Buttes persisted for over 2 m.y. Results of this study are consistent with the Metz model of mound formation in the forebulge of the Sevier orogeny during periods of maximum transgression. In the Metz model, the forebulge remained in the same area throughout the 10 my interval of mound formation potentially due to lithospheric weakness due to the Laramide and earlier faults, which provided conduits for methane to the sediment water interface. The forebulge also acted as a trap to accumulate the migrating methane, allowing for a larger reservoir than if the seeps were not on the forebulge.

The Stone City Bluff in Burleson Co., TX preserves unique elongate, cylindrical methane-derived septarian carbonate concretions in Middle Eocene transgressive system tract sediments. They formed vertically in the sediments and their exterior contours pinch and swell slightly in relation to layers in the surrounding sediment. These barrel concretions are up to 70 cm long and up to 20 cm in diameter and contain a small (1 cm) pyrite lined micropipe in the center. This micropipe contains cemented sediment, glauconite pellets, cement and even a small fossil which suggest fluid and gas migration. Convex bedding planes within the concretions are consistent with compaction which could be the driving force to methane migration. The stable isotopic ratios of carbonate from Stone City barrel concretions suggest formation from a mixture of marine DIC and bicarbonate from the oxidation of bacterial methane in the sulfate reduction zone. Methane expulsion may have been driven by compacting sediments as suggested by the doming of sediments seen in vertical slices of the barrel concretions. The barrel concretions occur at the base of a finer grained layer above a slightly coarser grained,

more porous layer, which may have forced methane to move upwards in vertical vents. Apparently, there was not enough methane produced at Stone City to reach the sediment water interface and form seep carbonates on the sea floor.

The Tepee Buttes represent the surface expression of a seep system, while the Stone City Bluffs provide a unique opportunity to investigate the subsurface plumbing of a seep system. By studying them together, my collaborators and I are able to look at the entire seep system as a whole, from the methane source, the migration through the subsurface, and finally the surface expressions of the seep.

REFERENCES

Aloisi, G., Bouloubassi, I., Heijs, S. K., Pancost, R. D., Pierre, C., Sinninghe Damste, J. S., Gottschal, J. C., Forney, L. J. and Rouchy, J. M., 2002, CH_4-consuming microorganisms and the formation of carbonate crusts at cold seeps: Earth and Planetary Science Letters, v. 203, p. 195-203.

Anderson, J., 2006, Petrological and Petrographical Analysis of Ancient Submarine Hydrocarbon Seep Deposits (Late Cretaceous) from the Tepee Buttes of Colorado [Bachelor of Arts Thesis]: Gustavus Adolphus College. 45 p.

Anderson, J., Shapiro, R. and Lyons, T., 2005, Petrology and Petrography of the Tepee Buttes (Cretaceous) Methane-Seep Carbonates: Geological Society of America Abstracts with Programs, v. 37, no. 7, p. 138.

Arthur, M. A., Kauffman, E. G., Scholle, P. A. and Richardson, R., 1982, Geochemical and Paleobiological Evidence for the Submarine Spring Origin of Carbonate Mounds in the Pierre Shale (Cretaceous) of Colorado: Geological Society of America Abstracts with Programs, v. 14, p. 435.

Bash, E., Shapiro, R., Anderson, J., Close, H., Dahl, R., Morgan, V., Parsons-Hubbard, K. and Rudolph, R., 2005, Distribution and Mapping of the Cretaceous Tepee Buttes of the Western Interior Seaway: Geological Society of America Abstracts with Programs, v. 37, no. 7, p. 138.

Beauchamp, B. and Savard, M., 1992, Cretaceous Chemosynthetic Carbonate Mounds in the Canadian Arctic: Palaios, v. 7, no. 4, p. 434-450.

Birgel, D., Peckmann, J., Klautzsch, S., Thiel, V. and Reitner, J., 2006, Anaerobic and Aerobic Oxidation of Methane at Late Cretaceous Seeps in the Western Interior Seaway, USA: Geomicrobiology Journal, v. 23, p. 565-577.

Callendar, R., 1992, Recognition of Deep-Water Assemblages in the Fossil Record: Taphonomy and Community Characteristics of Louisiana Continental Slope Petroleum Seep Assemblages: [Doctor of Philosophy Dissertation]: Texas A&M University. 289 p.

Callender, W. R. and Powell, E. N., 1999, Why did ancient chemosynthetic seep and vent assemblages occur in shallower water than they do today?: International Journal of Earth Sciences, v. 88, p. 377–391.

Campbell, K. A., 2006, Hydrocarbon seep and hydrothermal vent paleoenvironments and paleontology: Past developments and future research directions: Palaeogeography, Palaeoclimatology, Palaeoecology, v. 232, p. 362-407.

Chafetz, H. S., 1986, Marine Peloids: A Product of Bacterially Induced Precipitation of Calcite: Journal of Sedimentary Petrology, v. 56, no. 6, p. 812-817.

Close, H., 2006, Taphonomic and Sedimentologic Study of the Cretaceous Tepee Buttes Limestone [Unpublished Honors Thesis]: Oberlin College. 61 p.

Dahl, R. M., Close, H. G., Parsons-Hubbard, K. and Shapiro, R., 2005, Paleoecology and Topographic Expression of a Cretaceous Cold Seep: A Taphonomic Analysis of the Tepee Butte Limestone: Geological Society of America Abstracts with Programs, v. 37, no. 7, p. 138.

Darton, N. H., 1919, Newell Folio, South Dakota: U.S.G.S. Geological Atlas of the United States, v. 209, 11 p.

De Boever, E., Huysmans, M., Muchez, P., Lyubomir, D. and Swennen, R., 2009, Controlling factors on the morphology and spatial distribution of methane-related tubular concretions – Case study of an Early Eocene seep system: Marine and Petroleum Geology, v. 26, p. 1580-1591.

Dennis, K. J., Cochran, J. K., Landman, N. H. and Schrag, D. P., 2013, The climate of the Late Cretaceous: New insights from the application of the carbonate clumped isotope thermometer to Western Interior Seaway macrofossil: Earth and Planetary Science Letters, v. 362, p. 51-65.

Dickson, J. A. D., 1965, A Modified Staining Technique for Carbonates in Thin Section: Nature, v. 205, p. 587.

Enos, J. S., and Kyle, J. R., 2002, Diagenesis of the Carrizo Sandstone at Butler Salt Dome, East Texas basin, U.S.A.: evidence for fluid-sediment interaction near halokinetic structures: Journal of Sedimentary Research, v. 72, p. 68-81.

Fear, M. R., Gaffin, D. H., Hedrick, B. N., Limpus, B. A., Maertin, L. J., McClintock, J. S., Taylor, T. M. and Fluegeman, R. H., 2010, Planktonic:benthonic foraminiferal ratios from the Crockett Formation (Eocene; Bartonian) of the Texas Gulf coastal plain: Geological Society of America Abstracts with Programs v.42, no. 5, p. 250.

Feng, D., Chen, D., Qi, L. and Roberts, H. H., 2008, Petrographic and geochemical characterization of seep carbonate from Alaminos Canyon, Gulf of Mexico: Chinese Science Bulletin, v. 53, no. 11, p. 1716-1724.

Gaillard, C., Rio, M., Rolin, Y. and Roux, M., 1992, Fossil Chemosynthetic Communities Related to Vents or Seeps in Sedimentary Basins: The Pseudobioherms of Southeastern France Compared to Other World Examples: Palaios, v. 7, no. 4, p. 451-465.

Georgieva, M. N., Little, C. T. S., Watson, J. S., Sephton, M. A., Ball, A. D. and Glover, A. G., 2019, Identification of fossil worm tubes from Phanerozoic hydrothermal vents and cold seeps: Journal of Systematic Paleontology, v. 17, no. 4, p. 287-329.

Gilbert, G. K. and Gulliver, F. P., 1895, Tepee Buttes: Bulletin of the Geological Society of America, v. 6, p. 333-342.

Hays, P. D., and Grossman, E. L., 1991, Oxygen isotopes in meteoric calcite cements as indicators of continental paleoclimate: Geology, v. 19, p. 441-444.

Hendricks, J. K., Yancey, T. E., Flis, J. E., Flis, C. J. and Grossman, E. L., 2012, Formation of barrel concretions around methane seepage pathways in upper Middle Eocene shelf sediments, Stone City Bluff, Texas: Gulf Coast Association of Geological Societies Transactions, v. 62, p. 179-188.

Hendricks, J. K., Raymond, A., Pope, M. C., Metz, C. L., Grossman, E. L., and Gong, J., in review, Original Morphology of the Tepee Buttes Mounds: Implications for Mound Paleoecology and Formation: Journal of Sedimentary Research.

Higley, D. K., Pollastro, R. M., and Clayton, J. L., 1995, Denver Basin Province (039), in Gautier, D. L., Dolton, G. L., Takahashi, K. I., and Varnes, K. L., eds., National Assessment of United States oil and gas resources; Results, methodology, and supporting data, U.S. Geological Survey.

Higley, D. K. and Cox, D. O., 2007, Oil and gas exploration and development along the front range in the Denver Basin of Colorado, Nebraska, and Wyoming, in Higley, D. K., ed., Petroleum Systems and Assessment of Undiscovered Oil and Gas in the Denver Basin Province, Colorado, Kansas, Nebraska, South Dakota, and Wyoming—USGS Province 39 U.S. Geological Survey, p. 41.

Hilário, A., Capa, M., Dahlgren, T. G., Halanych, K. M., Little, C. T. S., Thornhill, D. J., Verna, C. and Glover, A. G., 2011, New Perspectives on the Ecology and Evolution of Siboglinid Tubeworms: PLoS ONE, v. 6, no. 2, p. 1-14.

Hovland, M., 2002, On the self-sealing nature of marine seeps: Continental Shelf Research, v. 22, p. 2387-2394.

Hovland, M., Talbot, M. R., Qvale, H., Olaussen, S. and Aasberg, L., 1987, Methane-Related Carbonate Cements in Pockmarks of the North Sea: Journal of Sedimentary Petrology, v. 57, no. 5, p. 881-892.

Howe, B., 1987, Tepee Buttes: A Petrological, Paleontological, Paleoenvironmental Study of Cretaceous Submarine Spring Deposits: [Master of Science Thesis]: University of Colorado. 182 p.

Hunter, A. W., Larson, N. L., Landman, N. H. and Oji, T., 2016, *Lakotacrinus brezinai* n. gen. n. sp., a new stalked crinoid from cold methane seeps in the Upper

Cretaceous (Campanian) Pierre Shale, South Dakota, United States: Journal of Paleontology, v. 90, no. 3, p. 506-524.

Kauffman, E. G., Arthur, M. A., Howe, B. and Scholle, P. A., 1996, Widespread venting of methane-rich fluids in Late Cretaceous (Campanian) submarine springs (Tepee Buttes), Western Interior seaway, U.S.A.: Geology, v. 24, no. 9, p. 799-802.

Kennicutt II, M. C., 2017, Oil and Gas Seeps in the Gulf of Mexico, in Ward, C. H., ed., Habitats and Biota of the Gulf of Mexico: Before the Deepwater Horizon Oil Spill: p. 275-358.

Kiel, S., 2010, On the potential generality of depth-related ecologic structure in cold-seep communities: Evidence from Cenozoic and Mesozoic examples: Palaeogeography, Palaeoclimatology, Palaeoecology, v. 295, p. 245-257.

Konhauser, K., 2006, Introduction to Geomicrobiology, Blackwell Science Ltd, 440 pg.

Krause, F. F., Clark, J., Sayegh, S. G. and Perez, R. J., 2009, Tube Worm Fossils or Relic Methane Expulsing Conduits?: Palaios, v. 24, p. 41–50.

Larson, N., Brezina, J., Landman, N. H., Tatsuo, O., Garb, M. P. and Handle, K. C., 2013, Hydrocarbon seeps: Habitats that preserved the diversity of fauna in the Late Cretaceous Western Interior Seaway: Wyoming Geological Society Field Guide, 20 p.

Levin, L. A., 2005, Ecology of Cold Seep Sediments: Interactions of Fauna with Flow, Chemistry and Microbes: Oceanography and Marine Biology: An Annual Review, v. 43, p. 1-46.

Lyons, T., Shapiro, R., Gill, B., Bates, S., Anderson, J., Gilhooly, W. and Parsons-Hubbard, K., 2007, Carbon and Sulfur Cycling in Cretaceous Cold Seeps Recorded in the Paragenesis and Geochemistry of Diagenetic Carbonates: Geological Society of America Abstracts with Programs, v. 39, no 6, p. 348.

MacDonald, I. R., Schroeder, W. W. and Brooks, J. M., 1995, Chemosynthetic Ecosystems Studies Final Report, U.S. Dept. of the Interior, Minerals Mgmt. Service, Gulf of Mexico OCS Region, v. 2, p. 1-338.

Metz, C. L., 2010, Tectonic Controls on the Genesis and Distribution of Late Cretaceous, Western Interior Basin Hydrocarbon-Seep Mounds (Tepee Buttes) of North America: The Journal of Geology, v. 118, p. 201-213.

Michaelis, W., Seifert, R., Nauhaus, K., Treude, T., Thiel, V., Blumenberg, M., Knittel, K., Gieseke, A., Peterknecht, K., Pape, T., Boetius, A., Amann, R., Barker Jorgensen, B., Widdel, F., Peckmann, J., Pimenov, N.V. and Gulin, M.B., 2002, Microbial reefs in the Black Sea Fueled by Anaerobic Oxidation of Methane: Science, v. 297, p. 1013-1015.

Nyman, S. L., Nelson, C. S. and Campbell, K.A., 2010, Miocene tubular concretions in East Coast Basin, New Zealand: Analogue for the subsurface plumbing of cold seeps: Marine Geology, v. 272, p. 319-336.

Parrish, J. T., Gaynor, G. C., and Swift, D. J. P., 1984, Circulation in the Cretaceous Western Interior Seaway of North America, A Review, in Stott, D. F., and Glass, D. J., eds., The Mesozoic of Middle North America, Volume 9, Canadian Society of Petroleum Geologists, p. 221-231.

Peckmann, J., and Thiel, V., 2004, Carbon cycling at ancient methane-seeps: Chemical Geology, v. 205, p. 443-467.

Reitner, J., Peckmann, J., Reimer, A., Schumann, G. and Thiel, V., 2005, Methane-derived carbonate build-ups and associated microbial communities at cold seeps on the lower Crimean shelf (Black Sea): Facies, v. 51, p. 66-79.

Scott, G. R. and Cobban, W. A., 1975, Geologic and biostratigraphic map of the Pierre shale in the Canon City-Florence Basin and the Twelvemile Park area, south-central Colorado: USGS, scale 1:48,000, 1 sheet

Scott, G. R. and Cobban, W. A., 1986, Geologic and biostratigraphic map of the Pierre Shale in the Colorado Springs-Pueblo area, Colorado: USGS, scale 1:100,000, 1 sheet.

Shapiro, R. and Fricke, H., 2002, Tepee Buttes: Fossilized methane-seep ecosystems: GSA Field Guides, v. 3, p. 94-101.

Sharps, J. A., 1976, Geologic map of the Lamar Quadrangle, Colorado and Kansas: USGS, scale 1:250,000, 1 sheet.

Sibuet, M. and Olu, K., 1998, Biogeography, Biodiversity and Fluid Dependence of Deep-Sea Cold-Seep Communities and Active and Passive Margins: Deep Sea Research II, v. 45, p. 517-567.

Stenzel, H. B., 1936, A new formation in the Claiborne Group: The University of Texas Bureau of Economic Geology Pub. No. 3501, p. 267-279.

Stenzel, H. B., Krause, E. K. and Twinning, J. T., 1957, Pelecypoda from the type locality of the Stone City Beds (Middle Eocene) of Texas: The University of Texas Bureau of Economic Geology Pub. No. 5704, 237 p.

Timm, K., and Sonnenberg, S. A., 2017, Increased Organic Content in the Presence of Floccules: A Case Study of the Sharon Springs Member of the Pierre Shale, Cañon City Basin, South-Central Colorado, AAPG Rocky Mountain Section Meeting: Billings, Montana, AAPG.

Thornton, C. A. and Stanton, Jr., R. J., 1994, Recognition of hardgrounds in terrigenous stratigraphic sections: the Moseley Limestone, Middle Eocene, southeast Texas: American Association of Petroleum Geologists Bulletin, v. 78, p. 1481.

van Cappelle, M., Hampson, G. J., and Johnson, H. D., 2018, Spatial and Temporal Evolution of Coastal Depositional Systems and Regional Depositional Process Regimes: Campanian Western Interior Seaway, U.S.A.: Journal of Sedimentary Research, v. 88, p. 873-897.

Waterman, A. S., Center, M. W., George, R. A., Vallette, N. S., Porter, Jr., A. F., Reilly, R. M., Roederer, R. V., Schmieder, J. and Filon, R. H., 2011, Paleogene Biostratigraphic Chart – Gulf Basin, USA: PaleoData Incorporated, 1 chart.

Whiticar, M. J., 1999, Carbon and hydrogen isotope systematics of bacterial formation and oxidation of methane: Chemical Geology, v. 161, p. 291-314.

Wright, E. K., 1987, Stratification and paleocirculation of the Late Cretaceous Western Interior Seaway of North America: Geological Society of America Bulletin, v. 99, p. 480-490.

Yancey, T. E. and Davidoff, A. J., 1991, Paleogene sequence stratigraphy and lithostratigraphy in the Brazos River Valley, Texas: Gulf Coast Association of Geological Societies Field Trip Guidebook, 112 p.

Yancey, T. E., 1995, Depositional trends in siliciclastic deposits of the Stone City transgressive systems tract, Middle Eocene, Texas: Gulf Coast Association of Geological Societies Transactions, v. 45, p. 581-586.

APPENDIX A

TEPEE BUTTES MOUND MORPHOLOGY

Fabric	**Lithofacies**	**$\delta^{18}O$ ‰ (VPDB)**	**$\delta^{13}C$ ‰ (VPDB)**	**Sample Name**	**Collection location**	**Sample Slab**
Peloids in Micrite	Brecciated	-5.99	-34.29	TB-BC 04	Boone South - 3C	BS-3C-10
Peloids in Micrite	Brecciated	-2.88	-40.51	TB-BC 13	Boone South - 3C	BS-3C-10
Peloids in Micrite	Brecciated	-8.14	-34.96	TB-BC 15	Boone South - 3C	BS-3C-10
Peloids in Micrite	Anastamosing ropey	-0.70	-42.24	TB-SV 03	Main Boone mound	B-32
Peloids in Micrite	Anastamosing ropey	-1.17	-43.84	TB-SV 12	Main Boone mound	B-32
Peloids in Micrite	Anastamosing ropey	-0.89	-44.45	TB-SV 24	Main Boone mound	B-32
Peloids in Micrite	Dense lucinid	-0.12	-41.85	TB-10	Main Boone mound	Boone DL
Peloids in Micrite	Dense lucinid	-0.65	-42.46	TB-04	Main Boone mound	Boone DL
Peloids in Micrite	Dense lucinid	-0.42	-44.35	TB-20	Main Boone mound	Boone DL
Peloids in Micrite	Vuggy	-9.94	-33.62	TB-V-02	Main Boone mound	B-11
Peloids in Micrite	Vuggy	-10.72	-32.59	TB-V-19	Main Boone mound	B-11
Peloids in Micrite	Vuggy	-10.20	-34.62	TB-V-24	Main Boone mound	B-11
	min	-10.72	-44.45			
	max	-0.12	-32.59			
Peloids in Calcite	Brecciated	-3.86	-42.07	TB-BC 10	Boone South - 3C	BS-3C-10
Peloids in Calcite	Brecciated	-9.28	-34.75	TB-BC 18	Boone South - 3C	BS-3C-10
Peloids in Calcite	Brecciated	-7.29	-35.16	TB-BC 23	Boone South - 3C	BS-3C-10
Peloids in Calcite	Anastamosing ropey	-0.21	-47.37	TB-SV 04	Main Boone mound	B-32
Peloids in Calcite	Anastamosing ropey	-1.22	-44.08	TB-SV 07	Main Boone mound	B-32
Peloids in Calcite	Anastamosing ropey	-1.22	-43.48	TB-SV 17	Main Boone mound	B-32

Table A-1. Raw Isotopic data of Tepee Butte fabric characterization samples.

Fabric	Lithofacies	$\delta^{18}O$ ‰ (VPDB)	$\delta^{13}C$ ‰ (VPDB)	Sample Name	Collection location	Sample Slab
Peloids in Calcite	Dense lucinid	-1.02	-42.53	TB-05	Main Boone mound	Boone DL
Peloids in Calcite	Dense lucinid	-1.14	-42.71	TB-05 DUP	Main Boone mound	Boone DL
Peloids in Calcite	Dense lucinid	-3.43	-34.81	TB-11	Main Boone mound	Boone DL
	min	-9.28	-47.37			
	max	-0.21	-34.75			
Peloids in ferroan Calcite	Vuggy	-10.97	-22.17	TB-V-07	Main Boone mound	B-11
Peloids in ferroan Calcite	Vuggy	-10.71	-25.44	TB-V-10	Main Boone mound	B-11
Peloids in ferroan Calcite	Vuggy	-10.87	-30.34	TB-V-11	Main Boone mound	B-11
	min	-10.97	-30.34			
	max	-10.71	-22.17			
Botryoidal cement	Brecciated	-8.40	-25.09	TB-BC 06	Boone South - 3C	BS-3C-10
Botryoidal cement	Brecciated	-2.41	-43.17	TB-BC 07	Boone South - 3C	BS-3C-10
Botryoidal cement	Brecciated	-2.74	-44.96	TB-BC 12	Boone South - 3C	BS-3C-10
Botryoidal cement	Brecciated	-2.86	-40.97	TB-BC 25	Boone South - 3C	BS-3C-10
Botryoidal cement	Anastamosing ropey	-4.78	-35.68	TB-SV 09	Main Boone mound	B-32
Botryoidal cement	Anastamosing ropey	-5.38	-35.75	TB-SV 19	Main Boone mound	B-32
Botryoidal cement	Anastamosing ropey	-5.87	-30.57	TB-SV 22	Main Boone mound	B-32
Botryoidal cement	Dense lucinid	-4.13	-38.68	TB-09	Main Boone mound	Boone DL
Botryoidal cement	Dense lucinid	-4.41	-37.78	TB-09 DUP	Main Boone mound	Boone DL
Botryoidal cement	Dense lucinid	-1.51	-46.14	TB-26	Main Boone mound	Boone DL
Botryoidal cement	Dense lucinid	-1.60	-44.37	TB-17	Main Boone mound	Boone DL

Table A-1 Continued.

Fabric	Lithofacies	$\delta^{18}O$ ‰ (VPDB)	$\delta^{13}C$ ‰ (VPDB)	Sample Name	Collection location	Sample Slab
Botryoidal cement	Dense lucinid	-1.75	-46.50	TB-28	Main Boone mound	Boone DL
Botryoidal cement	Dense lucinid	-1.50	-42.06	TB-08	Main Boone mound	Boone DL
Botryoidal cement	Dense lucinid	-4.21	-39.40	TB-07	Main Boone mound	Boone DL
Botryoidal cement	Dense lucinid	-4.34	-38.99	TB-07 DUP	Main Boone mound	Boone DL
Botryoidal cement	Dense lucinid	-4.19	-41.31	TB-24	Main Boone mound	Boone DL
Botryoidal cement	Vuggy	-5.69	-36.13	TB-V-13	Main Boone mound	B-11
Botryoidal cement	Vuggy	-4.78	-39.40	TB-V-14	Main Boone mound	B-11
Botryoidal cement	Vuggy	-5.49	-38.45	TB-V-17	Main Boone mound	B-11
Botryoidal cement	Vuggy	-4.32	-37.68	TB-V-20	Main Boone mound	B-11
Botryoidal cement	Vuggy	-4.32	-37.68	TB-V-25	Main Boone mound	B-11
	min	-8.40	-46.50			
	max	-1.50	-25.09			
Replaced Lucinid Shell	Brecciated	-12.71	-15.98	TB-BC 17	Boone South - 3C	BS-3C-10
Replaced Lucinid Shell	Brecciated	-12.77	-21.12	TB-BC 19	Boone South - 3C	BS-3C-10
Replaced Lucinid Shell	Anastamosing ropey	-12.58	-20.09	TB-SV 02	Main Boone mound	B-32
Replaced Lucinid Shell	Anastamosing ropey	-12.04	-19.63	SV-26	Main Boone mound	B-32
Replaced Lucinid Shell	Anastamosing ropey	-12.06	-19.13	SV-26 DUP	Main Boone mound	B-32
Replaced Lucinid Shell	Dense lucinid	-12.31	-14.50	TB-19	Main Boone mound	Boone DL
Replaced Lucinid Shell	Dense lucinid	-11.87	-14.37	TB-13	Main Boone mound	Boone DL

Table A-1 Continued.

Fabric	Lithofacies	$\delta^{18}O$ ‰ (VPDB)	$\delta^{13}C$ ‰ (VPDB)	Sample Name	Collection location	Sample Slab
Replaced Lucinid Shell	Dense lucinid	-11.90	-14.76	TB-13 DUP	Main Boone mound	Boone DL
Replaced Lucinid Shell	Dense lucinid	-11.91	-14.71	TB-22	Main Boone mound	Boone DL
Replaced Lucinid Shell	Dense lucinid	-11.70	-14.87	TB-21	Main Boone mound	Boone DL
Replaced Lucinid Shell	Vuggy	-11.41	-20.63	TB-V-03	Main Boone mound	B-11
Replaced Lucinid Shell	Vuggy	-12.02	-15.66	TB-V-05	Main Boone mound	B-11
Replaced Lucinid Shell	Vuggy	-11.87	-15.03	TB-V-09	Main Boone mound	B-11
Replaced Lucinid Shell	Ferroan micrite	-9.94	-10.71			
	min	-12.77	-21.12			
	max	-9.94	-10.71			
Inoceramid Shell	Ferroan micrite	-2.10	2.41	TB-MI-08	Florence 1	F1-11
Inoceramid Shell	Carbonate nodules	-3.46	-6.25	TB-N 04	Main Boone mound	B-25
Inoceramid Shell	Carbonate nodules	-6.37	-4.65	TB-N 05	Main Boone mound	B-25
Inoceramid Shell	Carbonate nodules	-3.34	-2.14	TB-N 08	Main Boone mound	B-25
Inoceramid Shell	Vuggy	-5.95	-4.62	TB-V-01	Main Boone mound	B-11
Inoceramid Shell	Vuggy	-4.42	-2.49	TB-V-08	Main Boone mound	B-11
Inoceramid Shell	Ferroan micrite	-3.51	0.86	MI-24	Florence 1	F-11
	min	-6.37	-6.25			
	max	-2.10	2.41			
Ferroan Sparry Calcite	Anastamosing ropey	-12.71	-15.38	TB-SV 13	Main Boone mound	B-32
Ferroan Sparry Calcite	Anastamosing ropey	-11.92	-15.03	TB-SV 16	Main Boone mound	B-32

Table A-1 Continued.

Fabric	Lithofacies	$\delta^{18}O$ ‰ (VPDB)	$\delta^{13}C$ ‰ (VPDB)	Sample Name	Collection location	Sample Slab
Ferroan Sparry Calcite	Anastamosing ropey	-8.44	-24.48	TB-SV 14	Main Boone mound	B-32
Ferroan Sparry Calcite	Anastamosing ropey	-11.70	-15.48	TB-SV 21	Main Boone mound	B-32
Ferroan Sparry Calcite	Dense lucinid	-12.01	-14.66	TB-18	Main Boone mound	Boone DL
Ferroan Sparry Calcite	Dense lucinid	-7.05	-11.88	TB-16	Main Boone mound	Boone DL
Ferroan Sparry Calcite	Dense lucinid	-12.05	-14.22	TB-14	Main Boone mound	Boone DL
Ferroan Sparry Calcite	Dense lucinid	-12.03	-14.15	TB-14 DUP	Main Boone mound	Boone DL
Ferroan Sparry Calcite	Dense lucinid	-11.90	-14.18	TB-15	Main Boone mound	Boone DL
Ferroan Sparry Calcite	Dense lucinid	-11.35	-16.74	TB-06	Main Boone mound	Boone DL
Ferroan Sparry Calcite	Dense lucinid	-11.81	-15.81	TB-06 DUP	Main Boone mound	Boone DL
Ferroan Sparry Calcite	Dense lucinid	-11.92	-15.63	TB-25	Main Boone mound	Boone DL
Ferroan Sparry Calcite	Dense lucinid	-11.65	-15.21	TB-12	Main Boone mound	Boone DL
Ferroan Sparry Calcite	Dense lucinid	-11.99	-15.75	TB-27	Main Boone mound	Boone DL
Ferroan Sparry Calcite	Brecciated	-11.72	-14.64	TB-BC 01	Boone South - 3C	BS-3C-10
Ferroan Sparry Calcite	Brecciated	-11.50	-15.71	TB-BC 02	Boone South - 3C	BS-3C-10
Ferroan Sparry Calcite	Brecciated	-11.33	-18.35	TB-BC 05	Boone South - 3C	BS-3C-10
Ferroan Sparry Calcite	Brecciated	-11.63	-17.78	TB-BC 09	Boone South - 3C	BS-3C-10
Ferroan Sparry Calcite	Brecciated	-11.81	-16.05	TB-BC 24	Boone South - 3C	BS-3C-10
Ferroan Sparry Calcite	Carbonate nodules	-11.84	-17.36	TB-N 01	Main Boone mound	B-25
Ferroan Sparry Calcite	Carbonate nodules	-11.16	-7.07	TB-N 13	Main Boone mound	B-25
Ferroan Sparry Calcite	Vuggy	-11.96	-16.33	TB-V-21	Main Boone mound	B-11
Ferroan Sparry Calcite	Vuggy	-11.30	-16.17	TB-V-22	Main Boone mound	B-11
Ferroan Sparry Calcite	Vuggy	-12.40	-15.54	TB-V-04	Main Boone mound	B-11
Ferroan Sparry Calcite	Vuggy	-12.42	-15.15	TB-V-06	Main Boone mound	B-11
Ferroan Sparry Calcite	Vuggy	-12.28	-15.49	TB-V-12	Main Boone mound	B-11

Table A-1 Continued.

Fabric	Lithofacies	$\delta^{18}O$ ‰ (VPDB)	$\delta^{13}C$ ‰ (VPDB)	Sample Name	Collection location	Sample Slab
	min	-12.71	-24.48			
	max	-7.05	-7.07			
Micrite	Anastamosing ropey	-1.32	-42.72	TB-SV 08	Main Boone mound	B-32
Micrite	Anastamosing ropey	-0.32	-42.26	TB-SV 15	Main Boone mound	B-32
Micrite	Anastamosing ropey	-0.54	-40.81	TB-SV 11	Main Boone mound	B-32
Micrite	Anastamosing ropey	-0.99	-41.74	SV-25	Main Boone mound	B-32
Micrite	Vuggy	-10.76	-34.98	TB-V-15	Main Boone mound	B-11
Micrite	Vuggy	-10.50	-34.46	TB-V-16	Main Boone mound	B-11
Micrite	Vuggy	-11.24	-34.80	TB-V-18	Main Boone mound	B-11
Micrite	Dense lucinid	-0.56	-44.45	DL-33	Main Boone mound	Boone DL
Micrite	Dense lucinid	-0.39	-44.87	DL-34	Main Boone mound	Boone DL
Micrite	Dense lucinid	-0.57	-44.63	DL-34 DUP	Main Boone mound	Boone DL
Micrite	Dense lucinid	-0.53	-42.84	DL-35	Main Boone mound	Boone DL
Micrite	Dense lucinid	-0.48	-42.69	DL-35 DUP	Main Boone mound	Boone DL
	min	-11.24	-44.87			
	max	-0.32	-34.46			
Dolomite	Anastamosing ropey	-12.60	-18.56	TB-SV 05	Main Boone mound	B-32
Dolomite	Anastamosing ropey	-12.84	-16.66	TB-SV 10	Main Boone mound	B-32
Dolomite	Anastamosing ropey	-12.07	-15.73	TB-SV 18	Main Boone mound	B-32
Dolomite	Anastamosing ropey	-12.76	-16.76	TB-SV 23	Main Boone mound	B-32
Dolomite	Brecciated	-10.21	-19.11	TB-BC 03	Boone South - 3C	BS-3C-10
Dolomite	Brecciated	-11.09	-19.24	TB-BC 08	Boone South - 3C	BS-3C-10
	min	-12.84	-19.24			
	max	-10.21	-15.73			

Table A-1 Continued.

Fabric	Lithofacies	$\delta^{18}O$ ‰ (VPDB)	$\delta^{13}C$ ‰ (VPDB)	Sample Name	Collection location	Sample Slab
Micritization	Vuggy	-10.19	-23.11	TB-V-26	Main Boone mound	B-11
Micritization	Vuggy	-9.74	-24.25	TB-V-27	Main Boone mound	B-11
Micritization	Vuggy	-10.20	-26.45	TB-V-28	Main Boone mound	B-11
Micritization	Brecciated	-12.80	-14.15	TB-BC 21	Boone South - 3C	BS-3C-10
Micritization	Brecciated	-13.09	-13.38	TB-BC 22	Boone South - 3C	BS-3C-10
Micritization	Anastamosing ropey	-10.96	-19.51	TB-SV 06	Main Boone mound	B-32
Micritization	Dense lucinid	-10.63	-12.61	TB-03	Main Boone mound	Boone DL
Micritization	Dense lucinid	-10.66	-12.66	TB-03 DUP	Main Boone mound	Boone DL
	min	-13.09	-26.45			
	max	-9.74	-12.61			
Ferroan Micrite	Ferroan micrite	-2.33	3.94	TB-MI 05	Florence 1	F1-11
Ferroan Micrite	Ferroan micrite	-1.66	4.94	TB-MI 09	Florence 1	F1-11
Ferroan Micrite	Ferroan micrite	-1.01	-4.69	TB-MI 10	Florence 1	F1-11
Ferroan Micrite	Ferroan micrite	-3.37	3.18	TB-MI 11	Florence 1	F1-11
Ferroan Micrite	Ferroan micrite	-1.72	4.55	TB-MI 13	Florence 1	F1-11
Ferroan Micrite	Ferroan micrite	-1.33	4.33	TB-MI 17	Florence 1	F1-11
Ferroan Micrite	Ferroan micrite	-0.12	5.30	MI-19	Florence 1	F-11
Ferroan Micrite	Ferroan micrite	-1.42	0.83	MI-20	Florence 1	F-11
Ferroan Micrite	Ferroan micrite	-0.43	4.55	MI-22	Florence 1	F-11
Ferroan Micrite	Ferroan micrite	-0.25	4.86	MI-23	Florence 1	F-11
	avg	-1.36	3.18			
	min	-3.37	-4.69			
	max	-0.12	5.30			
Tepee Butte characteri-zation samples	avg	-7.77	-28.06		without inoceramids and ferroan micrite	
	min	-13.09	-47.37			
	max	-0.12	-7.07			

Table A-1 Continued.

Figure A.1. I-25-118 Individual mound location, Google Earth image.

Figure A.2. I-25-118 Individual mound location outcrop view, lines pointing to seep carbonate, Google Earth image.

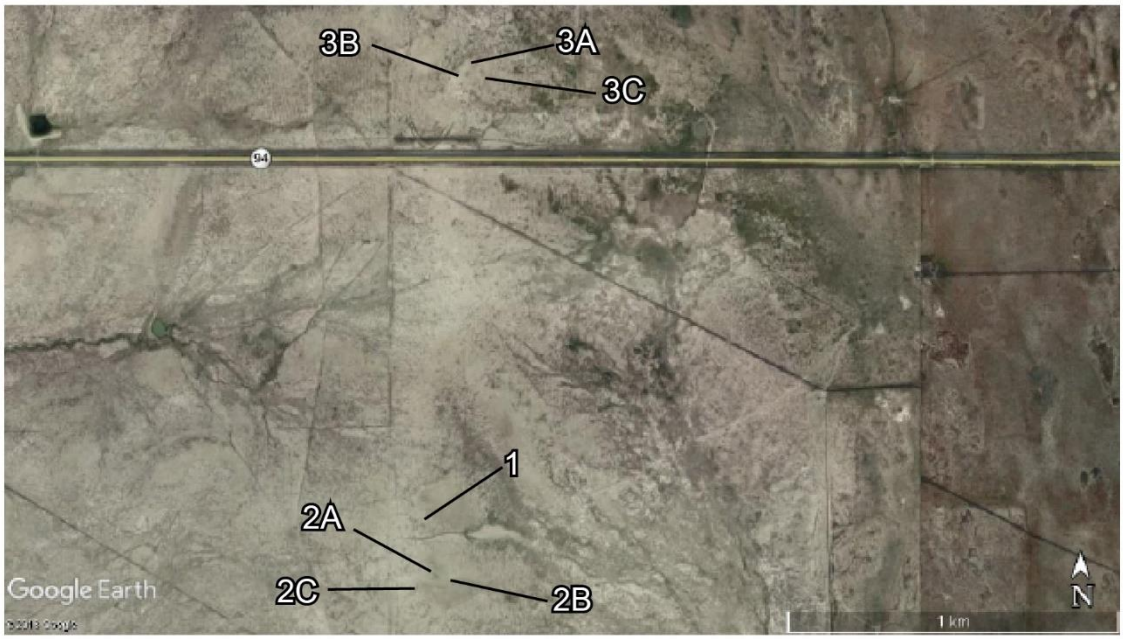

Figure A.3. Mosher individual mound location, Google Earth image.

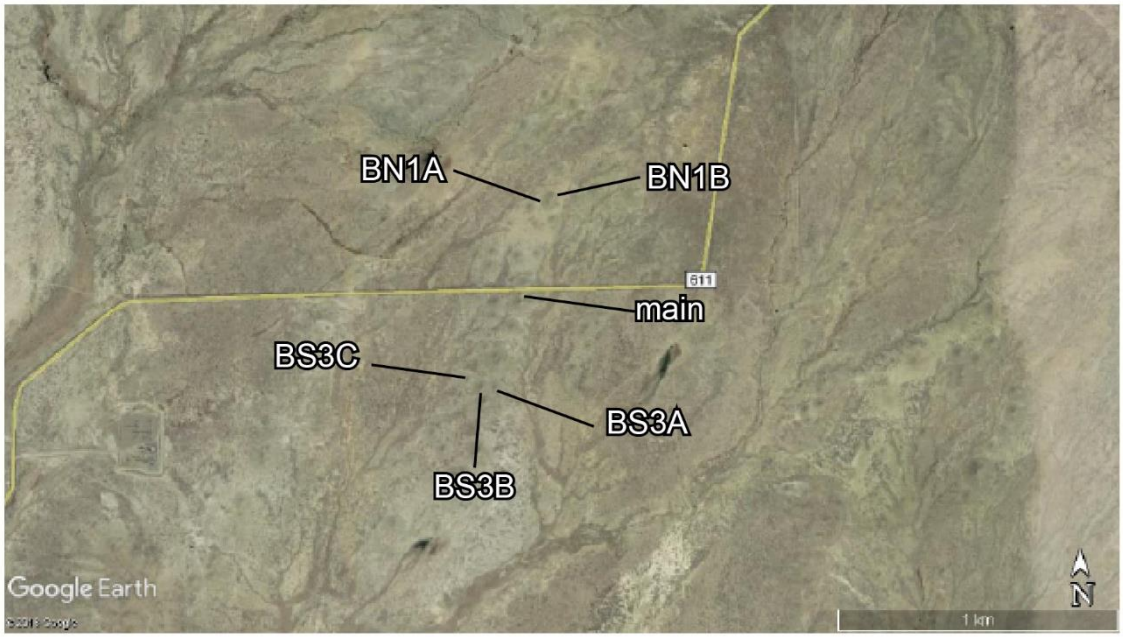

Figure A.4. Boone individual mound locations, Google Earth image. Note linear orientation of some mound arrays.

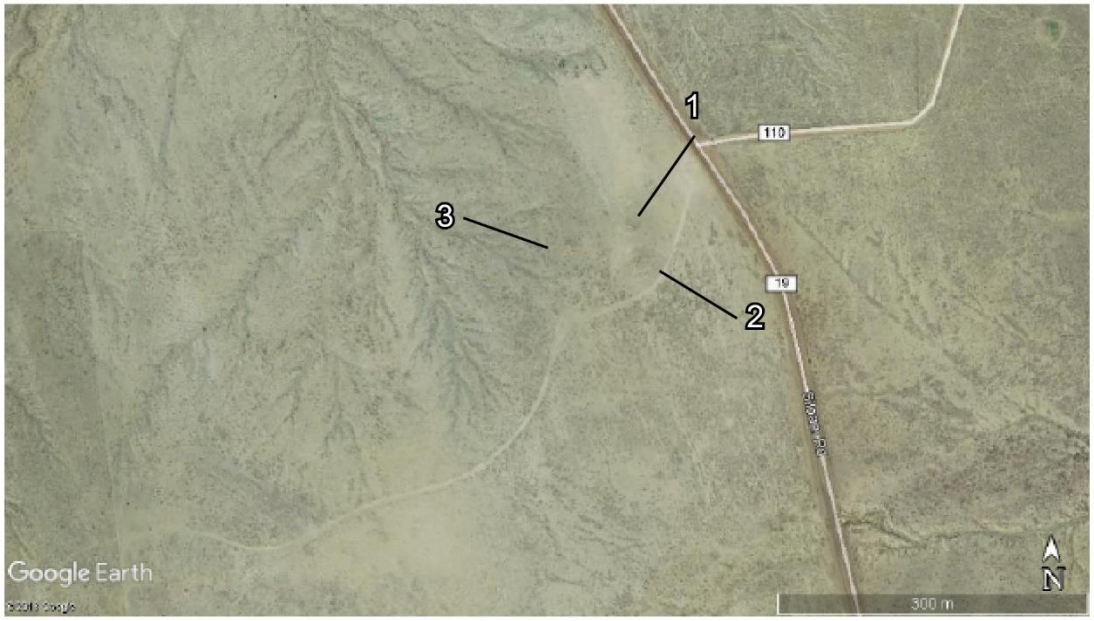

Figure A.5. Florence individual mound locations, Google Earth image.

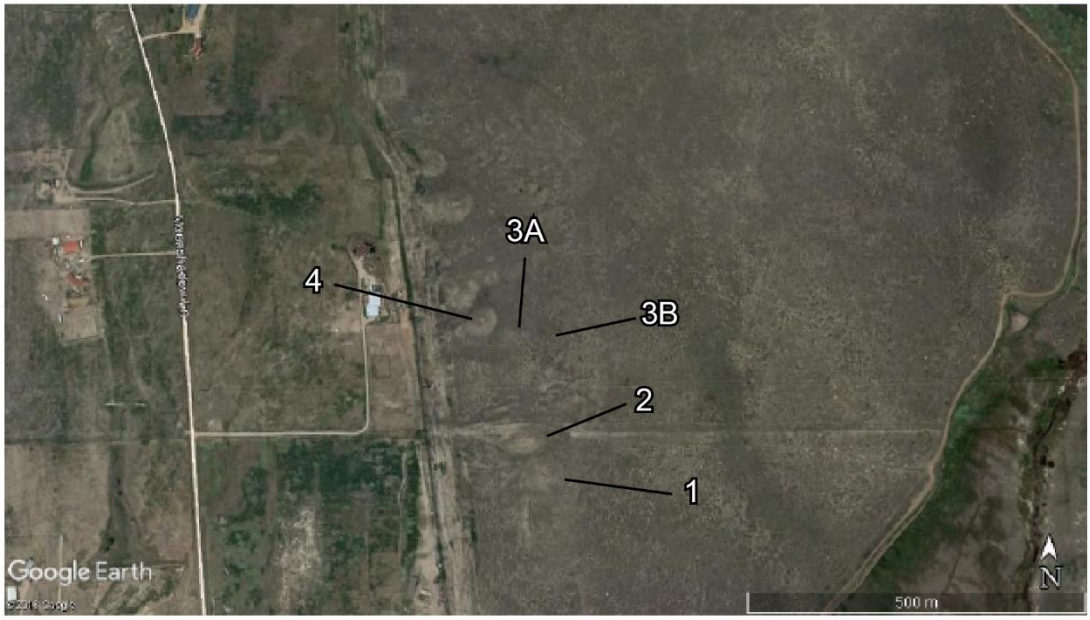

Figure A.6. JV Ranch individual mound locations, Google Earth image.

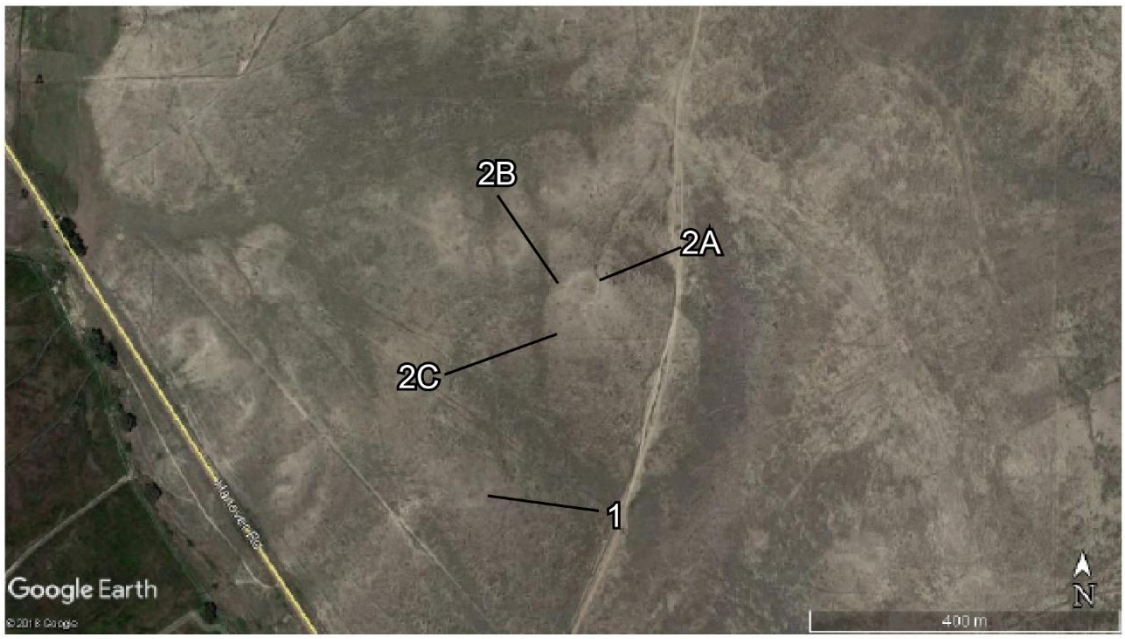

Figure A.7. Hanna Ranch individual mound locations, Google Earth image.

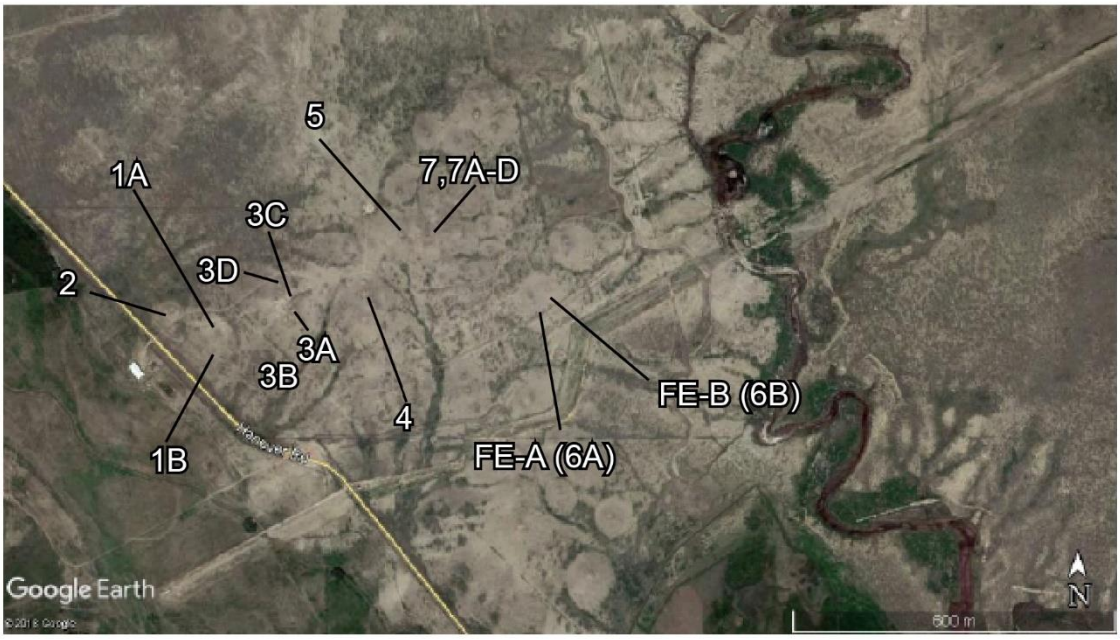

Figure A.8. Southeast Hanna Ranch individual mound locations, Google Earth image. Note linear arrangements of mounds.

Location	Mound name	Sample #	Sample Name	Date
Boone	Boone Main	1	B1	Oct 25 2010
Boone	Boone Main	2	B2	Oct 25 2010
Boone	Boone Main	3	B3	Oct 25 2010
Boone	Boone Main	4	B4	Oct 25 2010
Boone	Boone Main	5	B5	Oct 25 2010
Boone	Boone Main	6	B6	Oct 25 2010
Boone	Boone Main	7	B7	Oct 25 2010
Boone	Boone Main	8	B8	Oct 25 2010
Boone	Boone Main	9	B9	Oct 25 2010
Boone	Boone Main	10	B10	Oct 25 2010
Boone	Boone Main	11	B11	Oct 25 2010
Boone	Boone Main	12	B12	Oct 25 2010
Boone	Boone Main	13	B13	Oct 25 2010
Boone	Boone Main	14	B14	Oct 25 2010
Boone	Boone Main	15	B15	Oct 25 2010
Boone	Boone Main	16	B16	Oct 25 2010
Boone	Boone Main	17	B17	Oct 25 2010
Boone	Boone Main	18	B18	Oct 25 2010
Boone	Boone Main	19	B19	Oct 25 2010
Boone	Boone Main	20	B20	Oct 25 2010
Boone	Boone Main	21	B21	Oct 25 2010
Boone	Boone Main	22	B22	Oct 25 2010
Boone	Boone Main	23	B23	Oct 25 2010
Boone	Boone Main	24	B24	Oct 25 2010
Boone	Boone Main	25	B25	Oct 25 2010
Boone	Boone Main	26	B26	Oct 25 2010
Boone	Boone Main	27	B27	Oct 25 2010
Boone	Boone Main	28	B28	Oct 25 2010
Boone	Boone Main	29	B29	Oct 25 2010
Boone	Boone Main	30	B30	Oct 25 2010
Boone	Boone Main	31	B31	Oct 25 2010
Boone	Boone Main	32	B32	Oct 25 2010
Boone	Boone Main	33	B33	Oct 25 2010
Boone	Boone Main	34	B34	Oct 25 2010
Florence	F1	1	F1-1	Oct 26 2010
Florence	F1	2	F1-2	Oct 26 2010

Table A-2. Tepee Buttes Samples Data Sheet including mound location, mound name, sample number, the sample name, and date collected.

Location	Mound name	Sample #	Sample Name	Date
Florence	F1	3	F1-3	Oct 26 2010
Florence	F1	4	F1-4	Oct 26 2010
Florence	F1	5	F1-5	Oct 26 2010
Florence	F1	6	F1-6	Oct 26 2010
Florence	F1	7	F1-7	Oct 26 2010
Florence	F1	8	F1-8	Oct 26 2010
Florence	F1	9	F1-9	Oct 26 2010
Florence	F1	10	F1-10	Oct 26 2010
Florence	F1	11	F1-11	Oct 26 2010
Florence	F1	12	F1-12	Oct 26 2010
Florence	F2	1	F2-1	Oct 26 2010
Florence	F2	2	F2-2	Oct 26 2010
Florence	F2	3	F2-3	Oct 26 2010
Florence	F2	4	F2-4	Oct 26 2010
Florence	F2	5	F2-5	Oct 26 2010
Florence	F2	6	F2-6	Oct 26 2010
Florence	F2	7	F2-7	Oct 26 2010
Florence	F2	8	F2-8	Oct 26 2010
Florence	F2	9	F2-9	Oct 26 2010
Florence	F2	10	F2-10	Oct 26 2010
Florence	F2	11	F2-11	Oct 26 2010
Florence	F2	12	F2-12	Oct 26 2010
Florence	F2	13	F2-13	Oct 26 2010
Florence	F2	14	F2-14	Oct 26 2010
Florence	F2	15	F2-15	Oct 26 2010
Florence	F2	16	F2-16	Oct 26 2010
Florence	F2	17	F2-17	Oct 26 2010
Florence	F2	18	F2-18	Oct 26 2010
Florence	F2	19	F2-19	Oct 26 2010
Florence	F2	20	F2-20	Oct 26 2010
Florence	F2	21	F2-21	Oct 26 2010
Florence	F2	22	F2-22	Oct 26 2010
Florence	F2	23	F2-23	Oct 26 2010
Florence	F3	1	F3-1	Oct 26 2010
Florence	F3	2	F3-2	Oct 26 2010
Florence	F3	3	F3-3	Oct 26 2010
Florence	F3	4	F3-4	Oct 26 2010

Table A-2 Continued.

Location	Mound name	Sample #	Sample Name	Date
Florence	F3	5	F3-5	Oct 26 2010
Florence	F3	6	F3-6	Oct 26 2010
Florence	F3	7	F3-7	Oct 26 2010
Florence	F3	8	F3-8	Oct 26 2010
Florence	F3	9	F3-9	Oct 26 2010
Florence	F3	10	F3-10	Oct 26 2010
Florence	F3	11	F3-11	Oct 26 2010
Florence	F3	12	F3-12	Oct 26 2010
Florence	F3	13	F3-13	Oct 26 2010
Florence	F3	14	F3-14	Oct 26 2010
I25-118	I25-118	1	I25-118-1	Oct 26 2010
I25-118	I25-118	2	I25-118-2	Oct 26 2010
I25-118	I25-118	3	I25-118-3	Oct 26 2010
I25-118	I25-118	4	I25-118-4	Oct 26 2010
I25-118	I25-118	5	I25-118-5	Oct 26 2010
I25-118	I25-118	6	I25-118-6	Oct 26 2010
I25-118	I25-118	7	I25-118-7	Oct 26 2010
I25-118	I25-118	8	I25-118-8	Oct 26 2010
I25-118	I25-118	9	I25-118-9	Oct 26 2010
I25-118	I25-118	10	I25-118-10	Oct 26 2010
I25-118	I25-118	11	I25-118-11	Oct 26 2010
I25-118	I25-118	12	I25-118-12	Oct 26 2010
I25-118	I25-118	13	I25-118-13	Oct 26 2010
I25-118	I25-118	14	I25-118-14	Oct 26 2010
I25-118	I25-118	15	I25-118-15	Oct 26 2010
I25-118	I25-118	16	I25-118-16	Oct 26 2010
I25-118	I25-118	17	I25-118-17	Oct 26 2010
I25-118	I25-118	18	I25-118-18	Oct 26 2010
JV Ranch	JVR1	1	JVR1-1	Oct 26 2010
JV Ranch	JVR1	2	JVR1-2	Oct 26 2010
JV Ranch	JVR1	3	JVR1-3	Oct 26 2010
JV Ranch	JVR1	4	JVR1-4	Oct 26 2010
JV Ranch	JVR1	5	JVR1-5	Oct 26 2010
JV Ranch	JVR1	6	JVR1-6	Oct 26 2010
JV Ranch	JVR1	7	JVR1-7	Oct 26 2010
JV Ranch	JVR2	1	JVR2-1	Oct 26 2010
JV Ranch	JVR2	2	JVR2-2	Oct 26 2010

Table A-2 Continued.

Location	Mound name	Sample #	Sample Name	Date
JV Ranch	JVR2	3	JVR2-3	Oct 26 2010
JV Ranch	JVR2	4	JVR2-4	Oct 26 2010
JV Ranch	JVR2	5	JVR2-5	Oct 26 2010
JV Ranch	JVR2	6	JVR2-6	Oct 26 2010
JV Ranch	JVR2	7	JVR2-7	Oct 26 2010
JV Ranch	JVR2	8	JVR2-8	Oct 26 2010
JV Ranch	JVR2	9	JVR2-9	Oct 26 2010
JV Ranch	JVR2	10	JVR2-10	Oct 26 2010
JV Ranch	JVR2	11	JVR2-11	Oct 26 2010
JV Ranch	JVR2	12	JVR2-12	Oct 26 2010
JV Ranch	JVR2	13	JVR2-13	Oct 26 2010
JV Ranch	JVR2	14	JVR2-14	Oct 26 2010
JV Ranch	JVR3A	1	JVR3A-1	Oct 26 2010
JV Ranch	JVR3A	2	JVR3A-2	Oct 26 2010
JV Ranch	JVR3A	3	JVR3A-3	Oct 26 2010
JV Ranch	JVR3B	1	JVR3B-1	Oct 26 2010
JV Ranch	JVR4	1	JVR4-1	Oct 26 2010
JV Ranch	JVR4	2	JVR4-2	Oct 26 2010
JV Ranch	JVR4	3	JVR4-3	Oct 26 2010
JV Ranch	JVR4	4	JVR4-4	Oct 26 2010
Hanna Ranch	HR1	1	HR1-1	Oct 27 2010
Hanna Ranch	HR1	2	HR1-2	Oct 27 2010
Hanna Ranch	HR1	3	HR1-3	Oct 27 2010
Hanna Ranch	HR1	4	HR1-4	Oct 27 2010
Hanna Ranch	HR1	5	HR1-5	Oct 27 2010
Hanna Ranch	HR1	6	HR1-6	Oct 27 2010
Hanna Ranch	HR1	7	HR1-7	Oct 27 2010
Hanna Ranch	HR1	8	HR1-8	Oct 27 2010
Hanna Ranch	HR1	9	HR1-9	Oct 27 2010
Hanna Ranch	HR1	10	HR1-10	Oct 27 2010
Hanna Ranch	HR1	11	HR1-11	Oct 27 2010
Hanna Ranch	HR1	12	HR1-12	Oct 27 2010
Hanna Ranch	HR1	13	HR1-13	Oct 27 2010
Hanna Ranch	HR2A	1	HR2A-1	Oct 27 2010
Hanna Ranch	HR2A	2	HR2A-2	Oct 27 2010
Hanna Ranch	HR2A	3	HR2A-3	Oct 27 2010
Hanna Ranch	HR2A	4	HR2A-4	Oct 27 2010

Table A-2 Continued.

Location	Mound name	Sample #	Sample Name	Date
Hanna Ranch	HR2A	5	HR2A-5	Oct 27 2010
Hanna Ranch	HR2A	6	HR2A-6	Oct 27 2010
Hanna Ranch	HR2B	1	HR2B-1	Oct 27 2010
Hanna Ranch	HR2B	2	HR2B-2	Oct 27 2010
Hanna Ranch	HR2B	3	HR2B-3	Oct 27 2010
Hanna Ranch	HR2B	4	HR2B-4	Oct 27 2010
Hanna Ranch	HR2B	5	HR2B-5	Oct 27 2010
Hanna Ranch	HR2B	6	HR2B-6	Oct 27 2010
Hanna Ranch	HR2B	7	HR2B-7	Oct 27 2010
Hanna Ranch	HR2B	8	HR2B-8	Oct 27 2010
Hanna Ranch	HR2B	9	HR2B-9	Oct 27 2010
Hanna Ranch	HR2B	10	HR2B-10	Oct 27 2010
Hanna Ranch	HR2B	11	HR2B-11	Oct 27 2010
Hanna Ranch	HR2B	12	HR2B-12	Oct 27 2010
Hanna Ranch	HR2B-C	1	HR2B-C-1	Oct 27 2010
Hanna Ranch	HR2B-C	2	HR2B-C-2	Oct 27 2010
Hanna Ranch	HR2B-C	3	HR2B-C-3	Oct 27 2010
Hanna Ranch	HR2C	1	HR2C-1	Oct 27 2010
Hanna Ranch	HR2C	2	HR2C-2	Oct 27 2010
Hanna Ranch	HR2C	3	HR2C-3	Oct 27 2010
Hanna Ranch	HR2C	4	HR2C-4	Oct 27 2010
Hanna Ranch	HR2C	5	HR2C-5	Oct 27 2010
Southeast Hanna Ranch	SEHR1A	1	SEHR1A-1	Oct 27 2010
Southeast Hanna Ranch	SEHR1A	2	SEHR1A-2	Oct 27 2010
Southeast Hanna Ranch	SEHR1A	3	SEHR1A-3	Oct 27 2010
Southeast Hanna Ranch	SEHR1A	4	SEHR1A-4	Oct 27 2010
Southeast Hanna Ranch	SEHR1A	5	SEHR1A-5	Oct 27 2010
Southeast Hanna Ranch	SEHR1B	1	SEHR1B-1	Oct 27 2010
Southeast Hanna Ranch	SEHR1B	2	SEHR1B-2	Oct 27 2010
Southeast Hanna Ranch	SEHR1B	3	SEHR1B-3	Oct 27 2010
Southeast Hanna Ranch	SEHR1B	4	SEHR1B-4	Oct 27 2010
Southeast Hanna Ranch	SEHR2	1	SEHR2-1	Oct 27 2010
Southeast Hanna Ranch	SEHR2	2	SEHR2-2	Oct 27 2010
Southeast Hanna Ranch	SEHR2	3	SEHR2-3	Oct 27 2010
Southeast Hanna Ranch	SEHR2	4	SEHR2-4	Oct 27 2010
Southeast Hanna Ranch	SEHR2	5	SEHR2-5	Oct 27 2010
Southeast Hanna Ranch	SEHR2	6	SEHR2-6	Oct 27 2010

Table A-2 Continued.

Location	Mound name	Sample #	Sample Name	Date
Southeast Hanna Ranch	SEHR2	7	SEHR2-7	Oct 27 2010
Southeast Hanna Ranch	SEHR3A	1	SEHR3A-1	Oct 27 2010
Southeast Hanna Ranch	SEHR3A	2	SEHR3A-2	Oct 27 2010
Southeast Hanna Ranch	SEHR3A	3	SEHR3A-3	Oct 27 2010
Southeast Hanna Ranch	SEHR3A	4	SEHR3A-4	Oct 27 2010
Southeast Hanna Ranch	SEHR4	1	SEHR4-1	Oct 27 2010
Southeast Hanna Ranch	SEHR4	2	SEHR4-2	Oct 27 2010
Southeast Hanna Ranch	SEHR4	3	SEHR4-3	Oct 27 2010
Southeast Hanna Ranch	SEHR4	4	SEHR4-4	Oct 27 2010
Southeast Hanna Ranch	SEHR4	5	SEHR4-5	Oct 27 2010
Southeast Hanna Ranch	SEHR4	6	SEHR4-6	Oct 27 2010
Southeast Hanna Ranch	SEHR4	7	SEHR4-7	Oct 27 2010
Southeast Hanna Ranch	SEHR4	8	SEHR4-8	Oct 27 2010
Southeast Hanna Ranch	SEHR4	9	SEHR4-9	Oct 27 2010
Southeast Hanna Ranch	SEHR4	10	SEHR4-10	Oct 27 2010
Southeast Hanna Ranch	SEHR4	11	SEHR4-11	Oct 27 2010
Southeast Hanna Ranch	SEHR4	12	SEHR4-12	Oct 27 2010
Southeast Hanna Ranch	SEHR4	13	SEHR4-13	Oct 27 2010
Southeast Hanna Ranch	SEHR4	14	SEHR4-14	Oct 27 2010
Southeast Hanna Ranch	SEHR4	15	SEHR4-15	Oct 27 2010
Southeast Hanna Ranch	SEHR4	16	SEHR4-16	Oct 27 2010
Southeast Hanna Ranch	SEHR5	1	SEHR5-1	Oct 27 2010
Southeast Hanna Ranch	SEHR5	2	SEHR5-2	Oct 27 2010
Southeast Hanna Ranch	SEHRFE-A (6A)	1	SEHRFE-A (6A)-1	Oct 27 2010
Southeast Hanna Ranch	SEHRFE-A (6A)	2	SEHRFE-A (6A)-2	Oct 27 2010
Southeast Hanna Ranch	SEHRFE-A (6A)	3	SEHRFE-A (6A)-3	Oct 27 2010
Southeast Hanna Ranch	SEHRFE-A (6A)	4	SEHRFE-A (6A)-4	Oct 27 2010
Southeast Hanna Ranch	SEHRFE-A (6A)	5	SEHRFE-A (6A)-5	Oct 27 2010
Southeast Hanna Ranch	SEHRFE-A (6A)	6	SEHRFE-A (6A)-6	Oct 27 2010
Southeast Hanna Ranch	SEHRFE-A (6A)	7	SEHRFE-A (6A)-7	Oct 27 2010
Southeast Hanna Ranch	SEHRFE-A (6A)	8	SEHRFE-A (6A)-8	Oct 27 2010
Southeast Hanna Ranch	SEHRFE-A (6A)	9	SEHRFE-A (6A)-9	Oct 27 2010
Southeast Hanna Ranch	SEHRFE-A (6A)	10	SEHRFE-A (6A)-10	Oct 27 2010
Southeast Hanna Ranch	SEHRFE-A (6A)	11	SEHRFE-A (6A)-11	Oct 27 2010
Southeast Hanna Ranch	SEHRFE-A (6A)	12	SEHRFE-A (6A)-12	Oct 27 2010
Southeast Hanna Ranch	SEHRFE-A (6A)	13	SEHRFE-A (6A)-13	Oct 27 2010
Southeast Hanna Ranch	SEHRFE-B (6B)	1	SEHRFE-B (6B)-1	Oct 27 2010

Table A-2 Continued.

Location	Mound name	Sample #	Sample Name	Date
Southeast Hanna Ranch	SEHR7A	1	SEHR7A-1	Oct 27 2010
Southeast Hanna Ranch	SEHR7B	1	SEHR7B-1	Oct 27 2010
Southeast Hanna Ranch	SEHR7B	2	SEHR7B-2	Oct 27 2010
Southeast Hanna Ranch	SEHR7C	1	SEHR7C-1	Oct 27 2010
Southeast Hanna Ranch	SEHR7C	2	SEHR7C-2	Oct 27 2010
Mosher	M1	1	M1-1	Oct 28 2010
Mosher	M1	2	M1-2	Oct 28 2010
Mosher	M1	3	M1-3	Oct 28 2010
Mosher	M1	4	M1-4	Oct 28 2010
Mosher	M1	5	M1-5	Oct 28 2010
Mosher	M1	6	M1-6	Oct 28 2010
Mosher	M1	7	M1-7	Oct 28 2010
Mosher	M1	8	M1-8	Oct 28 2010
Mosher	M1	9	M1-9	Oct 28 2010
Mosher	M1	10	M1-10	Oct 28 2010
Mosher	M1	11	M1-11	Oct 28 2010
Mosher	M1	12	M1-12	Oct 28 2010
Mosher	M1	13	M1-13	Oct 28 2010
Mosher	M1	14	M1-14	Oct 28 2010
Mosher	M1	15	M1-15	Oct 28 2010
Mosher	M2A	1	M2A-1	Oct 28 2010
Mosher	M2A	2	M2A-2	Oct 28 2010
Mosher	M2A	3	M2A-3	Oct 28 2010
Mosher	M2A	4	M2A-4	Oct 28 2010
Mosher	M2A	5	M2A-5	Oct 28 2010
Mosher	M2A	6	M2A-6	Oct 28 2010
Mosher	M2A	7	M2A-7	Oct 28 2010
Mosher	M2A	8	M2A-8	Oct 28 2010
Mosher	M2B	1	M2B-1	Oct 28 2010
Mosher	M2B	2	M2B-2	Oct 28 2010
Mosher	M2B	3	M2B-3	Oct 28 2010
Mosher	M2B	4	M2B-4	Oct 28 2010
Mosher	M2B	5	M2B-5	Oct 28 2010
Mosher	M2B	6	M2B-6	Oct 28 2010
Mosher	M2C	1	M2C-1	Oct 28 2010
Mosher	M2C	2	M2C-2	Oct 28 2010
Mosher	M2C	3	M2C-3	Oct 28 2010

Table A-2 Continued.

Location	Mound name	Sample #	Sample Name	Date
Mosher	M2C	4	M2C-4	Oct 28 2010
Mosher	M2C	5	M2C-5	Oct 28 2010
Mosher	M2C	6	M2C-6	Oct 28 2010
Mosher	M2C	7	M2C-7	Oct 28 2010
Mosher	M2C	8	M2C-8	Oct 28 2010
Mosher	M2C	9	M2C-9	Oct 28 2010
Mosher	M2C	10	M2C-10	Oct 28 2010
Mosher	M3A	1	M3A-1	Oct 28 2010
Mosher	M3A	2	M3A-2	Oct 28 2010
Mosher	M3A	3	M3A-3	Oct 28 2010
Mosher	M3A	4	M3A-4	Oct 28 2010
Mosher	M3A	5	M3A-5	Oct 28 2010
Mosher	M3A	6	M3A-6	Oct 28 2010
Mosher	M3A	7	M3A-7	Oct 28 2010
Mosher	M3A	8	M3A-8	Oct 28 2010
Mosher	M3B	1	M3B-1	Oct 28 2010
Mosher	M3B	2	M3B-2	Oct 28 2010
Mosher	M3B	3	M3B-3	Oct 28 2010
Mosher	M3B	4	M3B-4	Oct 28 2010
Mosher	M3B	5	M3B-5	Oct 28 2010
Mosher	M3B	6	M3B-6	Oct 28 2010
Mosher	M3B	7	M3B-7	Oct 28 2010
Mosher	M3B	8	M3B-8	Oct 28 2010
Mosher	M3C	1	M3C-1	Oct 28 2010
Mosher	M3C	2	M3C-2	Oct 28 2010
Mosher	M3D	1	M3D-1	Oct 28 2010
Boone	BN1A	1	BN1A-1	Oct 29 2010
Boone	BN1A	2	BN1A-2	Oct 29 2010
Boone	BN1A	3	BN1A-3	Oct 29 2010
Boone	BN1A	4	BN1A-4	Oct 29 2010
Boone	BN1A	5	BN1A-5	Oct 29 2010
Boone	BN1A	6	BN1A-6	Oct 29 2010
Boone	BN1A	7	BN1A-7	Oct 29 2010
Boone	BN1A	8	BN1A-8	Oct 29 2010
Boone	BN1A	9	BN1A-9	Oct 29 2010
Boone	BN1A	10	BN1A-10	Oct 29 2010
Boone	BN1A	11	BN1A-11	Oct 29 2010

Table A-2 Continued.

Location	Mound name	Sample #	Sample Name	Date
Boone	BN1A	12	BN1A-12	Oct 29 2010
Boone	BN1B	1	BN1B-1	Oct 29 2010
Boone	BN1B	2	BN1B-2	Oct 29 2010
Boone	BN1B	3	BN1B-3	Oct 29 2010
Boone	BN1B	4	BN1B-4	Oct 29 2010
Boone	BN1B	5	BN1B-5	Oct 29 2010
Boone	BN1B	6	BN1B-6	Oct 29 2010
Boone	BN1B	7	BN1B-7	Oct 29 2010
Boone	BN1A/1B	1	BN1A/1B-1	Oct 29 2010
Boone	BN1A/1B	2	BN1A/1B-2	Oct 29 2010
Boone	BN1A/1B	3	BN1A/1B-3	Oct 29 2010
Boone	BN1A/1B	4	BN1A/1B-4	Oct 29 2010
Boone	BS3A	1	BS3A-1	Oct 29 2010
Boone	BS3A	2	BS3A-2	Oct 29 2010
Boone	BS3A	3	BS3A-3	Oct 29 2010
Boone	BS3A	4	BS3A-4	Oct 29 2010
Boone	BS3A	5	BS3A-5	Oct 29 2010
Boone	BS3A	6	BS3A-6	Oct 29 2010
Boone	BS3A	7	BS3A-7	Oct 29 2010
Boone	BS3A	8	BS3A-8	Oct 29 2010
Boone	BS3A	9	BS3A-9	Oct 29 2010
Boone	BS3A	10	BS3A-10	Oct 29 2010
Boone	BS3A	11	BS3A-11	Oct 29 2010
Boone	BS3A	12	BS3A-12	Oct 29 2010
Boone	BS3A	13	BS3A-13	Oct 29 2010
Boone	BS3A	14	BS3A-14	Oct 29 2010
Boone	BS3A	15	BS3A-15	Oct 29 2010
Boone	BS3A	16	BS3A-16	Oct 29 2010
Boone	BS3A	17	BS3A-17	Oct 29 2010
Boone	BS3B	1	BS3B-1	Oct 29 2010
Boone	BS3B	2	BS3B-2	Oct 29 2010
Boone	BS3B	3	BS3B-3	Oct 29 2010
Boone	BS3B	4	BS3B-4	Oct 29 2010
Boone	BS3B	5	BS3B-5	Oct 29 2010
Boone	BS3B	6	BS3B-6	Oct 29 2010
Boone	BS3B	7	BS3B-7	Oct 29 2010
Boone	BS3B	8	BS3B-8	Oct 29 2010

Table A-2 Continued.

Location	Mound name	Sample #	Sample Name	Date
Boone	BS3B	9	BS3B-9	Oct 29 2010
Boone	BS3B	10	BS3B-10	Oct 29 2010
Boone	BS3B	11	BS3B-11	Oct 29 2010
Boone	BS3B	12	BS3B-12	Oct 29 2010
Boone	BS3B	13	BS3B-13	Oct 29 2010
Boone	BS3B	14	BS3B-14	Oct 29 2010
Boone	BS3B	15	BS3B-15	Oct 29 2010
Boone	BS3B	16	BS3B-16	Oct 29 2010
Boone	BS3B	17	BS3B-17	Oct 29 2010
Boone	BS3B	18	BS3B-18	Oct 29 2010
Boone	BS3A/3B	1	BS3A/3B-1	Oct 29 2010
Boone	BS3A/3B	2	BS3A/3B-2	Oct 29 2010
Boone	BS3A/3B	3	BS3A/3B-3	Oct 29 2010
Boone	BS3A/3B	4	BS3A/3B-4	Oct 29 2010
Boone	BS3A/3B	5	BS3A/3B-5	Oct 29 2010
Boone	BS3A/3B	6	BS3A/3B-6	Oct 29 2010
Boone	BS3A/3B	7	BS3A/3B-7	Oct 29 2010
Boone	BS3A/3B	8	BS3A/3B-8	Oct 29 2010
Boone	BS3A/3B	9	BS3A/3B-9	Oct 29 2010
Boone	BS3A/3B	10	BS3A/3B-10	Oct 29 2010
Boone	BS3C	1	BS3C-1	Oct 29 2010
Boone	BS3C	2	BS3C-2	Oct 29 2010
Boone	BS3C	3	BS3C-3	Oct 29 2010
Boone	BS3C	4	BS3C-4	Oct 29 2010
Boone	BS3C	5	BS3C-5	Oct 29 2010
Boone	BS3C	6	BS3C-6	Oct 29 2010
Boone	BS3C	7	BS3C-7	Oct 29 2010
Boone	BS3C	8	BS3C-8	Oct 29 2010
Boone	BS3C	9	BS3C-9	Oct 29 2010
Boone	BS3C	10	BS3C-10	Oct 29 2010

Table A-2 Continued.

APPENDIX B

TEPEE BUTTES TEMPORAL AND SPATIAL VARIATIONS

Location	Name	Carbonate Type	Diagenetic Stage	$\delta^{18}O$ ‰	$\delta^{13}C$ ‰
I-25	I25-01	Peloids	Early	-2.18	-40.28
I-25	I25-02	Peloids	Early	-0.37	-46.05
I-25	I25-03	Peloids	Early	0.02	-45.68
I-25	I25-04	Micrite sans peloids	Early	-0.37	-43.61
I-25	I25-05	Micrite sans peloids	Early	-0.70	-34.51
I-25	I25-05 DUP	Micrite sans peloids	Early	-0.77	-35.15
I-25	I25-06	Botryoids	Late	-1.30	-44.23
I-25	I25-07	Botryoids	Late	-1.75	-43.92
I-25	I25-08	Botryoids	Late	-1.62	-48.03
I-25	I25-08 DUP	Botryoids	Late	-1.79	-47.76
I-25	I25-09	Botryoids	Late	-2.14	-43.73
			Min	-2.18	-48.03
			Max	0.02	-34.51
			Avg	-1.18	-43.00
Mosher	MS-01	Peloids in micrite	Early	-8.47	-36.27
Mosher	MS-02	Peloids in micrite	Early	-9.02	-38.47
Mosher	MS-03	Peloids in micrite	Early	-9.45	-41.08
Mosher	MS-04	Micrite sans peloids	Early	-6.94	-28.72
Mosher	MS-05	Micrite sans peloids	Early	-7.05	-26.94
Mosher	MS-05 DUP	Micrite sans peloids	Early	-6.97	-27.30
Mosher	MS-06	Botryoids	Late	-3.67	-49.33
Mosher	MS-06 DUP	Botryoids	Late	-3.71	-49.54
Mosher	MS-07	Botryoids	Late	-3.50	-45.65
Mosher	MS-07 DUP	Botryoids	Late	-3.43	-45.97
Mosher	MS-08	Botryoids	Late	-4.55	-49.03
Mosher	MS-09	Botryoids	Late	-10.09	-20.76
			Min	-10.09	-49.54
			Max	-3.43	-20.76
			Avg	-6.41	-38.25

Table B-1. Raw Isotopic data of Tepee Butte Temporal characterization samples from Mosher and I-25.

Location	Name	Carbonate Type	Diagenetic Stage	$\delta^{18}O$ ‰	$\delta^{13}C$ ‰
Florence	FL-01	Peloids in micrite	Early	-0.98	-43.86
Florence	FL-02	Peloids in micrite	Early	-0.90	-43.88
Florence	FL-03	Peloids in micrite	Early	-1.32	-44.32
Florence	FL-03DUP	Peloids in micrite	Early	-1.15	-42.45
Florence	FL-04	Peloids in calcite	Early	-1.52	-39.94
Florence	FL-05	Peloids in calcite	Early	-3.79	-26.71
Florence	FL-05 dup	Peloids in calcite	Early	-4.02	-26.71
Florence	FL-15	Micrite sans peloids	Early	-8.24	-26.77
Florence	FL-06	Botryoids	Late	-4.26	-36.68
Florence	FL-07	Botryoids	Late	-2.26	-44.77
Florence	FL-08	Botryoids	Late	-2.69	-45.08
Florence	FL-FM	Ferroan micrite		-2.33	3.94
Florence	FL-FM	Ferroan micrite		-1.66	4.94
Florence	FL-FM	Ferroan micrite		-1.01	-4.69
Florence	FL-FM	Ferroan micrite		-3.37	3.18
Florence	FL-FM	Ferroan micrite		-1.72	4.55
Florence	FL-FM	Ferroan micrite		-1.33	4.33
Florence	FL-FM	Ferroan micrite		-0.12	5.30
Florence	FL-FM	Ferroan micrite		-1.42	0.83
Florence	FL-FM	Ferroan micrite		-0.43	4.55
Florence	FL-FM	Ferroan micrite		-0.25	4.86
			Min	-8.24	-45.08
			Max	-0.90	-26.71
			Avg	-2.83	-38.29
JV Ranch	JVR-02	peloids in calcite	Early	-8.26	-38.18
JV Ranch	JVR-04	peloids in calcite	Early	-5.51	-19.37
JV Ranch	JVR-06	peloids in calcite	Early	-7.12	-39.34
JV Ranch	JVR-08	peloids in calcite	Early	-9.90	-37.06
JV Ranch	JVR-01	botryoids	Late	-3.71	-40.42
JV Ranch	JVR-03	botryoids	Late	-5.13	-40.43
JV Ranch	JVR-05	botryoids	Late	-4.50	-46.86
JV Ranch	JVR-07	botryoids	Late	-5.39	-40.10
			Min	-9.90	-46.86
			Max	-3.71	-19.37
			Avg	-6.19	-37.72

Table B-2. Raw isotopic data of Tepee Butte spatial characterization samples from the *Didymoceras nebrascense* biozone with the Florence, JV Ranch and Boone mounds.

Location	Name	Carbonate Type	Diagenetic Stage	$\delta^{18}O$ ‰	$\delta^{13}C$ ‰
Boone	TB-05	Peloids in calcite	Early	-1.02	-42.53
Boone	TB-05 DUP	Peloids in calcite	Early	-1.14	-42.71
Boone	TB-11	Peloids in calcite	Early	-3.43	-34.81
Boone	TB-10	Peloids in micrite	Early	-0.12	-41.85
Boone	TB-04	Peloids in micrite	Early	-0.65	-42.46
Boone	TB-20	Peloids in micrite	Early	-0.42	-44.35
Boone	DL-33	Micrite sans peloids	Early	-0.56	-44.45
Boone	DL-34	Micrite sans peloids	Early	-0.39	-44.87
Boone	DL-34 DUP	Micrite sans peloids	Early	-0.57	-44.63
Boone	DL-35	Micrite sans peloids	Early	-0.53	-42.84
Boone	DL-35 DUP	Micrite sans peloids	Early	-0.48	-42.69
Boone	TB-09	Botryoidal 1	Late	-4.13	-38.68
Boone	TB-09 DUP	Botryoidal 1	Late	-4.41	-37.78
Boone	TB-26	Botryoidal 2	Late	-1.51	-46.14
Boone	TB-17	Botryoidal 3	Late	-1.60	-44.37
Boone	TB-28	Botryoidal 4	Late	-1.75	-46.50
Boone	TB-08	Botryoidal	Late	-1.50	-42.06
Boone	TB-07	Botryoidal	Late	-4.21	-39.40
Boone	TB-07 DUP	Botryoidal	Late	-4.34	-38.99
Boone	TB-24	Botryoidal	Late	-4.19	-41.31
			Min	-4.41	-46.50
			Max	-0.12	-34.81
			Avg	-1.85	-42.17

Table B-2 Continued.

Location	Name	Carbonate Type	Diagenetic Stage	$\delta^{18}O$ ‰	$\delta^{13}C$ ‰
SEHR2	SEHR2-01	Peloids in micrite	Early	-9.75	-25.35
SEHR2	SEHR2-02	Peloids in micrite	Early	-10.41	-28.93
SEHR2	SEHR2-03	Peloids in micrite	Early	-10.64	-31.71
SEHR2	SEHR2-03 DUP	Peloids in micrite	Early	-10.59	-32.33
SEHR2	SEHR2-04	Botryoids	Late	-6.25	-37.10
SEHR2	SEHR2-05	Botryoids	Late	-6.92	-41.50
SEHR2	SEHR2-06	Botryoids	Late	-6.30	-41.94
			Min	-10.64	-41.94
			Max	-6.25	-25.35

Table B-3. Raw Isotopic data of Tepee Butte Temporal characterization samples from Southeast Hanna Ranch down a line of linear buttes.

Location	Name	Carbonate Type	Diagenetic Stage	$\delta^{18}O$ ‰	$\delta^{13}C$ ‰
			Avg	-8.69	-34.12
SEHR4	SEHR4-01	Peloids in micrite	Early	-8.94	-31.87
SEHR4	SEHR4-02	Peloids in calcite	Early	-9.20	-29.10
SEHR4	SEHR4-03	Peloids in micrite	Early	-10.69	-28.94
SEHR4	SEHR4-04	Peloids in micrite	Early	-9.52	-29.91
SEHR4	SEHR4-05	Botryoids	Late	-6.54	-32.88
SEHR4	SEHR4-05 DUP	Botryoids	Late	-6.81	-32.23
SEHR4	SEHR4-06	Botryoids	Late	-6.09	-35.07
SEHR4	SEHR4-07	Botryoids	Late	-3.48	-41.41
			Min	-10.69	-41.41
			Max	-3.48	-28.94
			Avg	-7.66	-32.68
SEHR6	SEHR6-01	Peloids in micrite/calcite	Early	-9.18	-39.93
SEHR6	SEHR6-02	Peloids in micrite/calcite	Early	-10.14	-37.67
SEHR6	SEHR6-02 DUP	Peloids in micrite/calcite	Early	-10.17	-37.40
SEHR6	SEHR6-03	Peloids in micrite	Early	-10.00	-38.39
SEHR6	SEHR6-04	Botryoids	Late	-3.43	-48.25
SEHR6	SEHR6-05	Botryoids	Late	-6.07	-40.32
SEHR6	SEHR6-06	Botryoids	Late	-4.77	-43.29
			Min	-10.17	-48.25
			Max	-3.43	-37.40
			Avg	-7.68	-40.75

Table B-3 Continued.

APPENDIX C

EOCENE STONE CITY BLUFF

Sample Type	Sample Name	$d^{13}C_{PDB}$	$d^{18}O_{PDB}$
Dark Matrix	SCB 5-4-13	-30.87	-1.76
Dark Matrix	SCB 5-4-14	-30.49	-1.81
Dark Matrix	SCB 5-4-17	-30.28	-0.82
Dark Matrix	SCB-04	-29.33	-1.82
Dark Matrix	SCB-08	-32.52	-1.45
Dark Matrix	SCB-09	-33.03	-1.64
Dark Matrix	SCB-04 dup.	-29.11	-1.42
Dark Matrix	SCB-09 dup.	-33.11	-1.58
Dark Matrix	SCB-5-7	-30.05	-1.74
Dark Matrix	SCB-5-9	-29.40	-1.82
Dark Matrix	SCB-5-10	-29.59	-1.81
Dark Matrix	SCB-5-11	-31.30	-1.59
Dark Matrix	SCB 5-13	-30.19	-1.57
Dark Matrix	SCB 5-13 dup.	-30.23	-1.60
Dark Matrix	SCB 5-15	-30.10	-1.78
Dark Matrix	SCB 5-17	-31.11	-1.54
Dark Matrix	SCB 5-19	-29.50	-1.88
Dark Matrix	SCB 5-20	-29.51	-1.86
Dark Matrix	SCB 5-21	-30.28	-0.20
Dark Matrix	SCB 5-4-07	-30.63	-1.68
Dark Matrix	SCB 5-4-09	-30.44	-1.71
Dark Matrix	SCB 5-4-10	-30.56	-1.68
Dark Matrix	SCB 5-4-11	-30.99	-1.44
Light Matrix	SCB 5-12	-30.75	-1.57
Light Matrix	SCB 5-14	-30.90	-1.56
Light Matrix	SCB 5-16	-31.24	-1.51
Light Matrix	SCB 5-18	-30.91	-1.58
Light Matrix	SCB 5-4-12	-31.31	-1.65
Light Matrix	SCB 5-4-15	-31.15	-1.66
Light Matrix	SCB 5-4-16	-31.69	-1.42
Light Matrix	SCB 5-4-18	-31.63	-1.56
Light Matrix	SCB-05	-28.85	1.06
Light Matrix	SCB-06	-29.56	-1.57
Light Matrix	SCB-06 dup.	-29.36	-1.67
Light Matrix	SCB-5-8	-30.74	-1.60
Light Matrix	SCB 5-4-08	-30.33	-1.76
Micropipe Fill	SCB 5-4-01	-32.09	-1.13
Micropipe Fill	SCB 5-4-02	-31.79	-1.08
Micropipe Fill	SCB 5-4-02 dup.	-32.27	-1.02

Table C-1. Raw data of the stable isotopic analysis on the barrel concretions.

Sample Type	Sample Name	$d^{13}C_{PDB}$	$d^{18}O_{PDB}$
Micropipe Fill	SCB 5-4-28	-32.65	-1.16
Micropipe Fill	SCB 5-4-29	-32.40	-1.15
Micropipe Fill	SCB 5-5-01	-32.38	-0.95
Micropipe Fill	SCB-5-01	-32.60	-1.12
Open Septarian Fill	SCB 5-4-03	-34.36	-1.34
Open Septarian Fill	SCB 5-4-04	-34.59	-1.33
Open Septarian Fill	SCB 5-4-05	-32.90	-1.05
Open Septarian Fill	SCB 5-4-06	-32.93	0.56
Open Septarian Fill	SCB 5-4-20	-32.92	-1.13
Open Septarian Fill	SCB 5-4-21	-33.01	-1.11
Open Septarian Fill	SCB 5-4-22	-34.51	0.29
Open Septarian Fill	SCB 5-4-22 dup.	-34.48	0.27
Open Septarian Fill	SCB 5-4-23	-33.05	-1.13
Open Septarian Fill	SCB 5-4-24	-34.31	-1.35
Open Septarian Fill	SCB 5-4-30	-32.96	-1.06
Open Septarian Fill	SCB 5-4-31	-34.10	-1.27
Open Septarian Fill	SCB-5-3	-33.03	-0.95
Open Septarian Fill	SCB-5-4	-33.55	-1.24
Open Septarian Fill	SCB-03	-33.89	-1.64
Healed Fracture Fill	SCB 5-4-25	-32.11	-1.40
Healed Fracture Fill	SCB 5-4-26	-33.00	-0.75
Healed Fracture Fill	SCB 5-4-27	-33.40	-1.14
Healed Fracture Fill	SCB 5-4-32	-33.10	-0.99
Healed Fracture Fill	SCB 5-4-33	-34.15	-1.23
Healed Fracture Fill	SCB 5-4-34	-32.69	-1.09
Healed Fracture Fill	SCB 5-4-35	-34.08	-1.20
Healed Fracture Fill	SCB-5-5	-33.59	-1.11
Healed Fracture Fill	SCB-5-6	-34.46	-1.55

Table C-1 Continued.